Progressive Quenching in Spin Networks

Charles Moslonka

PSL UNIVERSITÉ PARIS

THÈSE DE DOCTORAT

DE L'UNIVERSITÉ PSL

Préparée à l'ESPCI Paris
Laboratoire Gulliver, UMR 7083

Progressive Quenching in Spin Networks

Progressive Quenching et systèmes de spins

Soutenue par
Charles MOSLONKA
Le Vendredi 20 Octobre 2023

École doctorale n°624
École doctorale Physique en Île-de-France

Spécialité
Physique

Composition du jury :

M. Lev TRUSKINOVSKY Directeur de Recherche PMMH - ESPCI Paris - Université PSL	*Président du Jury*
Mme Hélène BERTHOUMIEUX Chargée de Recherche Gulliver - ESPCI Paris - Université PSL	*Examinatrice*
M. Raphaël CHETRITE Chargé de Recherche Laboratoire J.A Dieudonné - Université Côte-d'Azur	*Rapporteur*
M. David DEAN Professeur des Universités LOMA - Université de Bordeaux	*Rapporteur*
M. Matteo POLETTINI Researcher Université du Luxembourg	*Examinateur*
M. Ken SEKIMOTO Professeur Émerite Laboratoire MSC Université Paris-Cité Gulliver - ESPCI Paris - Université PSL	*Directeur de thèse*

ESPCI PARIS | PSL

Contents

À Djoudjou, François
Papy et Mamine.

Remerciements

Je voudrais tout d'abord remercier mon jury de thèse, et notamment M. Lev Truskinovsky pour m'avoir fait l'honneur de l'avoir présidé ainsi que par ses chaleureux encouragements. Merci à Matteo Polettini de s'être déplacé depuis le Luxembourg, et pour ses précieux commentaires sur le manuscrit. Merci aux deux rapporteurs, tout d'abord d'avoir accepté la lourde tâche de lire attentivement un manuscrit pas forcément digeste et surtout pour tous les commentaires qui ont, de manière certaine, amélioré la qualité globale de ce dernier. Merci donc à M. David Dean pour son écoute attentive en amont de la soutenance, et toutes ses questions. Un merci particulier à M. Raphaël Chétrite pour la profondeur de sa lecture et la pertinence de ses questions et remarques. Et merci à Mme Hélène Berthoumieux, pour ses bons conseils avant la soutenance quand le stress était au plus haut.

Merci également à MM. David Lacoste et Guilhem Semerjian d'avoir accepté de faire partie de mon comité de suivi de thèse !

Merci enfin à mon directeur de thèse, Ken, qui au cours de ses trois années et demie de travail commun, de par la profondeur abyssale de ses connaissances et par l'incroyable finesse de son analyse, m'a permis d'appréhender facilement bien des outils en physique et mathématiques, autrement bien velus. Merci aussi pour la liberté qu'il m'a accordée tout au long de ma thèse, de m'avoir laissé la conduire là où mon cœur pensait qu'il le fallait - souvent à tort - parfois à raison. Les moments de réalisation qu'une solution marche restent toujours mes plus beaux moments de recherche.

Le laboratoire Gulliver était un environnement de travail parfait pour moi, surtout grâce à ses occupants. Merci tout d'abord à son directeur Oliver Dauchot, toujours disponible que ce soit pour discuter sérieusement ou non. Merci aux différents gestionnaires que j'ai pu croiser et qui ont toujours tout fait pour faciliter mon accueil : l'indéboulonnable soleil Fée Sorrentino coté CNRS, ainsi qu'Elisa Silveira, Jeldy Cubas Hernandez et David Noël coté ESPCI. Je salue également les ingénieures Justine Laurent et Aurélie Lloret, que je n'ai pas beaucoup sollicitée, mais qui ont toujours eu le sourire.

Merci aux permanents du labo, toujours sympathiques et bienveillants, par ordre d'apparition dans leurs bureaux sur mon chemin jusqu'au H311: Élie, Matthieu, Michael, Tony, Vincent, David, Olivier, Zorana, Hélène (encore !), Mathilde, Teresa, Guillaume, Paddy, Yannick, Michel et enfin Josh.

Merci aux non-permanents, stagiaires, doctorants, postdocs et autres, les petites mains de la recherche et des vrais copains. En essayant de n'oublier personne, je tiens à citer : La team NL : Coline, Mats, Hedi et mon frère de galère Haggai, l'équipage du bureau du bout du monde H311: Maitane, Yann, Marion, Natalie, et Paul depuis le M2, ma "promo" des doctorants Jeremy et Yann, et tous les autres : Armand, Thibaut, Kostas, Vincent, Pierre, Antoine, Victoria, Léo-Paul, Angelo, Yorgos, Rocio, Maria, Samuel, Caroline,

Lars, Darka, Quentin, Amaury, Vas, Mengshi, Juliane, Claire, Martina, Martyna, Gabin, Mathéo et Martijn.

Après le labo, merci aux copains de l'ENS Kchan, et en particulier le Scooby-Gens: les OGs Élodie, Mathis, Jean-Louis, Olympio, Alice, Pierrick, Arnaud, Bastien, Corentin, Romane, Thomas et Pierre.

Encore une dernière couche avec les cœurs de la PC♡, merci en particulier à Aurélien, Ariane, Matthieu, Ben, Caroline, Émile, Émile (lequel est lequel ?), Joséphine et Adrien. Salut à Yehudi, avec qui j'ai fait un bon bout de chemin !

Merci à mes profs de physique, sans qui rien ne se serait passé, en particulier à MM. Galera, Barbet-Massin et Mme Daumont.

Enfin merci à ma famille, ma mère, mon père, Isaure, Sophie, Fred, Mamine, François et les autres, pour leur soutien que je sais éternel. Papy, cette thèse est en partie pour toi, même si tu ne le sais plus. J'aurais été fier de te l'expliquer.

Merci Thibaut, mon frère de cœur.

Marion, je perds 20 ans quand je suis avec toi, et j'aime ça. On sera toujours jeunes, même quand on sera vieux.

To the Reader's attention

This manuscript relates the evolution of my work on Progressive Quenching over the three years of my PhD. It therefore recontextualizes the model initially introduced by Bruno Ventéjou and Ken Sekimoto in 2018 [1], and extensively develops the ideas of our papers [2, 3, 4], taking much of the text from their bodies **without modification**. Reading this manuscript will offer the reader a smoothed compilation of the three articles. It is therefore not to be considered an original research work as such.

We have the following outline and article correspondence:

- Chapter 1 introduces the main concepts and tools used throughout this thesis, namely the Progressive Quenching, martingales and Markov chains. The latter section is extracted from lecture notes I took during the "(Post)-Modern Thermodynamics" conference held in December 2022 at he University of Luxembourg, following Ken Sekimoto's lecture, followed by Pedro Harunari's [5].

- Chapter 2 presents the original model of Progressive Quenching for globally coupled Ising Spins, first introduced by Ventéjou and Sekimoto in [1].

- Chapter 3 studies individual realizations of Progressive Quenching thanks to a martingale evolution law first derived in [1]. We include the exact derivation of the martingale from our 2022 article [3] and we re-write our prediction analysis with and without a perturbation from our 2020 article [2] without the $O(N_0^{-2})$ error bound.

- Chapter 4 links the magnetization probability distributions after a Progressive Quenching process to the canonical distribution of the initial system. We then show that they are equal under certain assumptions, namely the Markov property and detailed balance. Its content is taken from [3] (Sections 4.1 to 4.4) and our 2023 preprint article [4] (Section 4.4 onwards).

- Chapter 5 extends those results to all Markov processes, by redefining the Progressive Quenching as an operation on transition networks. It is extracted from [4], except Section 5.4 which is original.

- Chapter 7 explores the consequences of non-Markovianity. It is extracted from [4].

The overall structure of this thesis is quite linear. Each chapter follows and extends the results of the previous one. They all include a small appendix that extends the main

text. All codes, written in Python3 with Spyder syntax (and Mathematica for large-matrix eigenvalue analysis), used to generate the figures are publicly available on this GitHub repository [1].

[1] Available on `https://github.com/Chamiche/Progressive_Quenching/`

Résumé de cette thèse

Ce manuscrit relate l'évolution du Progressive Quenching (que l'on pourrait traduire par "trempe progressive") au cours de mes 3 années de thèses, dans ses linéarités et ses embranchements. Ce qui était au départ une adaptation aux spins d'Ising d'un concept développé pour l'étude des quasi-cristaux s'est vue généralisée et étendue aux chaînes de Markov et d'autre part devenir un terrain de jeu d'application de la théorie des martingales en physique.

Notre focalisation sur le modèle de Curie-Weiss (spins globalement couplés) lors des trois premiers chapitres est par nature restrictive mais nous a néanmoins permis de comprendre comment s'articulent les interactions entre les parties fixées (dites "quenchées") et libres du système soumis au Progressive Quenching.

Le chapitre 2 nous a permis de poser de manière systématique les bases du processus introduit lors de l'introduction, et de comprendre l'influence des différents paramètres du système. En fixant la température β, nous avons pu mettre en évidence deux cas limites, à savoir les limites du couplage entre les spins nul, aboutissant à des marches aléatoires non-biaisées, ainsi que du couplage infini aboutissant à un système nécessairement polarisé. Les cas d'intérêt sont donc situés à la frontière de ces deux limites, que nous avons identifiée comme le couplage critique, c'est-à-dire le couplage maximisant la susceptibilité magnétique du système. Nous avons également pu comprendre comment écrire la contribution de la partie fixée dans l'Hamiltonien du système, à savoir au travers d'un champ magnétique effectif agissant sur tout le système libre. Le modèle de Curie-Weiss permet la formulation simple de cette contribution.

Le chapitre 3 est centré autour de la notion de martingale qui gouverne la dynamique de la magnétisation du système. Cette loi, qui met en exergue la relation cyclique entre système figé et système libre au travers de quantités caractéristiques, nous permet de comprendre l'évolution temporelle du système. Ce dernier cherche à conserver sa magnétisation moyenne, et abouti ainsi à des trajectoires suivant les contours de magnétisation constante. Cette loi de martingale a d'abord été dérivée de manière approchée, mais il s'est ensuite avéré qu'elle était exacte. Nous avons pu en conclure qu'il était possible d'estimer l'état final d'un processus, par exemple prédire la valeur de la magnétisation des spins fixés M_T, car la valeur moyenne des spins non-fixés, $m^{(\mathrm{eq})}$, se conserve au cours d'une réalisation du Progressive Quenching. Nous pouvons donc projeter sur les contours iso-$m^{(\mathrm{eq})}$ ces trajectoires, afin d'estimer leurs valeurs finales. Un point crucial est que plus cette estimation est faite tardivement, plus elle est précise. Nous interprétons cette propriété comme étant une mémoire effective du système. Ce sont les premières positions de la trajectoire qui vont globalement déterminer sa direction et donc sa position finale. Nous avons quantifié cette dépendance grâce aux calculs de sensibilités du système. Ce dernier est d'autant plus sensible aux perturbations qu'il compte de spins non-fixés.

Nous pouvons offrir à ces conclusions un parallèle en termes de dynamique sociale. Lors d'un choix commun (typiquement, un référendum dans une population donnée), le débat public est surtout orienté par les premières personnes à donner leurs opinions. Ainsi, dans un groupe social ayant tendance à être homogène en termes d'opinion (c'est-à-dire avec des interactions typiquement ferromagnétiques), les questions et débats portés à l'actualité sont généralement dictés par les personnes donnant leur avis en premier, qui sont également les personnes ayant le plus d'exposition médiatique. Ce parallèle certes peu scientifique, nous permet néanmoins de justifier que lorsque l'opinion publique est peu stable, les interactions sociales sont, en moyenne, proches d'une valeur critique au sens de l'équation 3.

Une fois la dynamique d'une trajectoire ou d'une réalisation du Progressive Quenching étudiée, nous avons étudié leur répartition d'ensemble, à savoir la distribution de probabilité de la magnétisation finale M_{N_0}. C'est l'objet du chapitre 4. Tout d'abord, nous avons observé la dépendance avec la valeur du couplage spin-spin j_0 au chapitre 3. Nous nous sommes rendus compte que cette distribution coïncidait avec la distribution canonique du système à l'équilibre thermodynamique. D'abord au travers du Recycled Quenching, un processus sans fin dérivé du PQ, nous avons pu comprendre l'origine de cette conservation de distribution, alors que la fixation d'un spin est a priori un processus hors-équilibre. La propriété fondamentale ici en jeu est la formule des probabilités totales, qui nous permet d'établir que choisir la valeur des N_0 spins un à un ou bien tous ensemble ne change pas la probabilité de leur distribution. Une fois cette égalité établie, nous nous sommes concentré sur la dynamique d' équilibrage des spins et sur l'influence d'un *quench* sur celle-ci. À l'aide des algorithmes dynamiques de Glauber, nous avons pu mettre en évidence le fait que le temps entre les *quenches* n'avaient pas d'influence sur la distribution finale, quand bien même les systèmes étaient par nature du *quench* frustrés. Nous avons ensuite expliqué ce phénomène d'un point de vue thermodynamique, avec un parallèle avec la théorie de Landauer.

Nous avons ensuite entrepris une généralisation de nos résultats, portés par les résultats obtenus avec la dynamique de Glauber. Pour cette dernière, peu importe le temps de relaxation du système, la distribution canonique était la distribution stationnaire vers laquelle tendait le système sous les règles de l'algorithme. Nous nous sommes donc demandé si cela était généralisable aux chaines de Markov stationnaires (dont l'algorithme de Glauber fait partie). Nous avons donc formulé le Progressive Quenching pour n'importe quelle chaine de Markov, au travers de notre idée initiale, c'est-à-dire la représentation d'un système par ses degrés de liberté que nous pouvons ensuite fixer. Nous avons montré que la condition pour que la distribution finale de l'état d'un système après le Progressive Quenching corresponde à sa distribution stationnaire, était que les états vérifiaient entre eux le bilan détaillé. Autrement dit, lorsque deux états échangent entre eux des flux de probabilités équilibrés, nous pouvons supprimer les transitions entre ces deux états sans changer la distribution statique du système. Par exemple, l'algorithme de Glauber vérifie par construction le bilan détaillé, aspect fondamental de l'équilibre thermodynamique à l'échelle microscopique. Le Progressive Quenching nous donnera donc, dans ce cas, la distribution canonique. Nous avons ensuite ébauché ce résultat comme étant une représentation d'un invariant topologique du graphe dirigé représentatif des chaînes de Markov. Le dernier chapitre explore donc les conséquences du Progressive Quenching sur des systèmes non-Markoviens. Nous abandonnons donc notre cadre général des chaînes

de Markov pour retourner aux systèmes de spins d'Ising. Nous avons tout d'abord étudié les systèmes comprenant des degrés de liberté cachés couplant les spins visibles entre eux. Nous avons donc pu montrer que ce système est renormalisable via une intégration des degrés de liberté invisibles. Ces derniers modifient donc la dynamique d'équilibrage du système, mais pour autant l'état d'équilibre du système entier n'est pas modifié par le Progressive Quenching. Ainsi, nous observons des " overshoot " de la magnétisation lors de *quench*, mais la valeur d'équilibre de cette dernière reste inchangée. Nous avons donc entreprit d'introduire du délai dans les interactions des spins, en suivant la modélisation faite par Choi et Huberman. L'introduction de délai change complètement la donne, car cela rend l'état d'équilibre du système dépendant aux valeurs des coefficients cinétiques. Or, nous nous sommes rendu compte que l'action de *quench* un spin revient à faire tendre son temps de réponse typique vers $+\infty$. Le Progressive Quenching modifie donc la cinétique du système et donc sa distribution statique lorsque ses interactions comprennent du retard. À l'aide de simulations numériques, nous avons ainsi pu " cartographier " l'état stationnaire du modèle de Choi-Huberman, en fonction du temps de décalage entre les spins et du temps d'attente entre deux *quenches*. Cette cartographie nous a permis de montrer numériquement que le système atteint des états plus polarisés que le cas sans délai, correspondant à la distribution canonique. Il semble que cet effet est d'autant plus important que la taille du système est grande, mais cette conclusion reste à confirmer par des études numériques plus poussées.

Si finalement les résultats principaux exposés, à savoir la conservation de la distribution stationnaire dans le cas Markovien, peuvent apparaître décevants dans leur apparente simplicité, ils ouvrent néanmoins la voie pour l'étude des systèmes non-Markoviens, notamment le couplage entre retard entre interactions (paramètre a) et durée d'attente entre deux *quenches* (paramètre ΔT). Notre étude préliminaire semble indiquer qu'il existe une zone de domaine $(a, \Delta T)$ ou cet effet est optimal.

De plus, le Progressive Quenching appliqué au modèle de Curie-Weiss permet l'application de la théorie des martingales à des processus différents des standards de la thermodynamique stochastique. Étant donné la généralité des systèmes où certains paramètres se fixent avec le temps, en premier lieu les systèmes se refroidissant de manière non-homogène, nous sommes persuadés que ces processus dépassent le cadre de la pure physique statistique.

Chapter 1

Introduction

This Chapter will introduce the main ideas and models used throughout this thesis. We encourage the reader to browse through the first section about the general idea of Progressive Quenching, as this principle is common to all the results in the following chapters. We also briefly introduce martingale processes, Doob's optional stopping theorem in a dedicated section, and Markov chains. Both concepts will be helpful in the rest of the manuscript.

1.1 Progressive Quenching

1.1.1 Motivations

Since the end of the last century, much development has been made in the physics of stochastic processes out of equilibrium of a finite system interacting with heat baths and under the influences of an external system - or systems [6, 7, 8, 9, 10, 11]. world, however, we sometimes encounter situations where the system's degrees of freedom become progressively fixed. ity than the equivalent pure systems. Nevertheless, in our description, we model the progressive cooling-down process via its degrees of freedom without introducing fluctuations in interactions. Moreover, this paradigm could also be relevant for studying the evolution of mechanical properties of certain materials because of the long-ranged elasticity. For example, ripples propagate in graphene sheets [17] with quenched defects. A model of spins interacting indirectly through an elastic string has been studied in [18].

From a more socially oriented point of view, we might also consider the decision-making process of a community in which each member progressively makes up their mind before a referendum.

In those examples, the already fixed part can influence the behavior of the part whose degrees of freedom are not yet fixed. What types of generic aspects are in this type of problem is largely unknown, and our object is to find them out.

1.1.2 Setting up the process

Let us consider a dynamical system of n degrees of freedom, denoted by $\{x_1(t), x_2(t), \ldots, x_n(t)\}$. These parameters can evolve with time, obeying a set of evolution equations. It is in this very general description that the idea of progressive quenching

is defined. Imagine that at a certain time set by the operator, say t_1, we fix indefinitely the degree x_1 at the value it took at that exact time, that is :

$$\forall t \geq t_1 \qquad x_1(t) = x_1(t_1). \tag{1.1}$$

x_1 is now said to be **quenched**. We now let the rest of the system evolve under the same set of equations as before, except that now x_1 is fixed. This constraint may modify the overall dynamics completely, as it sets new boundary conditions. This constrained evolution continues for a certain time $\Delta t = t_2 - t_1$, until $t = t_2$. Then we fix similarly x_2 such that:

$$\forall t \geq t_2 \qquad x_2(t) = x_2(t_2). \tag{1.2}$$

This quenching procedure can then continue, for given fixation times $\{t_1, t_2, \ldots, t_n\}$, until all parameters are fixed. This idea is summed up schematically in Figure 1.1. The whole process is what we call **Progressive Quenching** - which we will abbreviate in "**PQ**". The action of quenching might be seen as an instantaneous cooling of a very specific part of the system or as an infinite increase of the kinetic response parameters of the part. This particular aspect is the object of Section 4.5.

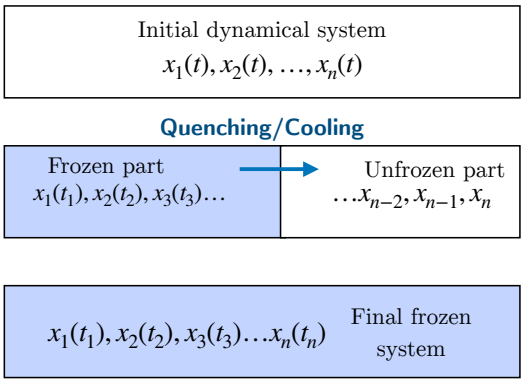

Figure 1.1: Schematic procedure of Progressive Quenching over a general dynamical system. The clear demarcation between the quenched (colored) and free (clear) parts is shown in the center. Only the free part is allowed to evolve under the constraints of the frozen part.

This quenching front propagation has been studied in the case of phasons in quasicrystals [19, 20], to study the propagation front of the apparent phase freezing of 2D Lennard-Jones atomic systems. The idea proposed by Sekimoto in [21] was an extending boundary condition at which the phase fields were frozen through a temperature decrease. In a nutshell, phasons are the quasiparticules associated to atomic rearrangement in quasicristals. Their evolution can be modeled by diffusive dynamics with a non-conservative thermal noise. In a 1D framework, a scalar phason field $\psi(x,t)$ obeys the evolution equation:

$$\partial\psi/\partial t = D\partial^2\psi/\partial x^2 + \xi(x,t), \tag{1.3}$$

where $\xi(x,t)$ is a Gaussian white noise uncorrelated in both space (x) and time (t). At

equilibrium, the spatial correlation scales like $\langle|\psi(x+r,t)-\psi(x,t)|^2\rangle \sim |r|$. The progressive quenching fixes the value of $\psi(x,t)$ at the front position, $x = Vt$, which moves in the $+x$ direction at a constant speed $V(>0)$. Then, the spatial correlation in the quenched part exhibits different statistics $\langle|\psi(x+r)-\psi(x)|^2\rangle \sim |r|^{3/2}/\ell_D^{1/2}$, over the length-scale inferior to the diffusion length, $\ell_D \equiv D/V$. Nearly three decades later, this idea was re-written in the terms described above for Ising spins networks [22, 1].

1.1.3 Choice of quenching time intervals and derived stochastic processes

The choice of the parameters $\{t_1, t_2, \ldots, t_n\}$ will dictate how long we leave the system to relax to the new constrained equilibrium until the next quench and may change the outcome of the process altogether. For example, if the suppose that the system has a typical relaxation time τ, setting $t_i \ll \tau$ for any $i \in \{1, \ldots, n\}$ will not allow a proper relaxation and will, in effect lower the quenching influence. On the other hand, setting $t_i \to \infty$ will allow the new equilibrium to be reached. With that consideration in mind, we chose at first to study the latter (in Chapters 2 to 4), and we extended the study to finite t_i later on in Chapters 4 to 6.

Another important aspect is that the quenching process effectively divides the initial system into two parts: quenched and free (as pictured in Fig.1.1) with different evolutions. When the systems behave apparently randomly, for example, systems in contact with a heat bath inducing thermal fluctuations, we can derive multiple stochastic processes characterizing those evolutions. First and foremost, the set of values of the quenched degrees of freedom $\{x_1(t_1), x_2(t_2), \ldots, x_i(t_i)\}_{i\in\{1,\ldots n\}}$ is a stochastic process indexed by the number of frozen degrees of freedom. It is usually the object of interest since it completely characterizes the evolution of the frozen part, and its final value is the system's final state. However, even though it is less well-defined and system-dependent, we can also consider the evolution of the free part as a stochastic process. For example, we can follow the evolution of a representative quantity $\mathcal{F}(x_{i+1}(t), x_{i+2}(t), \ldots, x_n(t))$ (magnetization, species count, density, etc.) during the quenching process. An exciting feature of this dichotomy is that both processes influence each other. The outcome of a quenching will set new constraints - through new boundary conditions or fixed interactions, see Fig. 1.2 - to which the rest of the system will react, thus modifying the probability distributions of the free degrees of freedom and therefore, the value of $\mathcal{F}$. Furthermore, since the distributions of the free x_i's are modified, it will influence the subsequent outcome of the quenching process. This retroactive phenomenon, coupled with the out-of-equilibrium nature of the quenching process, is at the center of our study, with interesting stochastic dynamics. In the case of Ising spins of a complete network, this retro-action gives rise to martingale properties. We will develop this aspect and its consequences in Chapter 3.

1.2 Martingale theory

In this section, we aim to introduce a key element of the stochastic process theory: martingales. Martingales play a crucial role in many critical applications of probability such as statistics and mathematical finance and are fundamental properties of essential unbi-

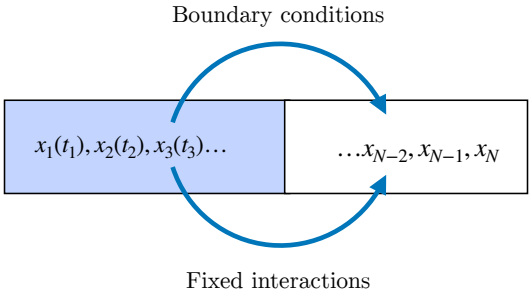

Figure 1.2: Mutual influences between the quenched and the unquenched part.

ased random walks, Brownian motion being a prime example [23]. Nevertheless, their applications in physics are relatively limited. However, they are now at the center of recent studies that explore their applications, extending the scope of fundamental relations such as the second law of thermodynamics, Jarzynski's equality, and many fluctuation relations [10, 24, 25, 26, 27, 28]. We will only focus on discrete-time martingales since it is the type that appears in our study. All results are adaptable to a continuous-time framework.

1.2.1 Discrete-time martingales in a nutshell

Martingales are, concisely, driftless integrable stochastic processes. Joseph Leo Doob introduced them to generalize random walks so that each new increment is "conditionally orthogonal" with respect to the past realizations [29]. Let us consider a stochastic process denoted by X_n, where $n \in \mathbb{N}$ is a discrete-time index. Formally, we will define martingales relative to the base process X_n. We say that M_n is a discrete time martingale relative to X_n if :

- M_n is a real-valued function defined on the set of trajectories $X_{[0,n]} = (X_0, X_1, \ldots, X_n)$;
- M_n is integrable, i.e., $\mathbb{E}[|M_n|] < \infty$ for all n;
- M_n has no drift, i.e., for all $0 \leq m \leq n$:

$$\mathbb{E}[M_n | X_{[0,m]}] = M_m, \tag{1.4}$$

.

Thus, the conditional expected value of any future observation, given all the past observations, is equal to the most recent observation. Formally, the set of all possible past observations up to time m constitutes a filtration $\mathcal{F}_m$.

When drift is introduced, that is $\mathbb{E}[M_n|X_{[0,m]}] \leq M_m$ or $\mathbb{E}[M_n|X_{[0,m]}] \geq M_m$, with the other properties still verified, we call those processes *super*-martingales and *sub*-martingales, respectively.

1.2.2 Example of discrete-time martingales

Let $(X_n)_{n\in\mathbb{N}^*}$ be a sequence of *iid*[1] random variables, with mean $m < \infty$, and let S_n be the sum-process, such that $S_0 = 0$ and

$$S_n = \sum_{i=1}^{n} X_i. \tag{1.5}$$

Then, the process $M_n = S_n - nm$ is a martingale. If $m = 0$, the sum process S_n is itself a martingale. Moreover, if $m > 0$, S_n is a *sub*-martingale, and inversely, if $m < 0$, S_n in a *super*-martingale.

Similarly, let $(X_n)_{n\in\mathbb{N}^*} > 0$ be a sequence of positive *iid* random variables with mean $m < \infty$. Let P_n be the product-process, such that $P_0 = 1$ and

$$P_n = \prod_{i=1}^{n} X_i. \tag{1.6}$$

Then, $M_n = P_n/m^n$ is a martingale.

Finally, for $(X_n)_{n\in\mathbb{N}^*}$ *iid* with zero mean and variance $\mathbb{E}[X_n^2] = \sigma^2$, and S_n the sum process defined by Eq.(1.5),

$$M_n = S_n^2 - n\sigma^2 \tag{1.7}$$

is a martingale.

1.2.3 Stopping times

There are many properties associated with martingales that are crucial to their applications. For the sake of concision, we will only focus on stopping times and Doob's optional stopping theorem since they will be of use in the perturbative analysis of our system (see Sec. 3.4).

A stopping time with respect to a sequence of random variables $X_1, X_2, \ldots$ is a random variable τ such that for every time t, the occurrence or non-occurrence of the event $\tau = t$ only depends on the values of the sequence up to time t: $X_1, X_2, X_3, \ldots, X_t$. The underlying idea behind this definition is that at any specific time t, one can examine the sequence up to that point and determine whether it is appropriate to halt. This determination of whether the event has occurred or whether the decision should be executed is solely contingent upon the information derived from the process until that precise moment. Mathematically speaking, τ is statistically independent of the future of the trajectory $(X_t)_{t>\tau}$.

An analogy in real-life could be the instance when a gambler departs from a gambling table; this decision might be contingent on their prior winnings (e.g., they might leave only when they have gone bankrupt), yet they cannot make their choice based on the outcomes of games that have not yet been played.

For example, a stochastic process's first-passage time (and more generally k-th passage times for any finite integer k) at a particular value or subset of its domain are stopping times. But, $\tau = \{n|X_n = \max(X_k)_{k>1}\}$, the time to reach the global maximum of a

[1]Independent and Identically Distributed, that is, they all follow the same probability law.

trajectory is not a stopping time since it requires a future knowledge, in this case, the certitude that the trajectory will not exceed a certain value.

A simple property is that, if $(M_n)_{n>1}$ is a martingale and τ is a stopping time, then the "stopped process" $(M_n^\tau)_{n>1}$ such that

$$M_n^\tau = M_{\min(n,\tau)} \tag{1.8}$$

is also a martingale, that is, for all $0 \leq m \leq n$:

$$\mathbb{E}[M_n^\tau | X_{[0,m]}] = M_m^\tau. \tag{1.9}$$

1.2.4 Optional Stopping

Now that we have set up the different tools we will use throughout the manuscript, we may write one of the key properties of martingales: Doob's optional stopping theorem.

Let M_n be a martingale and τ an almost-surely bounded stopping time (i.e. there exists a constant $c \in \mathbb{N}$ such that $\mathbb{P}(\tau \leq c) = 1$). Then:

$$\mathbb{E}[M_\tau] = \mathbb{E}[M_0] \tag{1.10}$$

This particular theorem can prove the impossibility of successful betting strategies for a gambler with a finite lifetime (or, in an equivalent way, a finite limit on bets), at least if the gambler cannot foresee the future. In other words, the gambler leaves with the same amount of money on average as when he started. As one can imagine, the optional stopping theorem is an essential tool of mathematical finance, for example, to price assets correctly and remove any possibility of making a profit without any risks. For a physicist, however, it may be used to derive new viewpoints of the second law of thermodynamics and fluctuation relations [30].

1.3 An introduction to Markov Chains

1.3.1 Introduction

In this section, we will introduce the main concepts and methods used in the study of Markov Chains that will be useful throughout this thesis, especially in Chapter 5. The content of this section is extracted from lecture notes I took during the "(Post)-Modern Thermodynamics" conference held in December 2022 in Luxembourg city, following Ken Sekimoto's lecture, followed by Pedro Harunari's. These lecture notes are available in ref [5].

It will be centered around Markov chains in continuous time. Our primary goal is to set up different tools, such as the transition network (TN), master equations, and modified networks (with applications to first-passage time problems). We will also connect the tools developed for continuous-time Markov chains to the discrete-time framework.

1.3.2 Continuous-time Markov Chains: basic notions

Notations and definitions

For basic notations, we will denote by $\{a, b, c, \dots\}$ or $\{a_1, a_2, \dots\}$ the discrete set of states, and $\hat{X}_t$ is the random variable representing the state X_t of the system at time t, where $t \in [0; +\infty)$. The time evolution of X is a stochastic process, and its history $\{X_t, t \in \mathbb{R}^+\}$ is also a random variable. The sample space Ω is the set of all possible histories. We will usually denote X_0 by a_0.

We recall the Markov property for such a stochastic process:

Definition 1 X_t is said to be a continuous-time **Markovian** process with respect to t if the conditional probability $p(\hat{X}_{t+dt} = b|\hat{X}_{[0,t]} = a)$ is independent of X_s for all $s < t$.

The statistics of $\hat{X}_{t+dt}$ only depends on the realization of $\hat{X}_t$. It is usually said that the system *forgets* the past after each time step of length dt.

Transition rates

For two different states $a \neq b$, the conditional probability $p(\hat{X}_{t+dt} = b|\hat{X}_t = a)$ is of the order $O(dt)$ for a Markovian process. We denote by $R_{ba} > 0$ the proportionality coefficient, such that:

$$p(\hat{X}_{t+dt} = b|\hat{X}_t = a) = R_{ba}dt + O(dt^2) \tag{1.11}$$

For several destinations $\{a_1, a_2, a_3\}$ we have in a similar way:

$$p(\hat{X}_{t+dt} = a_i|\hat{X}_t = a) = R_{a_i a}dt + O(dt^2) \tag{1.12}$$

A Markovian process is characterized by the set of states and the transition rates among

(a) A single transition

(b) Multiple transitions over several destinations

Figure 1.3: Possible transition configurations illustrating Eqs.(1.11) and (1.12)

them. Note that, to the linear order $O(dt)$, the transition rates do not interfere with each other.

On the time resolution of physical processes In physics, one may consider discrete problems derived from an underlying continuous process thanks to coarse-graining procedures. For example, consider a random walker traveling in Europe, as in Fig.1.4. We

only measure the country code with respect to time. Right after crossing a border, the walker has - for a short period - a significant probability of re-crossing the same border. Thus, if the temporal coarse-graining was not introduced, one might see multiple erratic transitions between two country codes before the walker finally moves far enough from the border.

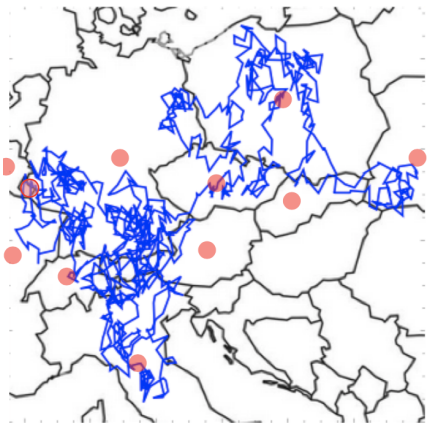

Figure 1.4: Continuous trajectory of a random traveler in Europe, with the different countries shown in red.

This discretization is typically non-Markovian. To obtain a Markovian trajectory in the new discrete-state continuous-time model, we need to weaken the time resolution of the trajectory, that is, introducing a time step Δt such that faster phenomena are integrated over. More precisely, transitions $a \to b$ such that $R_{ba} \gtrsim (\Delta t)^{-1}$ should not appear in the discrete-state model. Thermodynamically, this state coarse-graining is equivalent to adding a heat bath to mask details. Descriptions with different resolutions can thus have different thermodynamics.

Transition networks

We use a network -or graph- representation for each Markov chain, in which the nodes are the system states, and the directed edges represent the non-zero transition rates. For the following part, we consider ergodic transition networks i.e from any node, all the other nodes are reachable through directed edges. See Fig.1.6.

1.3.3 Simulating a trajectory: Gillespie's algorithm

Now that the basic notions of continuous-time Markov chains have been introduced, we may ask ourselves how to generate sample histories to verify the statistical properties. The main idea of such an algorithm is to generate a list of jumps at specific times, e.g., $X_t = a \to a_i$ with $i \in \{1, \dots, n\}$. A first but naive idea is to try a jump at every small time segment δt. This method may work but could be more practical, as it is inefficient and could be approximate if δt is too big.

A better -and exact - approach is the Gillespie algorithm. The idea is to generate a waiting time $\hat{T}$ between consecutive jumps. The probability of having $\hat{T} > \tau$ where $\tau > 0$

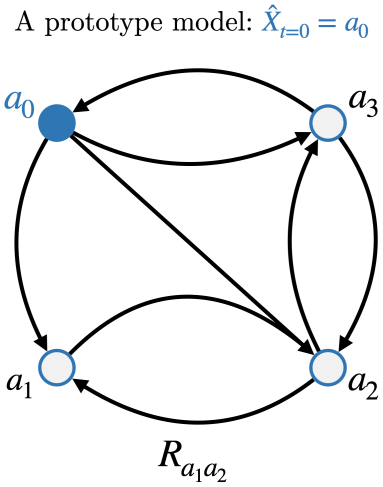

Figure 1.5: An example of ergodic transition network with four different states

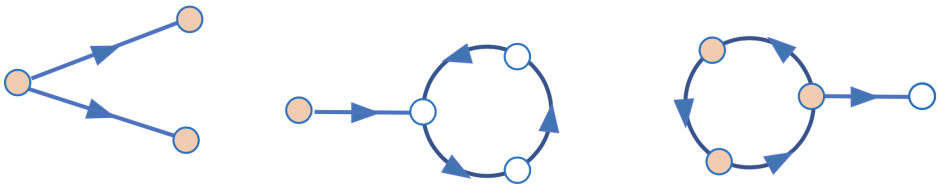

Figure 1.6: Three examples of non-ergodic transition networks. The nodes colored in red represent potentially unreachable states.

is:

$$p(\hat{T} > \tau) = \exp\left(-\sum_{i=1}^{n} R_{a_i a}\tau\right) \tag{1.13}$$

PROOF The event $\hat{T} > \tau$ is equivalent of having no transitions during time intervals $\left(\frac{\tau}{M}\right) k \leq t < \left(\frac{\tau}{M}\right)(k+1)$ for every $k \in \{0, 1, \ldots M-1\}$.

Thus, we have:

$$p(\hat{T} > \tau) = \left(1 - \sum_{i=1}^{n} R_{a_i a}\frac{\tau}{M}\right)^{M} \xrightarrow{M\to\infty} \exp\left(-\sum_{i=1}^{n} R_{a_i a}\tau\right)$$

We then generate such a waiting time $\hat{T}$ through a uniform random variable $\hat{Y}$. We have:

$$p(\hat{T} > \tau) = p(e^{-\sum_{i=1}^{n} R_{a_i a}\hat{T}} < e^{-\sum_{i=1}^{n} R_{a_i a}\tau}) \tag{1.14}$$

$$= e^{-\sum_{i=1}^{n} R_{a_i a}\tau}. \tag{1.15}$$

Introducing $\hat{Y} := e^{-\sum_{i=1}^{n} R_{a_i a}\hat{T}}$ and $y := e^{-\sum_{i=1}^{n} R_{a_i a}\tau}$, we have:

$$p(\hat{Y} < y) = y \Rightarrow \hat{Y} \text{ is a uniform random variable on } [0, 1] \tag{1.16}$$

After generating $\hat{Y}$ with a built-in function, we can find $\hat{T}$ such that $\hat{Y} = e^{-\sum_{i=1}^{n} R_{a_i a}\hat{T}}$.

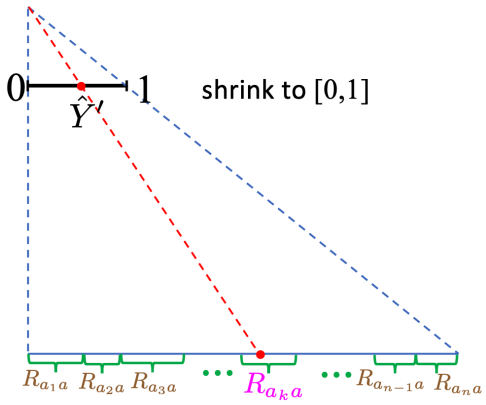

Figure 1.7: Choice protocol for the arrival state: the transition rates are "shrunk" to map the interval $[0, 1]$.

To determine the arrival state, we notice that, in Markovian processes, the destination is determined at the last infinitesimal interval dt. We thus have:

$$p(\text{destination is } a_k) = \frac{R_{a_k a}}{\sum_{i=1}^{n} R_{a_i a}} \tag{1.17}$$

and the state can be decided with another uniform random variable on $[0, 1]$, see Fig.1.7.
Remark: We can generalize this idea: given a 1D probability density $\rho(x)$, we can construct a random variable $\hat{X}$ that obeys $\rho(x)$. The cumulative probability up to $x \in \mathbb{R}$ is:

$$p(\hat{X} < x) = \int_{-\infty}^{x} \rho(x')dx'.$$

Since this is equivalent to $p(\int_{-\infty}^{\hat{X}} \rho(x')dx' < \int_{-\infty}^{x} \rho(x')dx') = \int_{-\infty}^{x} \rho(x')dx'$, we can define $\hat{Y} := \int_{-\infty}^{\hat{X}} \rho(x')dx'$, which is a uniform random variable on $[0, 1]$, and find $\hat{X}$ by this relation.

1.3.4 First-passage time problems

Consider a Markovian transition network like the one depicted in Fig.1.5. Given an initial condition $\hat{X}_{t=0} = a_0$ and the ergodic hypothesis, the probability of the process $\hat{X}_t$ never visiting a state a_i is zero. We can, therefore, define a time $\hat{T}_{FP}$ at which $\hat{X}_t$ visits a_i *for the first time*. The random variable $\hat{T}_{FP}$ is called the first-passage time (usually abridged FPT [31]) and is a special case of stopping time. We have in particular $p(\hat{T}_{FP} < +\infty) = 1$. Numerically, the sampling of T_{FP} can be done with a Gillespie algorithm. Moreover, we can obtain analytical results for its statistics, such as $p(\hat{T}_{FP} > \tau)$.

1.3.4.1 Master equation

Let us consider N ($\gg 1$) copies of the transition network, starting at $\hat{X}_{t=0} = a_0$. For $t > 0$, each copy evolves independently. At a time t we find $\simeq N p_t(a_i)$ copies in the state $\hat{X}_t = a_i$, with $0 \leq p_t(a_i) \leq 1$ and $\sum_{i=0}^{n} p_t(a_i) = 1$. Between t and $t + dt$, the *population*, i.e., the probability of finding the system in a certain state, changes by $N p_{t+dt}(a_i) - N p_t(a_i)$. In parallel, counting all the possible transitions coming to the state a_i from other states allow

us to write the population influx as $+\sum_{k(\neq i)}(R_{a_i a_k}dt)\,(Np_t(a_k))$. Likewise, the probability out-flux coming from the state a_i to all of the other states is: $-\sum_{k(\neq i)}(R_{a_k a_i}dt)\,(Np_t(a_i))$. Therefore, we have the following equality between time variation and flux:

$$Np_{t+dt}(a_i) - Np_t(a_i) = \sum_{k(\neq i)} (R_{a_i a_k}dt)\,(Np_t(a_k)) - \sum_{k(\neq i)} (R_{a_k a_i}dt)\,(Np_t(a_i)). \tag{1.18}$$

Dividing by Ndt and taking the $N \to \infty$ limit, we obtain the so-called master equation:

$$\frac{dp_t(a_i)}{dt} = \sum_{k(\neq i)} R_{a_i a_k}\, p_t(a_k) - \sum_{k(\neq i)} R_{a_k a_i}\, p_t(a_i). \tag{1.19}$$

We can define the net probability flow from a_i to a_k: $J_{a_k a_i} \coloneqq -R_{a_i a_k}\, p_t(a_k) + R_{a_k a_i}\, p_t(a_i)$ so that:

$$\frac{dp_t(a_i)}{dt} = -\sum_{k(\neq i)} J_{a_k a_i}. \tag{1.20}$$

The probability flow $J_{a_k a_i}$ can be seen as the difference of two *semi* -flows: the outgoing flow

$$\mathcal{J}_{a_k a_i} \coloneqq R_{a_k a_i}\, p_t(a_i) \tag{1.21}$$

and the in-coming flow

$$\mathcal{J}_{a_i a_k} \coloneqq R_{a_i a_k}\, p_t(a_k). \tag{1.22}$$

Thus

$$J_{a_k a_i} = \mathcal{J}_{a_k a_i} - \mathcal{J}_{a_i a_k}. \tag{1.23}$$

The semi-flows characterize the effect of each possible transition and are of particular importance when considering transition network modifications. For a pair of states a_i and a_k, we say that the $a_i \leftrightarrow a_k$ transition is reciprocal if $\mathcal{J}_{a_k a_i} = \mathcal{J}_{a_i a_k}$. In this case, there is no net flow between them.

We have now switched from an individual history framework to a flow of population framework. We can now obtain a solution to the set of master equations. We regroup the state probabilities in a column vector: $\vec{p_t} \coloneqq (p_t(a_0), \ldots, p_t(a_n))^\dagger$. We also introduce the diagonal elements, such that: $R_{a_i a_i} \coloneqq -\sum_{k(\neq i)} R_{a_k a_i}$. We can now write all of the master equations as a vector-matrix equation:

$$\frac{d\vec{p_t}}{dt} = \mathbf{R}\,\vec{p_t} \tag{1.24}$$

The matrix $\mathbf{R}$ is called the rate matrix, and its off-diagonal elements are the transition rates: $(\mathbf{R})_{ki} = R_{a_k a_i}$. A formal solution for every t is thus:

$$\vec{p_t} = e^{\mathbf{R}t}\,\vec{p}_0. \tag{1.25}$$

Remark: We recall the definition of the exponential of a matrix $\mathbf{M}$:

$$e^{\mathbf{M}} \coloneqq \sum_{n=0}^{\infty} \frac{\mathbf{M}^n}{n!} \tag{1.26}$$

We can write the propagator - that is the path integral from an initial state to a

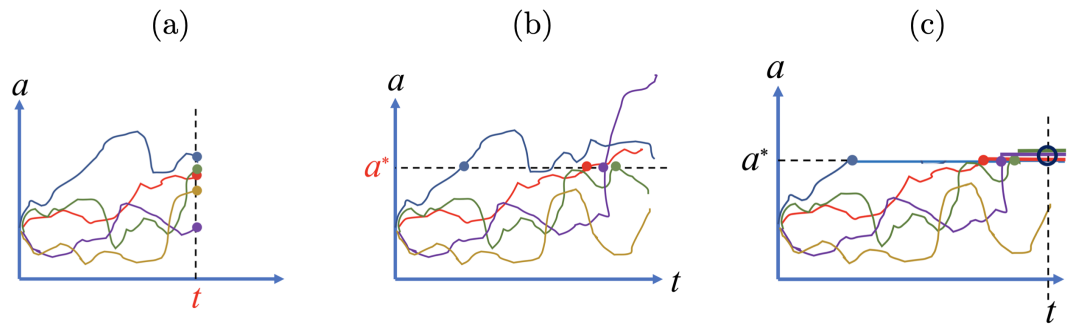

Figure 1.8: **(a)** Trajectories generated by the master equation $\frac{d\vec{p}_t}{dt} = \mathbf{R}\,\vec{p}_t$ representing a state variable a with respect to time t. **(b)** Illustration of the first-passage time of each trajectory at the state a^*. **(c)** The same trajectories on the modified network, with an absorbing state at a^*.

particular later state (in this case $p(\hat{X}_t = a_k|X_0 = a_i)$) - as:

$$p(\hat{X}_t = a_k|X_0 = a_i) = \left(e^{\mathbf{R}t}\right)_{a_k a_i} \tag{1.27}$$

1.3.4.2 First-Passage time from master equation

We can use the vector master equation to study the statistics of $\hat{T}_{FP}$ through the usage of *absorbing boundary conditions* (for more details, the reader may refer to Chapter XII of [6]). Figure 1.8 represents the procedure qualitatively. The master equation allows the generation of individual trajectories up to a time t. In a way, we know the intersection (and the subsequent statistics) of the trajectories $\{a(t)\}$ with a vertical line of coordinate t (Fig.1.8(a)). In this framework, the first-passage time problem is a reverse problem. We want to know the (first) intersection time of the trajectories with a horizontal line representing a particular state (a^* in Fig.1.8(b)). The main idea is to modify the transition network by introducing particular absorbing states, meaning that all outgoing transitions from them are removed. In the trajectory-space of Figure 1.8, that means that once a trajectory has reached the state of interest a^*, it becomes stationary (Fig.1.8(c)). We then solve the master equation (Eq.1.24) for the now-modified rate matrix. From this, we can deduce the statistics of interest, such as $p(\hat{T}_{FP} < t)$ or the mean first-passage time. Below, we detail this procedure applied to the network depicted in Fig.1.5.

Step-by-step example procedure of network modification of first-passage times
We consider the 4-states transition network depicted in Figs. 1.5 and 1.9 (a), with a (4×4) rate matrix $\mathbf{R}$. Our goal is to compute the statistics of the FPT reaching the state a_2 starting from a_0.

- We first remove the destination node (or nodes if we consider more than one state of arrival) of the FPT problem, in this case a_2, and replace it with an absorbing state, that is, a state from which no transitions are possible. This transformation of the transition network is depicted in Fig.(1.9)(b). We denote the modified rate matrix by $\mathbf{R}^*$, Eq.(1.29).

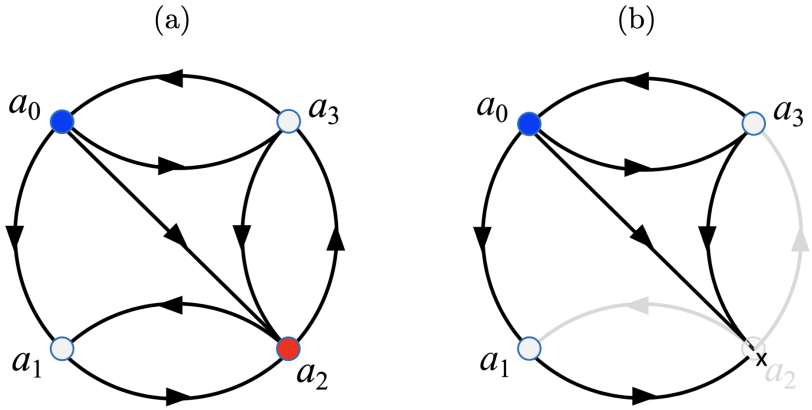

Figure 1.9: **(a)**: Example of a first-passage time problem at the state a_2 (in red) where a_0 (in blue) is the starting state. **(b)**: Modified transition network, where a_2 is now an absorbing state (cross), with outgoing transitions having been removed (light-gray lines).

- We now consider the **reduced** state space, where all the absorbing states have been removed. In our example, the reduced state space is (a_0, a_1, a_3), and the corresponding probability vector is $\vec{p_t^*} = (p_t^*(a_0), p_t^*(a_1), p_t^*(a_3))^\dagger$. The reduced master equation reads:

$$\frac{d\vec{p_t^*}}{dt} = \mathbf{R}^* \, \vec{p_t^*} \tag{1.28}$$

with

$$\mathbf{R}^* = \begin{pmatrix} -R_{a_1a_0} - R_{a_2a_0} - R_{a_3a_0} & 0 & R_{a_0a_3} \\ R_{a_1a_0} & -R_{a_2a_1} & 0 \\ R_{a_3a_0} & 0 & -R_{a_0a_3} - R_{a_2a_3} \end{pmatrix}. \tag{1.29}$$

- From Eq.(1.28), we obtain the solution, given the initial condition $\vec{p_0^*}$: $\vec{p_t^*} = \exp(\mathbf{R}^* t)\, \vec{p_0^*}$

- We can now compute the cumulative probability of the first passage as an integral of the probability semi-flow towards the absorbing state over time:

$$p(\hat{T}_{FP} < t) = \int_0^t [\mathcal{J}^*_{a_2a_0} + \mathcal{J}^*_{a_2a_1} + \mathcal{J}^*_{a_2a_3}]ds \tag{1.30}$$

$$= \int_0^t [R_{a_2a_0} p_s^*(a_0) + R_{a_2a_1} p_s^*(a_1) + R_{a_2a_3} p_s^*(a_3)]ds \tag{1.31}$$

$$. \tag{1.32}$$

Moreover, we have for the complementary event:

$$p(\hat{T}_{FP} < t) = 1 - p(\hat{T}_{FP} \geq t) \tag{1.33}$$

$$= 1 - (p_t^*(a_0) + p_t^*(a_1) + p_t^*(a_3)) = 1 - \langle 1^* | p_t^* \rangle \tag{1.34}$$

with $\langle 1^* | = (1, 1, \ldots 1)$ the unit row vector over the reduced state space and $\langle . | . \rangle$ denotes the Euclidean scalar product. We may note that those equations have a

"Gauss divergence theorem" -like structure, relating a probability flux to probability values.

- The FPT probability density $\rho_{FP}(t)$ is then obtained from Eqs.(1.28) and (1.33):

$$\rho_{FP}(t) = \frac{d}{dt}p(\hat{T}_{FP} < t) = -\langle 1^*|\mathbf{R}^*|p_t^*\rangle. \tag{1.35}$$

From Eq.(1.35), we can compute the quantities of interest - for example, the mean first-passage time, starting from a_0. With $|p_0^*\rangle = (1,0,0)^\dagger$, we get:

$$\begin{aligned}
\langle \hat{T}_{FP}|\hat{X}_0 = a_0\rangle &= \int_0^\infty t\rho_{FP}(t)dt \\
&= \int_0^\infty t\frac{d}{dt}p(\hat{T}_{FP} < t)dt = \int_0^\infty t\frac{d}{dt}\left[p(\hat{T}_{FP} < t) - 1\right]dt \\
&= \Big[t(p(\hat{T}_{FP} < t) - 1)\Big]_0^{+\infty} - \int_0^\infty (p(\hat{T}_{FP} < t) - 1)dt \\
&= 0 + \int_0^\infty \langle 1^*|p_t^*\rangle dt \\
&= \int_0^\infty \langle 1^*|\exp(\mathbf{R}^*t)|p_0^*\rangle dt = -\langle 1^*|\mathbf{R}^{*-1}|p_0^*\rangle
\end{aligned} \tag{1.36}$$

where $\mathbf{R}^{*-1}$ denotes the inverse of the modified rate matrix, knowing that $\lim_{t\to+\infty}\exp(\mathbf{R}^*t)|p_0^*\rangle = |0^*\rangle$. Note that the original matrix $\mathbf{R}$ is not invertible since 0 is an eigenvalue. Note also that $\langle 1^*|\mathbf{R}^* \neq 0$.

Remark 1 We can derive this last result with a different approach attributed to Kramers [32]. We consider the reduced master equation, Eq.(1.28), complemented by a source term J on the initial state $\vec{p_0^*}$. The equation reads:

$$\frac{d\vec{p_t^*}}{dt} = \mathbf{R}^*\,\vec{p_t^*} + J\vec{p_0^*}. \tag{1.37}$$

The steady-state, denoted $\vec{p_\infty^*}$, is:

$$\vec{p_\infty^*} = -J\mathbf{R}^{*-1}\vec{p_0^*} \tag{1.38}$$

By multiplying $\frac{1}{J}\langle 1^*|$ from the left,

$$\frac{1}{J}\langle 1^*|p_\infty^*\rangle = -\langle 1^*|\mathbf{R}^{*-1}|p_0^*\rangle = \langle \hat{T}_{FP}|\hat{X}_0 = a_0\rangle \tag{1.39}$$

Reminder **: Linear algebra of master equation** We recall the spectral decomposition of a diagonalizable matrix $\mathbf{R}$: $\mathbf{R} = \mathbf{Q}\mathbf{\Lambda}\mathbf{Q}^{-1}$ where $\mathbf{\Lambda} = \mathrm{diag}(\lambda_1, \lambda_2, \ldots, \lambda_n)$ is the diagonal matrix of eigenvalues, and $\mathbf{Q}$ is the eigenbasis representation matrix.

We have $\mathbf{RQ} = \mathbf{Q\Lambda}$, and the columns of $\mathbf{Q}$ denoted by $|v_\mu\rangle$ are the *right*-eigenvectors of $\mathbf{R}$. Similarly, we have $\mathbf{Q}^{-1}\mathbf{R} = \mathbf{\Lambda}\mathbf{Q}^{-1}$, so the rows of $\mathbf{Q}^{-1}$, denoted by $\langle u_\nu|$ are the *left*-eigenvectors of $\mathbf{R}$. We have: $\mathbf{Q}^{-1}\mathbf{Q} = I \Leftrightarrow \langle u_\nu|v_\mu\rangle = \delta_{\nu\mu}$ (orthonormality of the dual bases) and $\mathbf{QQ}^{-1} = \sum_\mu |v_\mu\rangle\langle u_\mu| = I$ (completeness). The latter follows from the former.

Figure 1.10: Columns and rows of the matrices $\mathbf{Q}$ and $\mathbf{Q}^{-1}$.

Since

$$\begin{aligned}\exp(\mathbf{R}t) &= \exp(\mathbf{Q}\mathbf{\Lambda}\mathbf{Q}^{-1}t) \\ &= \sum_{n=0}^{+\infty} \frac{(\mathbf{Q}\mathbf{\Lambda}\mathbf{Q}^{-1})^n t^n}{n!} \\ &= \mathbf{Q}\left(\sum_{n=0}^{+\infty} \frac{\mathbf{\Lambda}^n t^n}{n!}\right)\mathbf{Q}^{-1} = \mathbf{Q}\exp(\mathbf{\Lambda}t)\mathbf{Q}^{-1},\end{aligned} \tag{1.40}$$

we have

$$\exp(\mathbf{R}t) = \sum_{\mu} |v_\mu\rangle e^{\lambda_\mu t}\langle u_\mu|. \tag{1.41}$$

Remark 2 Numerically the exponential $e^{\mathbf{R}^* t}$ is computed using spectral decomposition, $\mathbf{R}^* = \sum_\mu |v_\mu^*\rangle\lambda_\mu\langle u_\mu^*|$, that is, $e^{\mathbf{R}^* t} = \sum_\mu |v_\mu^*\rangle e^{\lambda_\mu t}\langle u_\mu^*|$. Once $e^{\mathbf{R}^* t}$ is obtained, $\vec{p_t^*}$ is given by the matrix-vector product, $\vec{p_t^*} = e^{\mathbf{R}^* t}\vec{p_0^*}$

- The matrix $\mathbf{R}$ or $\mathbf{R}^*$ can have complex eigenvalues. Nevertheless, when $\mathbf{R}$ or $e^{\mathbf{R}t}$ are applied to a "physically meaningful" $\vec{p^*}$ are real matrices.
- All eigenvalues of $\mathbf{R}^*$ must have strictly negative real part. While this can be shown using the Perron-Frobenius theorem, it is intuitively understandable by the fact $p_t^* = e^{R^* t}p_0^*$ vanishes for$t \to \infty$ because all the probability eventually goes to the absorbing states.
- The (non-reduced) rate matrix $\mathbf{R}$ must have at least one null eigenvalue: the steady-state distribution, $|\nu_0\rangle$ satisfies $\mathbf{R}|\nu_0\rangle = 0$. The corresponding left null eigenvector $\langle\nu_0|$ has all components 1, a consequence of the conservation of the total probability: for all $|p_t\rangle$, we have $d/dt\langle\nu_0|p_t\rangle = \nu_0|\mathbf{R}|p_t\rangle = 0$. For further spectral properties of the rate matrix, the reader may refer to Perron-Frobenius theorems and their consequences [33].

1.3.5 Discrete-time Markov Chains

Consider the previously studied transition network; see Fig.1.11. The large dots represent the different states of the systems, and the arrows represent possible transitions between them. In discrete time, the network has a similar shape. However, the steps iteration creates the possibility of periods when the system remains in the same state[2]. Those

[2]Some transitions may happen at a finer resolution, but are not visible at the present level of description (see Section 1.3.2).

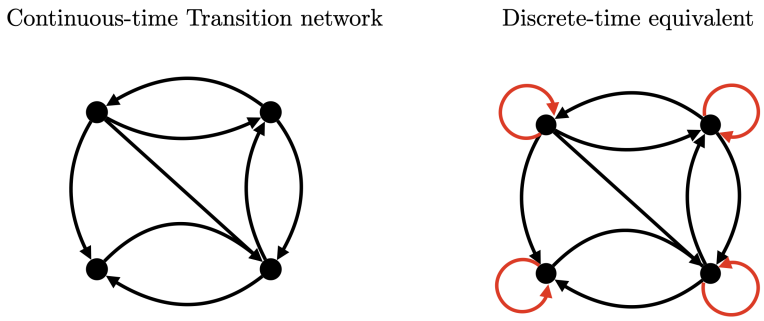

Figure 1.11: Discretization of time on the transition network. Stationary transitions are shown in red.

transitions are added to the graph, symbolized by the circular arrows. We now consider time as a discrete variable: $t = n\Delta t$ with $n \in \mathbb{N}$ and Δt is the unitary step duration. We define the stochastic [3] matrix $\mathbf{P}$ by

$$\mathbf{P} \coloneqq \mathbf{I} + \Delta t \mathbf{R}\,, \tag{1.42}$$

where $\mathbf{R}$ is the rate matrix for the continuous-time master equation. $\mathbf{P}$ defines how the population probability is dynamically flowing in the network. The off-diagonal elements are given by:

$$(P)_{\substack{ab \\ a\neq b}} = \Delta t (R)_{ab} = p(\hat{X}_{n+1} = a | \hat{X}_n = b) \tag{1.43}$$

for a and b two states of the system. Since $(R)_{ab}$ is the probability per unit of time that the system jumps from b to a, $(P)_{ab}$ is the probability of jumping to state a at time $(n+1)\Delta t$ given that state are in b at time $n\Delta t$. Here, $\hat{X}_n$ represents the random variable associated with the state occupied at time n, and p is the probability measure.

The diagonal elements are:

$$(P)_{aa} = 1 + \Delta t (R)_{aa} = 1 - \Delta t \sum_{b(\neq a)} (R)_{ba} \tag{1.44}$$

The diagonal element $(R)_{aa}$ is, according to the continuous-time framework, the negative sum of all transition rates from state a (this result comes from the conservation of the probability norm during processes). P_{aa} is thus the probability of not jumping at all:

$$(P)_{aa} = p(\hat{X}_{n+1} = a | \hat{X}_n = a) \tag{1.45}$$

Note that those transitions do not appear explicitly in the continuous-time framework.

The evolution equation of the probability vector $\vec{p}$ over the state space is:

$$\vec{p}_{n+1} = \mathbf{P}\vec{p}_n \tag{1.46}$$

[3] also referred as the transfer matrix

which gives element-wise:

$$p_{n+1}(b) = \sum_a (P)_{ba} p_n(a) \tag{1.47}$$

$$= \sum_a p(\hat{X}_{n+1} = b | \hat{X}_n = a) p_n(a) \tag{1.48}$$

$$= \sum_{a(\neq b)} (P)_{ba} p_n(a) + (P)_{bb} p_n(b). \tag{1.49}$$

From Eqs.(1.43) and (1.44), we obtain:

$$p_{n+1}(b) = \sum_{a(\neq b)} \Delta t (R)_{ba} p_n(a) + [1 + \Delta t (R)_{bb}] \, p_n(b) \tag{1.50}$$

or, equivalently:

$$\frac{p_{n+1}(b) - p_n(b)}{\Delta t} = \sum_{a(\neq b)} (R)_{ba} p_n(a) - \sum_{a(\neq b)} (R)_{ab} p_n(b). \tag{1.51}$$

Taking the limit $\Delta t \to 0^+$ in Eq.(1.51) with $n = t$ allow us to verify the continuous-time master equation $\mathrm{d}\vec{p}/\mathrm{d}t = \mathbf{R}\vec{p}$. For this reason, everything said in the discrete-time framework holds in the continuous-time limit, given that we take a small enough time step Δt. This equivalence is sometimes used in the other direction, switching from continuous to discrete time to prevent dealing with exponentially distributed time intervals. This description shift can make proofs easier, with the results holding in both cases as there is a time limit away.

Now, we discuss the solution to the evolution equation. In order to write a propagator for the evolution equation, we apply Eq.(1.46) n times:

$$\begin{aligned} \vec{p}_n &= \mathbf{P}^n \vec{p}_0 \\ &= (\mathbf{I} + \Delta t \mathbf{R})^n \vec{p}_0. \end{aligned} \tag{1.52}$$

$\mathbf{P}^n$ is, therefore, the propagator. If we let $\Delta t \to 0^+$ with $n\Delta t$ fixed, we again recover the exponential propagator of the continuous-time formulation:

$$\vec{p}_n = (\mathbf{I} + \Delta t \mathbf{R})^{t/\Delta t} \vec{p}_0 \xrightarrow[\Delta t \to 0^+]{} e^{\mathbf{R}t} \vec{p}_0. \tag{1.53}$$

In the following table, we sum up the differences between the continuous and discrete formulations.

Element	Continuous framework	Discrete framework
Stochastic Matrix	Rate Matrix $\mathbf{R}$	Transition probability matrix $\mathbf{P}$
Dynamics	Master Equation $\frac{\mathrm{d}\vec{p}}{\mathrm{d}t} = \mathbf{R}\vec{p}$	Evolution Equation $\vec{p}_{n+1} = \mathbf{P}\vec{p}_n$
$p(\hat{X}_{t+\Delta t} = b \vert \hat{X}_t = a)$	$(R)_{ba}\Delta t$	$(P)_{ba}$
Diagonal elements	$(R)_{aa} = -\sum_{b(\neq a)}(R)_{ba} \leq 0$	$0 \leq (P)_{aa} \leq 1$
Propagator	$(e^{\mathbf{R}t})_{ba}$	$(\mathbf{P}^n)_{ba}$
Conservation of probability	$\sum_b (R)_{ba} = 0$	$\sum_b (P)_{ba} = 1$

Note that the elements of $\mathbf{R}$ have the dimension of the inverse of time, whereas the elements of $\mathbf{P}$ are dimensionless. It is also worth mentioning that discrete-time processes are simpler to simulate in a computer program as we do not have to draw random time steps with a Gillespie algorithm (as described in Section 1.3.3). In the discrete case, Δt is fixed, and the operator only has to draw the probabilities $(P)_{ba}$ from a uniform distribution between 0 and 1.

Chapter 2

Globally coupled models

2.1 Introduction

Following the main ideas of Progressive Quenching (this will be denoted by **PQ** along the whole manuscript) introduced in Section 1.1 of the Introduction, we can highlight the feedback mechanisms between the fixed and free parts of a system using a simple toy-model: the Curie-Weiss model. This relatively simple process has been at the very heart of our work for the past three years, resulting in multiple publications [1, 22, 2, 3, 4]. In the present chapter, we will explain how the PQ protocol is defined for globally-coupled spins and the relevant parameters to keep track of the evolution of both parts of the system. We will also highlight the computation techniques of thermodynamic quantities and the subsequent simulations, which are the starting point of our analysis. Those concepts were originally introduced in [1].

2.2 System setup

2.2.1 Globally coupled Ising Spins

After introducing progressive quenching and its different parameters, we choose a simple system to apply its principles. Ising spins are perfect toy models in this context, as they constitute simple interacting degrees of freedom with a rich phenomenology of physical properties that arise in large systems. We chose to study the simplest topology of Ising spin systems: the globally coupled one. Below, we introduce this model and develop the main results used throughout this manuscript.

The Ising model, developed by Lenz and his student Ising during the 1920s, is a typical statistical mechanics model of ferromagnets and has since been the subject of many development and studies - to the point of being a fundamental aspect of the study of phase transitions and more generally in statistical mechanics. While Ising quit academia after his conclusions on the 1D model that showed no global magnetization at finite temperature - and his thinking that the model was useless - others pursued higher-dimensional analysis yielding fundamental results about phase transitions and their universality. An Ising spin s in an discrete variable that can only take two values: $+1$ or -1. It is a very simple approximation of the atomic magnetic dipoles that, when aligned in a material, create a

macroscopic magnetic field. This alignment is mainly caused by a purely quantum effect: the exchange interaction.

Named after Pierre Curie and Pierre-Ernest Weiss, the Curie-Weiss Model (or infinite-range model) is used to describe the behavior of magnetic materials. While it is a relatively simple model that can be solved exactly, its power lies in the insights it provides about phase transitions and its coincidence with the mean-field approximation of the Ising model.

Let us consider a ferromagnetic model consisting of N_0 Ising spins, denoted by $\{s_i\}_{i\in\{1,\dots,N_0\}}$, on a complete network. All spins thus interact with every over spin, with a fixed coupling constant. While we could set a specific coupling $j_{ij} = j_{ji}$ for every pair of spins (s_i, s_j), with $i \neq j$, we first chose to set it equal along the network:

$$\forall (i,j) \text{ such that } i \neq j \qquad j_{ij} = j_0. \tag{2.1}$$

Under an external magnetic field h, the ferromagnetic Hamiltonian $\mathcal{H}$ of the system is:

$$\begin{aligned}\mathcal{H} &= -\frac{j_0}{N_0} \sum_{1\leq i<j\leq N_0} s_i s_j - h\sum_{i=1}^{N_0} s_i &(2.2)\\ &= -\frac{j_0}{2N_0}\left(\sum_{i=1}^{N_0} s_i\right)\left(\sum_{j\neq i}^{N_0} s_j\right) - h\sum_{i=1}^{N_0} s_i \\ &= -\frac{j_0}{2N_0}\left(\sum_{i=1}^{N_0} s_i\right)^2 - h\sum_{i=1}^{N_0} s_i + C &(2.3)\end{aligned}$$

where we choose the normalization convention by N_0, and $C = j_0/2$ is a constant term that can be ignored[1]. This system is in contact with a thermal bath that sets the inverse temperature $\beta = \frac{1}{k_B T}$. The statistical properties are thus given by the canonical partition function Z [34, 35] :

$$Z = \sum_{\{s_1,\dots,s_{N_0}\}} e^{-\beta\mathcal{H}} \tag{2.4}$$

Since the values of β, j_0, and h are fixed, we can set $\beta = 1$ without loss of generality. Hereafter, we will write βj_0 and βh as j_0 and h, respectively. An important quantity for later is the mean magnetization of the system, denoted by $m^{(\mathrm{eq})}$:

$$m^{(\mathrm{eq})} = \langle s_i \rangle^{(\mathrm{eq})} \equiv \frac{1}{N_0}\frac{\partial \ln Z}{\partial h}, \tag{2.5}$$

where $\langle \dots \rangle^{(\mathrm{eq})}$ denotes the average over the canonical ensemble.

2.2.2 Quenching protocol and notations

Let us set the external magnetic field h to 0 and consider the system at equilibrium. Under those assumptions, the symmetry of the problem imposes that every spin - taken individually - has a 1/2 probability of being either in a $+1$ or -1 state:

$$\forall i, \mathbb{P}[s_i = +1] = \mathbb{P}[s_i = -1] = 1/2. \tag{2.6}$$

[1]Since the energy is always defined to within a constant, this term will not change the statistics

Now, let us define a PQ protocol. We will fix the spins in the order in which they are numbered since they are all statistically equivalent - and let the system re-equilibrate itself after each quench. This procedure is equivalent to setting the "inter-quenching time" to $+\infty$ and allows us not to consider relaxation dynamics for now. This aspect will be studied later in Chapter 4. Under this assumption, the "time" parameter that describes the advancement of the process is the number of quenched spins, denoted by T.

The first spin s_1, following Eq.(2.6), has a 1/2 probability to be fixed at ± 1. This breaks the system's symmetry, as s_1 now acts as a small external magnet that polarizes the system to a $+1$ or -1 state, depending on the result of the first quench. For a ferromagnetic system (*i.e* $j_0 > 0$), the next spin s_2 has a higher probability to be in the same state as s_1. Remarking that the remaining $N_0 - 1$ spins are still statistically equivalent because of the connected graph, we want the s_2 quench probability to reflect how polarized the free part is. We can thus write :

$$\mathbb{E}[s_2|s_1] = \langle s_i \rangle^{(\mathrm{eq})}_{T=1} \qquad \forall i \in \{2, \dots, N_0\}. \tag{2.7}$$

Note that the left-hand-side (l.h.s) expectation in Equation (2.7) corresponds to the quenching probability measure, which is entirely different from the canonical one of the right-hand-side (r.h.s). More explicitly, the object s_2 of the l.h.s is among the quenched part of the system, whereas on the r.h.s, it is among the free part.

Now that we understand how the quenching process works initially let us consider that T spins have already been quenched. The number of remaining free spins is denoted by $N = N_0 - T$, and the quenched magnetization is $M_T = \sum_{i=1}^{T} s_i$. The Hamiltonian given by Eq.(2.3) now reads:

$$\mathcal{H}_{T,M_T} = -\frac{j_0}{2N_0}\left(M_T + \sum_{i=T+1}^{N_0} s_i\right)^2 \tag{2.8}$$

$$= -\frac{j_0}{N_0} \sum_{T+1 \le i < j \le N_0} s_i s_j - h_T \sum_{i=T+1}^{N_0} s_i \quad + C_T, \tag{2.9}$$

where $h_T \equiv (j_0/N_0)M_T$ is the quenched molecular field, and C_T is an additive constant which depends of M_T. From Eq.(2.8), we can notice that the influence of the quenched part on the free part depends only on M_T and not individual spin values. Moreover, with the parallel between Eqs. (2.2) and (2.9), this influence is equivalent to the effect of an external magnetic field of intensity h_T that may polarize the system.

The mean magnetization of the unquenched part, denoted by ${m^{(\mathrm{eq})}}_{T,M_T}$, is given by :

$${m^{(\mathrm{eq})}}_{T,M_T} = \langle s_i \rangle^{(\mathrm{eq})}_{i \in \{T+1,\dots,N_0\}} = \frac{1}{N}\frac{\partial \ln Z_{T,M_T}}{\partial h} \tag{2.10}$$

with the partition function Z_{T,M_T} being:

$$Z_{T,M_T} = \sum_{\{s_{T+1},\dots,s_{N_0}\}} e^{-\beta \mathcal{H}_{T,M_T}}. \tag{2.11}$$

Note that ${m^{(\mathrm{eq})}}_{T,M_T}$ is function of both T and M_T. Moreover, during the PQ process, the effective size of the system N is decreasing, whereas T is increasing. Following the rea-

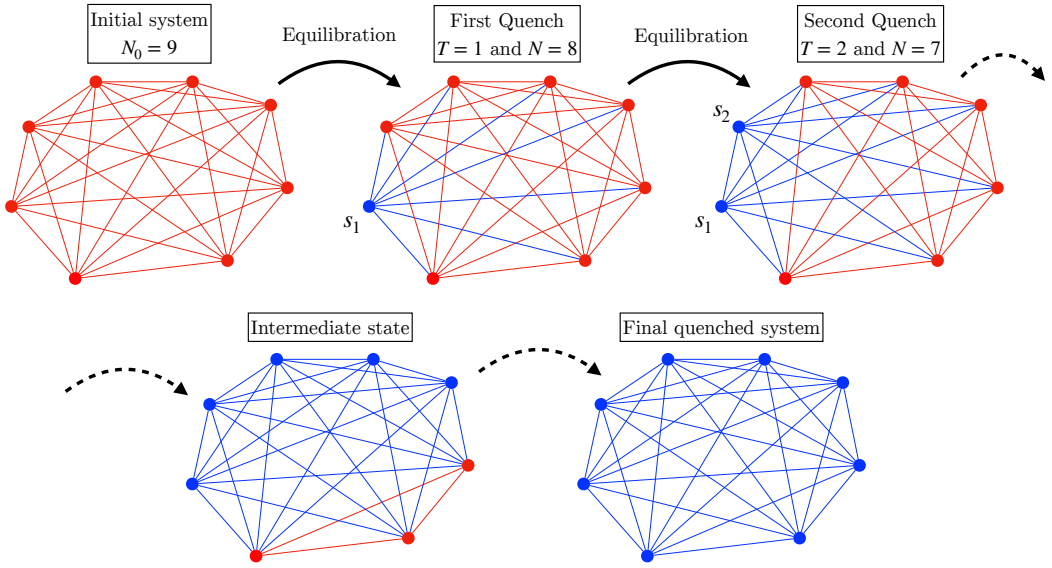

Figure 2.1: Schematic summary of the PQ process defined on the Curie-Weiss model, drawn for $N_0 = 9$ spins. The red dots and connections correspond to the free spins and their interactions, whereas the blue ones correspond to their quenched equivalents.

soning of Eq.(2.7), the next quenched spin, s_{T+1}, will take the ± 1 value with expectation:

$$\mathbb{E}[s_{T+1}|s_1, s_2, \ldots, s_T] = \langle s_i \rangle_T^{(\mathrm{eq})} \qquad \forall i \in \{T+1, \ldots, N_0\} \tag{2.12}$$

$$= m^{(\mathrm{eq})}{}_{T,M_T} \tag{2.13}$$

and from the normalization condition we get:

$$\mathbb{P}[s_{T+1} = \pm 1|s_1, s_2, \ldots, s_T] = \frac{1 \pm m^{(\mathrm{eq})}{}_{T,M_T}}{2}. \tag{2.14}$$

We can now repeat this process until all the N_0 spins are quenched and the whole system is fixed. Figure 2.1 summarizes the process graphically.

2.2.3 An integral formulation of the magnetization

For numerical computations and simulations, we may want to have a different formulation of $m^{(\mathrm{eq})}{}_{T,M_T}$ from Eq.(2.10), which is demanding in CPU time. Let us first re-write the Hamiltonian, starting from Eq.2.8. We will denote the unquenched magnetization by $\mu = \sum_{i=T+1}^{N_0} s_i$

$$\mathcal{H}_{T,M_T} = -\frac{j_0}{2N_0}\left(M_T + \sum_{i=T+1}^{N_0} s_i\right)^2$$

$$= -\frac{j_0}{2N_0}\left(M_T^2 + \mu^2 + 2\mu M_T\right) \tag{2.15}$$

$$= -a\mu - b\mu^2 - bM_T \tag{2.16}$$

with $a \equiv \frac{j_0 M_T}{N_0}$ and $b \equiv \frac{j_0}{2N_0}$. From the Gaussian integral

$$\int_{-\infty}^{+\infty} \exp\left(-by^2 + 2b\mu y\right) dy = \sqrt{\frac{\pi}{b}} e^{b\mu^2}, \tag{2.17}$$

we get the integral formulation for the exponential of the Hamiltonian :

$$\exp(-\mathcal{H}_{T,M_T}) = \exp\left(a\mu + b\mu^2 + bM_T\right) \tag{2.18}$$

$$= e^{bM_T^2} \sqrt{\frac{b}{\pi}} \int_{-\infty}^{+\infty} e^{-by^2} e^{(a+2by)\mu} \mathrm{d}y. \tag{2.19}$$

We can now compute the partition function from Eq.(2.11):

$$\begin{aligned} Z_{T,M_T} &= \sum_{\{s_{T+1},\ldots,s_{N_0}\}} e^{-\beta \mathcal{H}_{T,M_T}} \\ &= e^{bM_T^2} \sqrt{\frac{b}{\pi}} \int_{-\infty}^{+\infty} e^{-by^2} \sum_{\{s_{T+1},\ldots,s_{N_0}\}} e^{(a+2by)\mu} \mathrm{d}y, \end{aligned} \tag{2.20}$$

where the sum of exponentials yields:

$$\sum_{\{s_{T+1},\ldots,s_{N_0}\}} e^{(a+2by)\mu} = 2^N \cosh^N(a + 2by). \tag{2.21}$$

We finally get the Hubbard-Stratonovitch transformation [36, 37] of the partition function:

$$Z_{T,M_T} = \sqrt{\frac{b}{\pi}} \int_{-\infty}^{+\infty} \exp\left[bM_T^2 - by^2 + N \log[2\cosh(a + 2by)]\right] \mathrm{d}y. \tag{2.22}$$

Moreover, we get from Eqs. (2.11) and (2.16):

$$Z_{T,M_T} = \sum_{\{s_{T+1},\ldots,s_{N_0}\}} e^{bM_T^2 + a\mu + b\mu^2}, \tag{2.23}$$

that allows for an alternative derivative definition of ${m^{(\mathrm{eq})}}_{T,M_T}$:

$$\mathbb{E}[\mu] = \frac{\partial}{\partial a} \log Z_{T,M_T} = N {m^{(\mathrm{eq})}}_{T,M_T} \tag{2.24}$$

$$\Leftrightarrow {m^{(\mathrm{eq})}}_{T,M_T} = \frac{1}{N} \frac{\partial}{\partial a} \log Z_{T,M_T} \tag{2.25}$$

The numerical values of $m^{(\mathrm{eq})}$ used to simulate PQ processes for the following analyses were computed with both symbolic and numerical libraries (SymPy and Numpy in Python3 or using built-in Mathematica functions) from Eqs. (2.23) and (2.25). We avoided the usage of the saddle-point evaluation since such approximation brought non-negligible differences in the system-size dependence.

2.3 Trajectories and biased random walks

At the end of a PQ process, we obtain a series of quenched spin values $\{s_1, \ldots, s_{N_0}\}$ that can be seen as a random walk. We can indeed follow the evolution of the quenched magnetization M_T with respect to T, respectively, as a "position" and a "time". This discrete random walk is Markovian, as the next position probability distribution only depends on the present one. Thus, we may view its evolution it in a triangular network, parametrized by T and M_T, with each node corresponding to a value of $m^{(\mathrm{eq})}{}_{T,M_T}$. (see Fig.2.2 for an illustration).

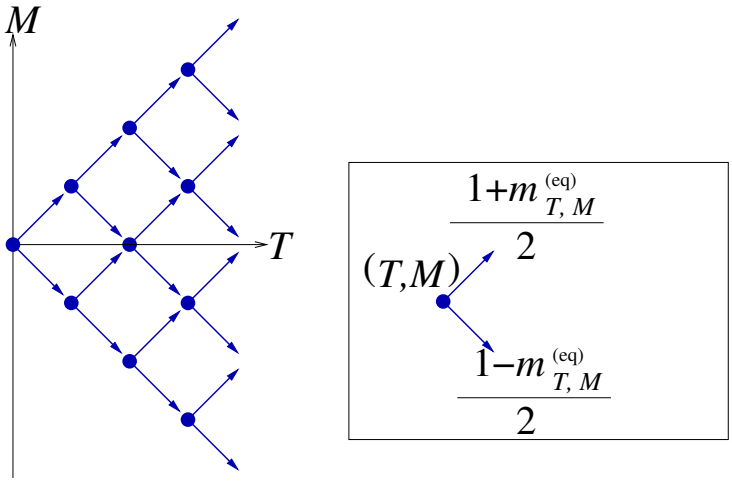

Figure 2.2: Markovian biased random walk corresponding to the present model of progressive quenching. From each node (blue (thick) dot) in the transition network, (T, M), the possible branched transitions, $M \to M \pm 1$, occur with the probabilities, $(1 \pm m^{(\mathrm{eq})}{}_{T,M})/2$, which corresponds, respectively, to fixing s_{T+1} at ± 1.

The stochastic evolution is given by:

$$M_{T+1} = M_T + s_{T+1}. \tag{2.26}$$

trajectories (i.e realizations of $\{M_T\}_{T\in\{1,2,\ldots,N_0\}}$ with respect to T) are plotted for different values of j_0 in figures 2.3a and 2.3b. Those two pictures showcase how j_0 controls how polarized the trajectories are. We may understand the typical behaviors with two-limit cases.

Simulations techniques We can simulate PQ individual trajectories, either by sampling spin configurations with a local Metropolis-Hastings algorithm [38], or for larger systems, a cluster Metropolis procedure [39, 40], or either with an exact enumeration, by computing all possible values of $m^{(\mathrm{eq})}$ at each node of the triangular network (see Fig.2.2) using Eq.2.25. The implementation of the PQ process in the first case is relatively straightforward. Once we reach an equilibrium configuration, the quench spin is removed from the "spin-flip" routine implemented in the Metropolis algorithm to freeze it effectively. However, the CPU time needed to reach a statistically relevant probability distribution for large systems was very high, so the second option was preferred.

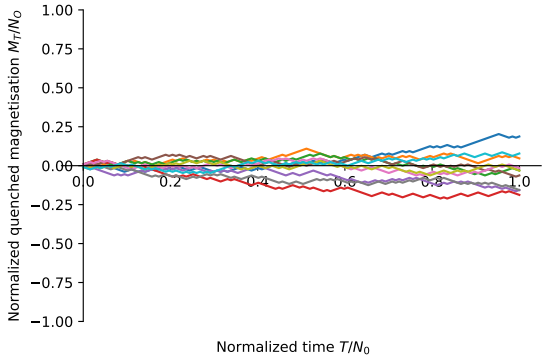

(a) Sample PQ trajectories in the normalized triangular network $(T/N_0, M_T/N_0)$, with a "small" ($j_0 = 0.05$) coupling.

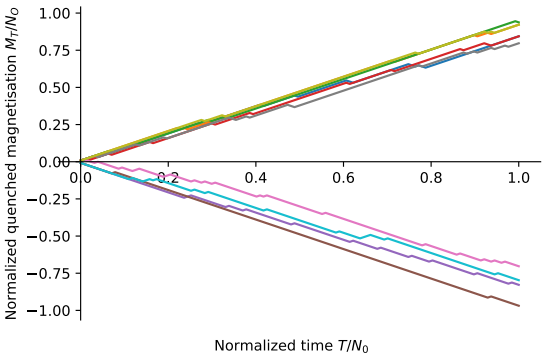

(b) Sample PQ trajectories in the normalized triangular network $(T/N_0, M_T/N_0)$, with a "high" ($j_0 = 1.5$) coupling.

Figure 2.3: Trajectories (evolution of M_T) in the two limit cases plotted for $N_0 = 2^8 = 256$

2.3.1 No-coupling limit

If we set the coupling constant j_0 to 0, all spins are decoupled and independent. Then, at equilibrium, all spin configurations are equiprobable regardless of the quenched part and $\forall T \in \{1, \dots \mathbb{N}_0\}, \forall M_T$ with $-T \leq M_T \leq +T$, we have $m^{(\mathrm{eq})}{}_{T,M_T} = 0$. This corresponds to an unbiased random walk with a binomial distribution. More precisely, the probability of having a final quenched magnetization $M_{N_0} = M$ is:

$$\mathbb{P}[M_{N_0} = M] = \frac{1}{2^{N_0}} \binom{N_0}{\frac{M+N_0}{2}}, \tag{2.27}$$

since they are exactly $\binom{N_0}{\frac{M+N_0}{2}}$ spin configurations with a magnetization M, all having a probability $1/2^{N_0}$. The maximum probability corresponds to the paramagnetic (i.e., unmagnetized) state$M = 0$. The shapes (i.e., the re-scaled probabilities so that all maximum values are 1) of the distribution given by Eq.2.27 with respect to the system size N_0 are plotted in Figure 2.4. The central-limit theorem [41] allows us to write $\mathbb{P}[M_{N_0} = M] \approx \sqrt{\frac{2}{\pi N_0}} \exp(-2M^2/N_0)$ for large N_0

2.3.2 Strong-coupling limit

On the contrary, if we set j_0 to $+\infty$, the only possible configurations are the two completely polarized ones: $\{+1, +1, \dots, +1\}$ and $\{-1, -1, \dots, -1\}$, which both have, by symmetry, a 1/2 probability. The result of the first quench, inducing a complete polarization of the other spins, will then decide in which direction the trajectory will go. The maximum probability thus corresponds to a non-zero magnetization and a ferromagnetic state. For high but not infinite j_0, the trajectories still have a polarized -or ferromagnetic - profile, as pictured in Fig.2.3b. From this short analysis, we can distinguish two cases depending on the value of j_0: whether the maximum probability is reached for $M = 0$ - in this case, the probability distribution is said "unimodal" - or for a non-zero magnetization ("bimodal" distributions). The frontier between those two cases is closely related to the Curie point and the ferromagnetic/paramagnetic transition in infinite models. Below, we explore this

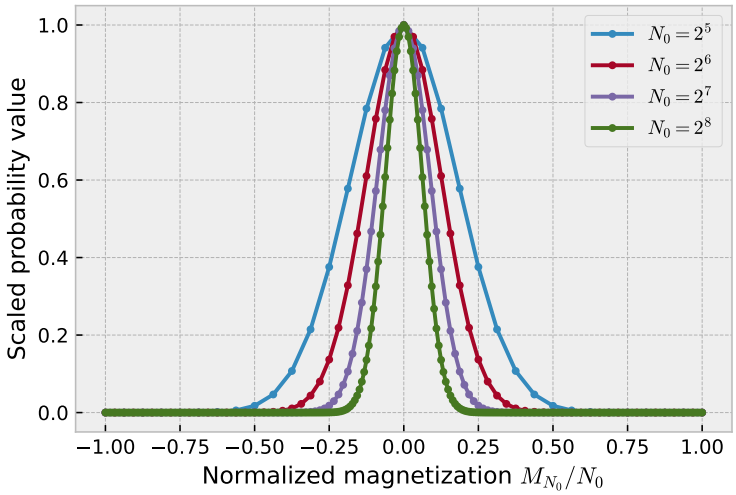

Figure 2.4: Scaled PQ distribution for $j_0 = 0$, with respect to M/N_0, plotted for different N_0. Each curve was rescaled so that $\mathbb{P}[M_{N_0} = 0] = 1$, to compare the relative shapes. Note that each curve has N_0+1 points (the number of possible magnetization values with N_0 spins).

"critical" case for finite systems.

2.3.3 Critical coupling and general formulation

Our interest is to set our problem between those two limit cases, where the results are not as predictable. From here, and for the rest of the analysis of the simulations, we will focus on the system that starts from the "critical" point under zero external field ($h = 0$). For finite systems, the "critical" point, $j_{0,\text{crit}}$, is defined as the value of coupling j_0 at which the magnetic susceptibility $\chi = \partial m^{(\text{eq})}/\partial h|_{h=0}$ is at its maximum - as an analogy to the infinite case where $j_{\text{crit}} = 1$ and $\chi \to +\infty$. We recall that for $N_0 \to \infty$ the Curie point is $j_0 = 1$ because $m^{(\text{eq})}$ verifies the self-consistent equation $m^{(\text{eq})} = \tanh(\beta[j_0 m^{(\text{eq})} + h])$ in this limit. Its numerical value is determined through extrapolation of the Curie law from the paramagnetic side, represented by the form:

$$\chi^{-1} \propto j_{0,\text{crit}} - j_0, \qquad j_{0,\text{crit}} > j_0. \tag{2.28}$$

Empirically, the value of $j_{0,\text{crit}}$ fits well with the power-law

$$j_{0,\text{crit}} \simeq 1 + 5.06\, {N_0}^{-0.933} \tag{2.29}$$

over the size-range $N_0 = 2^5$-2^{13}. We do have $j_{0,\text{crit}} \to 1$ as $N_0 \to +\infty$, recovering the mean-field results of the infinite-range Ising model. The numerical computations of $m^{(\text{eq})}$ for different $j_0 j$ were performed following Eq.(2.25).

Some trajectories at the critical coupling $j_{0,\text{crit}}$ are plotted in Fig.2.5b. We immediately notice that the curves are not like the unbiased random walk of Fig.2.3a. Rather, M_T in the late stages varies mostly linearly with T. This feature is also common to the

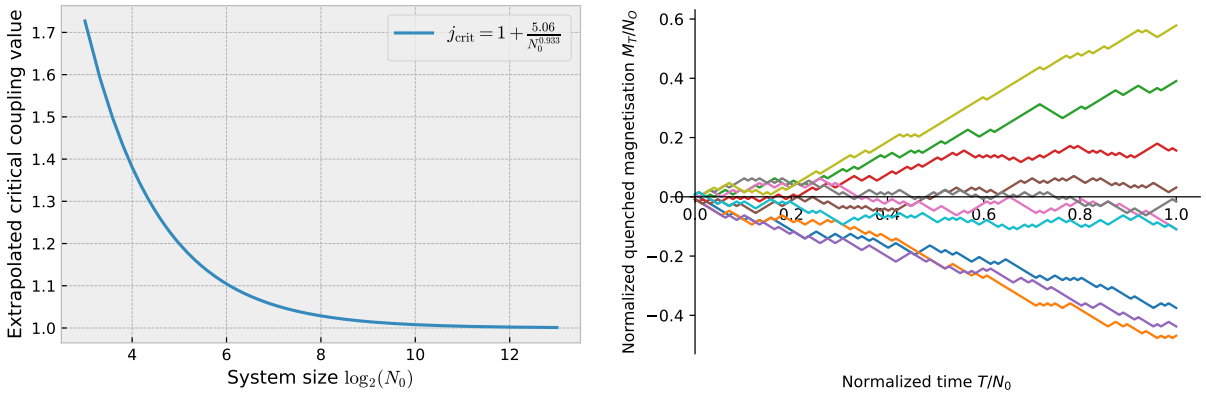

(a) Plot of the empirical power-law fit of j_{crit} from Eq.2.29

(b) Sample PQ trajectories at critical coupling $j_0 = j_{0,\text{crit}}$, plotted for $N_0 = 2^8$ spins.

Figure 2.5

"ferromagnetic" case ($j_0 = 1.5$) in Fig.2.3b. In Fig. 2.6 we superposed trajectories over a contour map of the equilibrium spin $m^{(\text{eq})}$. We observe qualitatively that the individual evolutions tend to follow a trajectory where the value of ${m^{(\text{eq})}}_{T,M_T}$ is kept mostly constant. The system thus exhibits a long-term memory of this value. This particular point is the starting point of the martingale analysis that will follow in the next chapter.

In general, the path probability $\mathbb{P}[\{s_1, \ldots, s_T\}]$ of the history of quenched spins up to the step T, $\{s_1, \ldots, s_T\}$, can be constructed and is written as

$$\mathbb{P}[\{s_1, \ldots, s_T\}] = \frac{1}{2^T} \prod_{T'=1}^{T} \left(1 + s_{T'} {m^{(\text{eq})}}_{T'-1,M_{T'-1}}\right). \tag{2.30}$$

Since 2^{-T} is the path probability of an unbiased ($j_0 = 0$) quenching of T spins, the product $R_T \equiv \prod_{T'=1}^{T} \left(1 + s_{T'} {m^{(\text{eq})}}_{T'-1,M_{T'-1}}\right)$ can be identified as the so-called Radon-Nikodym derivative (or functional), that relates both current biased and unbiased path probabilities [42]. Moreover, R_T is a martingale with respect to this unbiased process, meaning $\mathbb{E}0[RT + 1|s_1, \ldots, s_T] = R_T$, where $\mathbb{E}_0$ represents the conditional expectation over the unbiased process. This perspective aligns with the work of [24, 43] and their interpretation of the martingale in the context of the Jarzynski and Crooks equalities [7, 44]. However, in the case of Progressive Quenching, we will demonstrate that the mean equilibrium spin, ${m^{(\text{eq})}}_T$, eventually exhibits martingale-like behavior through a distinct physical mechanism compared to path probability ratios. This, along with the study of the magnetization probability distribution, will be the study of the next chapter.

2.4 Conclusion

This chapter presents how Progressive Quenching may be applied to the Curie-Weiss model when we set the quenching time intervals to several equilibration times (strictly speaking, it is set to ∞). In this case, the coupling between the quenched and free parts appears explicitly in the update rule (Eqs. (2.14) and (2.26)) - through the free

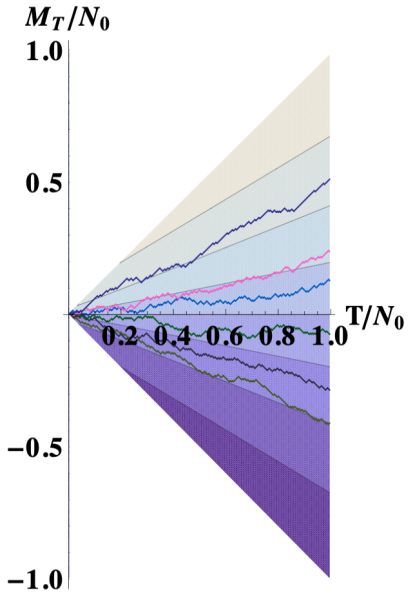

Figure 2.6: Trajectories plotted for $j_{0,\text{crit}}$ overlayed with iso-$m^{(\text{eq})}$ contour areas in the network. The darker the contour is, the lower the corresponding $m^{(\text{eq})}$ value is. (Figure extracted from [1])

mean magnetization $m^{(\text{eq})}$. By following the evolution of the quenched magnetization $M_T = \sum_{i=1}^{T} s_i$, we can distinguish two limit cases according to the value of the coupling constant j_0 and deduce a limit case corresponding to the finite equivalent of the critical coupling. Nevertheless, in general, we noticed *graphically* that trajectories tend to follow straight lines, which corresponds to iso-$m^{(\text{eq})}$ lines. This aspect, as well as the structure of equation (2.30), puts us on the track of a martingale governing the process evolution. We will follow this track in the next chapter and use some specific martingale theorems to study the effect of perturbations during the PQ.

A possible real-life example of such systems is found in the context of decision-making where the results of preliminary surveys are updated frequently (*e.g.*. online opinion surveys) before a referendum will represent those who already made up their mind. They can influence all those people who do not yet make up their minds. The choice of being at the critical coupling may be justified since important referendums are often done when the public opinion is little stable. In this context, the memory effects showcased by simulations show that the opinion of the first few determined persons may have a decisive impact. The PQ procedure is also reminiscent of greedy algorithms. Those algorithms make a sequence of choices that are in some way the best available at each step, and never go back on earlier decisions. See [45] and the references cited therein.

Appendix: Martingale property of path probability ratios.

In the context of stochastic processes within physics, martingale properties can manifest, particularly in the study of path probability ratios, which are integral to understanding entropic contributions and play a significant role in stochastic thermodynamics [26].

The path probability of a Progressive Quenching (PQ) process, up to T quenched spins, can be expressed as follows:

$$\mathbb{P}(s_1,\dots,s_T) = \frac{1}{2^T}\prod_{T'=1}^{T}\left(1+s_{T'}m^{(\mathrm{eq})}{}_{T'-1,M_{T'-1}}\right) \tag{2.31}$$

$$= \left(\frac{d\mathcal{P}}{d\mathcal{P}_0}\right)_T \times \mathbb{P}_0(s_1,\dots,s_T), \tag{2.32}$$

where $\mathbb{P}_0(s_1,\dots,s_T) \equiv 2^{-T}$ represents the probability of an unbiased, uncorrelated spin configuration. Additionally, the expression:

$$\left(\frac{d\mathcal{P}}{d\mathcal{P}_0}\right)_T = \prod_{T'=1}^{T}\left(1+s_{T'}m^{(\mathrm{eq})}_{T'-1,M_{T'-1}}\right) \tag{2.33}$$

denotes the "Radon-Nikodym derivative", acting as the conversion factor from the unbiased random walk to the biased random walk defined by Eqs.(2.14) and (2.26). In this case, $(d\mathcal{P}/d\mathcal{P}_0)_T$ is denoted as R_T in the main text. The marginal normalization condition for $1 \le T \le N_0 - 1$, which can be rephrased as:

$$\mathbb{E}_0\left[\left(\frac{d\mathcal{P}}{d\mathcal{P}_0}\right)_{T+1}\middle| s_1,\dots,s_T\right] = \left(\frac{d\mathcal{P}}{d\mathcal{P}_0}\right)_T, \tag{2.34}$$

where $\mathbb{E}_0$ represents the conditional expectation of $(d\mathcal{P}/d\mathcal{P}_0)_{T+1}$ with respect to the unbiased spin (in this case, s_{T+1} only) given the values $\{s_1,\dots,s_T\}$. Consequently, the stochastic process $(d\mathcal{P}/d\mathcal{P}_0)_T$ exhibits a martingale property concerning the unbiased stochastic process $s_1,\dots,s_T$. The path-probability normalization condition, $\sum_{s_1,\dots,s_T}\mathbb{P}(s_1,\dots,s_T) = 1$, can be expressed in terms of the unconditional expectation over all the unbiased stochastic processes as follows:

$$\mathbb{E}_0\left[\left(\frac{d\mathcal{P}}{d\mathcal{P}_0}\right)_T\right] = 1. \tag{2.35}$$

The last relation can be obtained through iterative application of (2.34) down to $T = 0$, when $\left(\frac{d\mathcal{P}}{d\mathcal{P}_0}\right)_{T=0}$ equals unity. This is a general consequence of the martingale property under specific conditions and is referred to as the optional stopping theorem (for more details, refer to [46]).

The martingale property of the Radon-Nikodym derivative has recently been intro-

duced into the field of physics by [24, 43], where $\mathcal{P}$ and $\mathcal{P}_0$ represented the path probabilities for the forward and time-reversed processes, respectively. Equation (2.35) essentially corresponds to the equalities of Jarzynski [7] and Crooks [44]. Their work advanced our comprehension of entropy production as an action functional and introduced the concept of stopping time [47, 48, 49, 27], such as the random cycle duration of autonomous mesoscopic heat engines [50].

Chapter 3

Distributions, Perturbations and Martingales

3.1 Introduction

Following the paradigm established in the last chapter, we study the probability distributions of magnetizations during and after a PQ process. First, we will establish the martingale property that governs the system's evolution. This property corresponds to the case where an observable undergoing a stochastic process - say, for example, $\hat{m}_T$, where T is time - evolves such that the conditional expectation of $\hat{m}_{T+1}$ at time $T+1$ remains equal to $\hat{m}_T$ under the given history of the system up to T, that is:

$$\mathbb{E}[\hat{m}_{T+1}|\mathcal{F}_T] = \hat{m}_T. \tag{3.1}$$

The notation $\mathbb{E}[\hat{X}|\mathcal{F}_T]$ corresponds to the conditional expectation of the random variable $\hat{X}$ given the history up to T, with $\mathcal{F}_T$ being the corresponding filtration. Physically, $\mathcal{F}_T$ corresponds to the sum of available information about the system up to time T - so we cannot see the future. Indeed, as our notation may suggest, the equilibrium average of the unfixed spins after the fixation of the T-th spin ${m^{(\mathrm{eq})}}_T$ verifies Eq.(3.1). For the sake of simplicity, we will drop the hat symbol of random variables in probability and expectation equations. Therefore $\mathbb{E}[\hat{m}^{(\mathrm{eq})}_{T,M_T}]$ will read $\mathbb{E}[{m^{(\mathrm{eq})}}_{T,M_T}]$. Similarly, when the value of M_T is not specified, we simplify ${m^{(\mathrm{eq})}}_{T,M_T}$ to ${m^{(\mathrm{eq})}}_T$.

While physics has used martingale properties as a technical tool, their physical meanings and consequences have rarely been exploited. Besides, detailed fluctuation theorems have recently been recognized as martingales of path probability ratios [24, 43, 51]. The reader may refer to Section 1.2 for a short introduction to martingales in stochastic processes. The present analysis aims at uncovering a different physical mechanism of the martingale property, whose necessary consequence is that the initial stochastic history has strong and long-lasting effects on the subsequent process.

Once this claim is proven, we need to study the final magnetizations' statistical distribution resulting from the previous chapter's trajectories. We will, therefore, study their probability distributions and the effect of system size on them. In particular, we will show that the distributions at critical coupling are all bimodal.

Finally, we will explore the mechanics of magnetization and apparent memory of the

system during PQ with a perturbative approach. Indeed, if we recall the observations of Sec. 2.3.3, the evolution of the fixed magnetization showed signs of long-term memory. *A priori*, the action of quenching breaks the local detailed balance associated with the micro-reversibility at thermal equilibrium, thus linear response theory [52, 53] and its fluctuation dissipation theorems [54] are not applicable [55, 56]. Much less is known about the dynamic response of systems far from equilibrium, primarily when the elementary processes do not satisfy local detailed balance. Nevertheless, we want to quantify this memory effect through a perturbative approach. Recently, the Malliavin weight sampling technique, derived from Malliavin derivatives in the context of stochastic calculus [57, 58, 59], has been introduced to study the dynamic response of stochastic systems undergoing a general Markovian process without assuming local DB [60, 61, 62]. Thus, we will revisit the PQ problem and directly analyze its response to the external field perturbations using Malliavin weighting. We will also focus on the response of the total magnetization in the final state when all spins have been fixed. The power of the martingale property of $\hat{m}_T^{(\mathrm{eq})}$ will be demonstrated by estimating both perturbed and unperturbed magnetization distributions from only early knowledge of the system. By this framework, we will assert that when a physical observable of a system possesses the martingale property, this property acts as a kind of stochastic conservation law, causing a long-term memory in the system's response, just like the proper conservation laws played essential roles in the response theory of the equilibrium systems through the emergence of hydrodynamic modes, either diffusive or propagative [63].

Most of this chapter is extracted from our 2020 paper [2], and the exact martingale derivation is extracted from [3].

3.2 Martingale property

3.2.1 The original approximate approach

Ventéjou and Sekimoto [1] were the first to derive the martingale property, by an approximate approach, and is the starting point of our interest in Progressive Quenching. They originally showed that, for a large enough unquenched system (i.e. $N_0 \gg 1$ and $N = N_0 - T \sim N_0$), the stochastic process corresponding to the equilibrium value of $m_T^{(\mathrm{eq})}$ at stage T (defined by Eq.(2.10)) followed:

$$\mathbb{E}[m_{T+1}^{(\mathrm{eq})} | \{s_1, \dots, s_T\}] = m_T^{(\mathrm{eq})} + \mathcal{O}(\frac{1}{{N_0}^2}). \tag{3.2}$$

This equation, denoted "hidden-martingale" because it does not involve the quenched process M_T directly, has then sparked a lot of interested, even though it had error bounds. In the original paper [1], the authors were able to deduce from it the "quasi-straightness" of the contour plots observed in Fig. 2.6, and the fact that trajectories tend to follow those contours. More precisely, the mean tangent of each trajectory approximately gives the equilibrium mean spin value in the free part:

$$\frac{dM}{dT} = m_{T,M_T}^{(\mathrm{eq})} + \mathcal{O}({N_0}^{-1}). \tag{3.3}$$

along the contour $m_T^{(\mathrm{eq})} = \mathrm{cst}$. This particular equation showcases how a PQ realization retains a sort of memory of the value of $m_T^{(\mathrm{eq})}$, which mostly depends on the early stages of the process. We then extended this particular observation to predict the future states of a trajectory, see Section 3.5, and derived an exact formulation of the martingale property, shown below.

3.2.2 An exact derivation for any homogeneous Ising spins

This derivation was performed later [3] when we understood the importance of the complete coupling between each spin in the memory effects, as it is an essential parameter for this exact derivation.

Let us consider an Ising system $\{s_k\}_{k=1}^{N_0}$ that evolves under the rule such that each unquenched spins are statistically equivalent (the system is then said "homogeneous"). For example, when the spins up to T-th, $\{s_T, \ldots, s_1\}$, with $0 \leq T < N_0$ have been quenched, the expectation m_{T,M_T} should verify :

$$m_{T,M_T} \equiv \mathbb{E}[s_{T+1}|M_T, \ldots, M_0] = \mathbb{E}[s_{N_0}|M_T, \ldots, M_0] \tag{3.4}$$

Here the conditional expectation $\mathbb{E}[s_{N_0}|M_T, \ldots, M_0](= m_{T,M_T})$ should be defined in the path-space such that the condition "$M_T, \ldots, M_0$" represents the history of quenching under a given time protocol, and that the value of s_{N_0}, or equivalently that of s_{T+1}, should be observed at the right moment when the latter spin is quenched.

The standard martingale theory tells : *If Z and $\{Y_i\}$'s are random variables with finite expectations, the process $\{X_T\}$ defined by $X_T = \mathbb{E}[Z|Y_T, \ldots, Y_0]$ is martingale with respect to $\{Y_T, \ldots, Y_0\}$.* In order to prove this, it suffices to use the following *tower rule* property (also called the *law of total expectations*):

$$\mathbb{E}[\mathbb{E}[Z|Y_{T+1}, Y_T \ldots, Y_0]|Y_T, \ldots, Y_0]] = \mathbb{E}[Z|Y_T, \ldots, Y_0]. \tag{3.5}$$

In our context, we apply the mapping, $\{Y_T, \ldots, Y_0\} \mapsto \{M_T, \ldots, M_0\}$ (or, equivalently $\{s_T, \ldots, s_1\}$), $X_T \mapsto m_{T,M_T}$ and $Z \mapsto s_{N_0}$. We latter mapping as to be carefully justified since the value of Z is effectively taken further in time. In our case, the mapping holds thanks to the homogeneity mentioned above. We therefore have:

$$m_{T,M_T} = \mathbb{E}[s_{N_0}|M_T, \ldots, M_0], \tag{3.6}$$

thus yielding

$$\begin{aligned} \mathbb{E}[m_{T+1,M_{T+1}}|M_T, \ldots, M_0] &= \mathbb{E}[\mathbb{E}[s_{N_0}|M_{T+1}, \ldots, M_0]|M_T, \ldots, M_0] \\ &= \mathbb{E}[s_{N_0}|M_T, \ldots, M_0] \\ &= m_{T,M_T}. \end{aligned} \tag{3.7}$$

Therefore, m_{T,M_T} is martingale process with respect to $\{M_T, \ldots, M_0\}$. This result holds even for non-Markovian dynamics since the conditional expectation considers the whole history, not just the last magnetization. However, our model of equilibrium quenching is Markovian. Then (3.6) simply reads

$$m^{(\mathrm{eq})}{}_{T,M_T} = \mathbb{E}[s_{N_0}|M_T] = \mathbb{E}[s_i|M_T], \tag{3.8}$$

that results in the martingale expression:

$$\mathbb{E}[{m^{(\mathrm{eq})}}_{T+1}|M_T] = {m^{(\mathrm{eq})}}_{T,M_T}. \tag{3.9}$$

Moreover, since any $T \in \{1, \ldots, N_0\}$ is a stopping time (see Sec. 1.2), we get from Doob's optional stopping theorem:

$$\mathbb{E}[{m^{(\mathrm{eq})}}_{T'}|M_T] = {m^{(\mathrm{eq})}}_{T}, \qquad \text{with} \quad T' > T. \tag{3.10}$$

For the approximate martingale given by Eq.(3.2), we also have a similar equation, with the propagation of error:

$$\mathbb{E}[{m^{(\mathrm{eq})}}_{T'}|M_T] = {m^{(\mathrm{eq})}}_{T} + \mathcal{O}\left(\frac{T'-T}{N_0^2}\right), \qquad T' > T. \tag{3.11}$$

3.2.3 A stochastically conserved quantity

Between two Progressive Quenching steps, the magnetization value of the free spins remains, on average, constant. While in the early stages of the process, variations in its value are substantial, they gradually diminish with each step. This effect is intuitively understandable, as the individual contribution of each new spin to the external field h_T is of the order of $1/T$. We may extrapolate this effect for large systems and write

$$\left\| \frac{{m^{(\mathrm{eq})}}_{T+1,M_T\pm1}}{{m^{(\mathrm{eq})}}_{T,M_T}} \right\| \xrightarrow[T\to\infty]{T/N_0=\mathrm{cte}} 1. \tag{3.12}$$

Therefore, adding one spin to an already large quenched part does not modify the free part's equilibrium much. Hence, we may understand the martingale equation (3.9) as a *stochastic* conservation law, that is, conservation in expectation. Furthermore, since the establishment of Lagrangian mechanics and Emmy Noether's work, it is known that behind every conserved quantity, there is usually an invariance or symmetry in the problem. The exact derivation of the martingale law above showcases that the coupling between spins on a complete lattice - and, therefore, the statistical equivalence of free spins is undoubtedly the underlying symmetry. Please note that this discussion is an interpretation and does not rely on any Lagrangian formulation of the problem.

3.3 Distributions of magnetization

Now that the mechanisms governing the evolution of single trajectories are developed, it is now time to delve deeper into the analysis of the statistical distribution of the final magnetization M_{N_0} and move beyond the basic analysis we conducted in the previous chapter (Section 2.3).

3.3.1 A transfer matrix formulation of the master equation

Instead of simulating the path ensemble, which would cost $\mathcal{O}(2^{N_0})$ trials, we can solve the master equation for the distribution of $\hat{M}_T$, the random variable associated to the value

of M at stage T, which costs no more than an algebraic power of N_0. By definition of PQ, the partition between the system and the external system (i.e., fixed spins) is not static. We can, nevertheless, reformulate the evolution as that of a super-system which is adapted to the transfer matrix method: The stochastic process of $\hat{M}_T$ vs T with $0 \leq T \leq N_0$ is represented as the transfer of $(2N_0+1)$-dimensional vector, $\vec{P}^{(T)} = \{P_M^{(T)}\}_{M=-N_0}^{N_0}$. The initial state $\vec{P}^{(0)}$ is $P_0^{(0)} = 1$ for $M = 0$ and $P_M^{(0)} = 0$, otherwise. The transition from stage T to the next one can be represented by a transfer matrix, $\mathbf{W}^{(T+1\leftarrow T)}$, such that

$$P_M^{(T+1)} = \sum_{M'=-T}^{T} (\mathbf{W}^{(T+1\leftarrow T)})_{M,M'} P_{M'}^{(T)} \tag{3.13}$$

or, in vector-matrix notation,

$$\vec{P}^{(T+1)} = \mathbf{W}^{(T+1\leftarrow T)} \vec{P}^{(T)} \tag{3.14}$$

for $0 \leq T \leq N_0 - 1$. The component of the matrix, $(\mathbf{W}^{(T+1\leftarrow T)})_{M',M}$, is the conditional probability that the fixation of the $(T+1)$-th spin makes the total fixed magnetization change from M to M'. By definition of PQ the only non-zero components of $\mathbf{W}^{(T+1\leftarrow T)}$ are $(\mathbf{W}^{(T+1\leftarrow T)})_{M\pm1,M}$ with $|M| \leq T$ and $M \equiv T \,(\mathrm{mod}\ 2)$. The transitions in the absence of perturbation (i.e., with $T \neq T_0$) gives

$$(\mathbf{W}^{(T+1\leftarrow T)})_{M\pm1,M} = (1 \pm m_{T,M}^{(\mathrm{eq})})/2 \tag{3.15}$$

corresponding to the fixation of the spin, $\hat{s}_{T+1} = \pm 1$, respectively. Using this notation, the final probability distribution of the total magnetization M_{N_0} in the absence of the perturbation reads,

$$\vec{P}^{(N_0)} = \mathbf{W}^{(N_0\leftarrow N_0-1)} \cdots \mathbf{W}^{(1\leftarrow 0)} \vec{P}^{(0)}. \tag{3.16}$$

This method was used to compute numerically all of the distributions shown below.

3.3.2 Fixed magnetization distribution description

The martingale property of individual histories holds memory of early stages of the trajectory that, we anticipate, will significantly affect the subsequent process's outcome. Figure 3.1 illustrates the evolution of the probability distribution's of the mean fixed spin value, M_T/T, from stage $T = 2^4$ up to the final stage $T = N_0 = 2^8$. Calculations were performed by solving the discrete "time" master equation for the biased random walk described in Fig. 2.2. At the critical coupling $j_{0,\mathrm{crit}}$, the Progressive Quenching results in a split of peak of the M_T/T distribution: the distribution switches from a "unimodal" shape (that is, the distribution reaches its maximum for $M = 0$) to a "bimodal" one (where the maximum is reached for any $M \neq 0$ values). Nonetheless, no bifurcation appears in the transition network, as can be seen from the example histories in Fig. 2.5b. In order to understand this transition, we may plot the probability densities of M_T/T for those histories starting from the polarized state $M_1 = +1$ (Fig. 3.2). The distribution in Fig. 3.1 can be recovered by taking the average of the result in Fig. 3.2 and its mirror image about the vertical axis, which corresponds to the $M_1 = -1$ initial condition. In Fig. 3.2, the peak is well off the vertical axis from the beginning, and it only sharpens with the progression of quenching.

These results highlight the significance of the stochastic events during the initial phases of the process, and will be extended by the perturbation analysis in the next section.

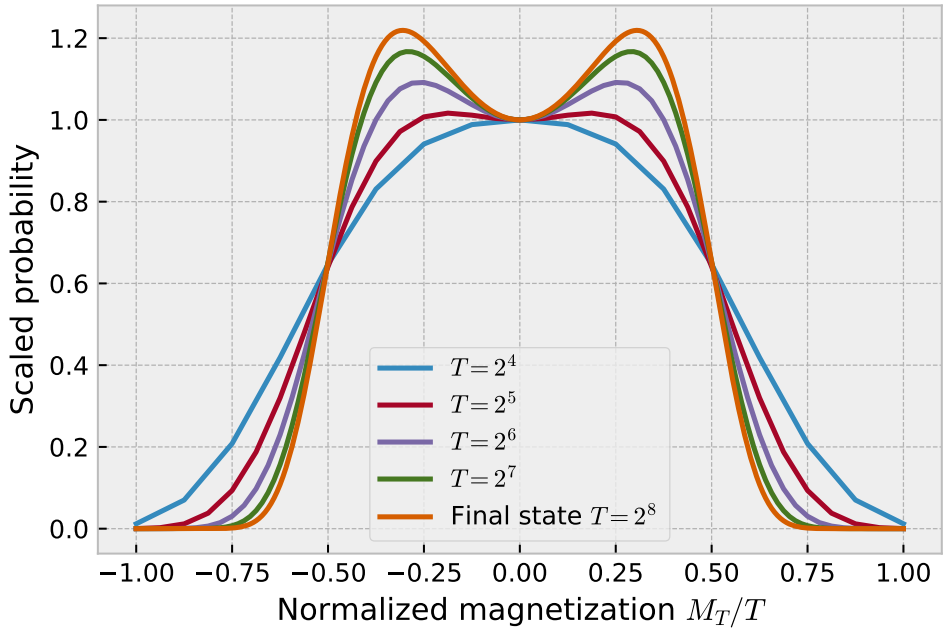

Figure 3.1: Probability distributions (rescaled) of the mean spin value, M_T/T, in the quenched part at different stages, $T = 2^k$ for $k = 4 - 8$ with fixed system size, $N_0 = 2^8 = 256$. The initial condition is $M_0 = 0$, and $j_0 = j_{0,\mathrm{crit}}$.

3.4 Perturbation analysis

3.4.1 Unperturbed evolution

Let us briefly recapitulate the case where no external perturbations were applied. We only show the evolution of the probability distribution of M_T, which is relevant to the following analysis. Fig.3.3(a) shows individual snapshots of the distribution of M_T for the system of $N_0 = 2^8$ spins (same system as Figure 3.1). These have been obtained essentially by interrupting the calculation of Eq.(3.16) at the midpoint; $\vec{P}^{(T)} = \mathbf{W}^{(T\leftarrow T-1)} \cdots \mathbf{W}^{(1\leftarrow 0)} \vec{P}^{(0)}$.

The coupling parameter j_0 is on the single phase side, i.e., $j_0 \leq j_{0,\mathrm{crit}}$. But if j_0 is not far below the critical one, the distribution develops a bimodal shape, as seen in Figs.3.1 and 3.3(a). On the other hand, if $0 \leq j_0 < j_0^* (< j_{0,\mathrm{crit}})$ with some threshold coupling j_0^*, then the peak remains unimodal until the final stage. For example, with $j_0 = 0$ the $\vec{P}^{(T)}$ is a symmetric binomial distribution. Whether or not $\vec{P}^{(T)}$ develops a bimodal profile depends on the relative importance of the memory of the early stages, such as the value of $\hat{s}_1 = \pm 1$. The memory of these stages is kept tenaciously in any case. However, it can be blurred by the noises if the system's (paramagnetic) susceptibility in the early stages is not large enough. This qualitative explanation will become clearer later regarding the hidden martingale (Sec.3.5.3).

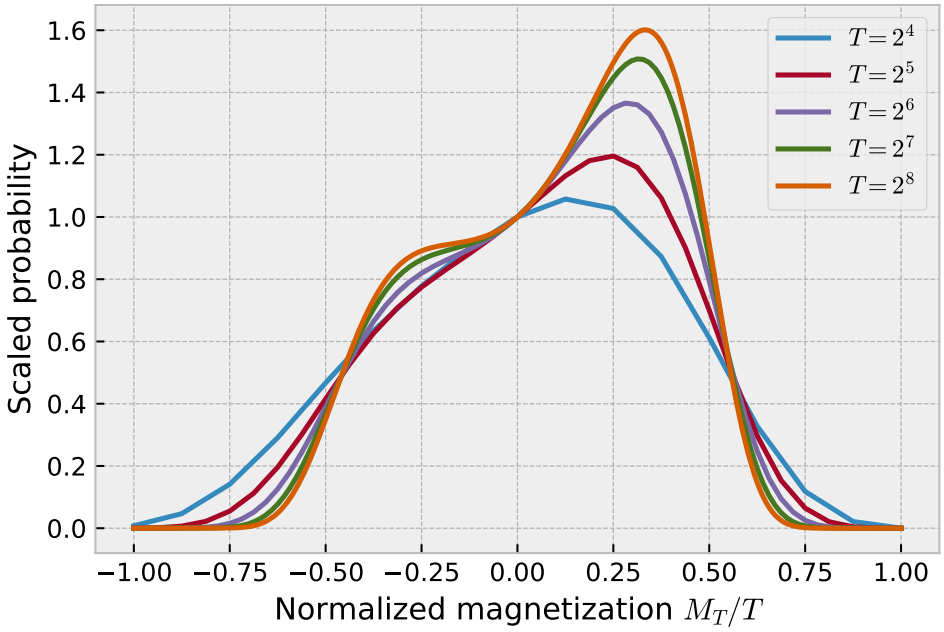

Figure 3.2: Rescaled probability distributions of the mean spin value, M_T/T, in the quenched part at different stages, $T = 2^k$ for $k = 4 - 8$ with the fixed system size, $N_0 = 2^8 = 256$. The initial condition is $M_1 = 1$ and $j_0 = j_{0,\mathrm{crit}}$.

We recall that the appearance of the bimodal profile of $P^{(N_0)}$ is *not* the result of the first order transition. The system is finite, therefore the magnetic susceptibility χ cannot diverge. Moreover, the system of unfrozen spins is in the single para-magnetic phase because the effective coupling among them, $j_{\mathrm{eff}} = (1 - \frac{T}{N_0})j_{0,\mathrm{crit}}$, is below critical for all $\mathbf{W}^{(T+1\leftarrow T)}$ $(1 \leq T \leq N_0)$.

3.4.2 Application of the perturbation:

In the next section we will study the influences of the external field perturbation h_{ext} which is applied uniquely at the stage-$(T_0 - 1)$. That is, in the presence of $h_{\mathrm{ext}} + h_{T_0-1}$, where h_{T_0-1} is the quenched molecular field by the fixed spins, we re-equilibrate $N_0 - (T_0 - 1)$ spins before fixing the T_0-th spin. If the external field is applied at the stage-$(T_0 - 1)$, the matrix $\mathbf{W}^{(T_0\leftarrow T_0-1)}$ should be modified; we denote the corresponding transfer matrix by $\mathbf{W}^{(T_0\leftarrow T_0-1)}_{h_{\mathrm{ext}}}$. The perturbed process and the resulting final distribution, $\vec{P}^{(N_0)}_{h_{\mathrm{ext}}}$ reads,

$$\begin{aligned}\vec{P}^{(N_0)}_{h_{\mathrm{ext}}} &= \mathbf{W}^{(N_0\leftarrow N_0-1)}\cdots\mathbf{W}^{(T_0+1\leftarrow T_0)} \\ &\quad \mathbf{W}^{(T_0\leftarrow T_0-1)}_{h_{\mathrm{ext}}}\mathbf{W}^{(T_0-1\leftarrow T_0-2)}\cdots\mathbf{W}^{(1\leftarrow 0)}\vec{P}^{(0)}. \end{aligned} \tag{3.17}$$

The martingale property of $\hat{m}^{(\mathrm{eq})}_T$ [1] is, therefore, interrupted upon the transition from the stage-(T_0-1) to the stage-T_0. From the stage-T_0 the martingale property of $\hat{m}^{(\mathrm{eq})}_T$ with $T \geq T_0$ holds *de nouveau* with the total fixed spin $\hat{M}_{T_0}$ being the new initial condition. The question is how the perturbation given to $\hat{M}_{T_0}$ propagates up to the final value $\hat{M}_{N_0}$

and how the martingale property of $\hat{m}_T^{(\mathrm{eq})}$ manifests itself in this propagation.

3.4.3 Sensitivity of final-state distribution to perturbations

The response to the perturbation given at the stage-(T_0-1) can be studied in two complementary ways, like the Fokker-Planck versus Langevin dynamics. In the present subsection we follow how the perturbation given to $\vec{P}^{(T_0)}$ is transferred to that in the final distribution $\vec{P}^{(N_0)}$ through (3.17). This Fokker-Planck type approach is in line with the Malliavin weighting [60, 61] when the perturbation is infinitesimal (see below). In the following subsection (3.5.1), we instead focus on the evolution of $\hat{M}_T$ from $T=T_0$ up to $T=N_0$, similar to the Langevin equation but through the filter of the conditional expectation, $\mathbb{E}[\hat{M}_T|M_{T_0}]$.

The direct consequence of the perturbation at the stage-(T_0-1) is the shift of the transfer matrix, $\Delta\mathbf{W}^{(T_0\leftarrow T_0-1)} \equiv \mathbf{W}_{h_{\rm ext}}^{(T_0\leftarrow T_0-1)} - \mathbf{W}^{(T_0\leftarrow T_0-1)}$. As the result of the propagation of the shift, the final shift of the probability density reads,

$$\begin{aligned}\vec{P}_{h_{\rm ext}}^{(N_0)} - \vec{P}^{(N_0)} \quad &= \mathbf{W}^{(N_0\leftarrow N_0-1)}\cdots\mathbf{W}^{(T_0+1\leftarrow T_0)} \\ &\Delta\mathbf{W}^{(T_0\leftarrow T_0-1)}\mathbf{W}^{(T_0-1\leftarrow T_0-2)}\cdots\mathbf{W}^{(1\leftarrow 0)}\vec{P}^{(0)}. \end{aligned} \tag{3.18}$$

In the case of the infinitesimal perturbing field, we deal with the linear response to $h_{\rm ext}$ and calculate, instead of (3.18), the sensitivity

$$\begin{aligned}\frac{\partial\vec{P}_{h_{\rm ext}}^{(N_0)}}{\partial h_{\rm ext}} \quad &= \quad \mathbf{W}^{(N_0\leftarrow N_0-1)}\cdots\mathbf{W}^{(T_0+1\leftarrow T_0)} \\ &\frac{\partial\mathbf{W}_{h_{\rm ext}}^{(T_0\leftarrow T_0-1)}}{\partial h_{\rm ext}}\,\mathbf{W}^{(T_0-1\leftarrow T_0-2)}\cdots\mathbf{W}^{(1\leftarrow 0)}\vec{P}^{(0)}, \end{aligned} \tag{3.19}$$

where the partial derivative with respect to $h_{\rm ext}$ should be evaluated at $h_{\rm ext}=0$ and the only non-zero components of $\partial\mathbf{W}_{h_{\rm ext}}^{(T_0\leftarrow T_0-1)}/\partial h_{\rm ext}$ are $\partial(\mathbf{W}_{h_{\rm ext}}^{(T_0\leftarrow T_0-1)})_{M\pm1,M}/\partial h_{\rm ext} = \pm\chi_{T_0-1,M}^{(\mathrm{eq})}/2$ for $|M|\le T_0-1$ with $\chi_{T,M}^{(\mathrm{eq})} \equiv \partial m_{T,M}^{(\mathrm{eq})}/\partial h_{\rm ext}$ being the susceptibility at the stage-T under a molecular field, $h_T = \frac{j_0}{N_0}M$. The approach of Malliavin weighting [60, 61] is essentially the path-wise expression of (3.19), see Appendix 3.6 for a more detailed account. In Fig.3.3 (b) we plotted the result in (3.19) vs M_{N_0}/N_0 of the system with the size $N_0=2^8=256$. Depending on the stage of perturbation ($T_0=2^4=16$ or $T_0=2^7=128$) the sensitivity qualitatively changes; see below.

In the case of the infinite perturbing field $h_{\rm ext}=+\infty$, we calculate directly (3.18), where the transition rates upon the perturbed stage read $(\mathbf{W}_{h_{\rm ext}}^{(T_0\leftarrow T_0-1)})_{M+1,M}=1$ with $|M|\le T_0-1$ and all the remaining components of $\mathbf{W}_{h_{\rm ext}}^{(T_0\leftarrow T_0-1)}$ are zero. Therefore the only non-zero components of $\Delta\mathbf{W}^{(T_0\leftarrow T_0-1)}$ are $\Delta(\mathbf{W}^{(T_0\leftarrow T_0-1)})_{M\pm1,M} = \pm(1-m_{T_0-1,M}^{(\mathrm{eq})})/2$ for $|M|\le T_0-1$. In Fig.3.3(c) we monitored $\vec{P}_{h_{\rm ext}}^{(N_0)} - \vec{P}^{(N_0)}$ vs M_{N_0} as the response to the infinite perturbation, $h_{\rm ext}=+\infty$. This response is qualitatively similar to the linear response of the distribution (Fig.3.3(b)), except for a positive bias around $M_{N_0}=0$ in the former case. We notice the two common trends for both types of perturbation: (i) The response is stronger when the perturbation is given at the early stage, which is contrasting to the equilibrium system for which the impact of perturbation should be strongest if given most recently, i.e., with the largest T_0. (ii) The profiles of the

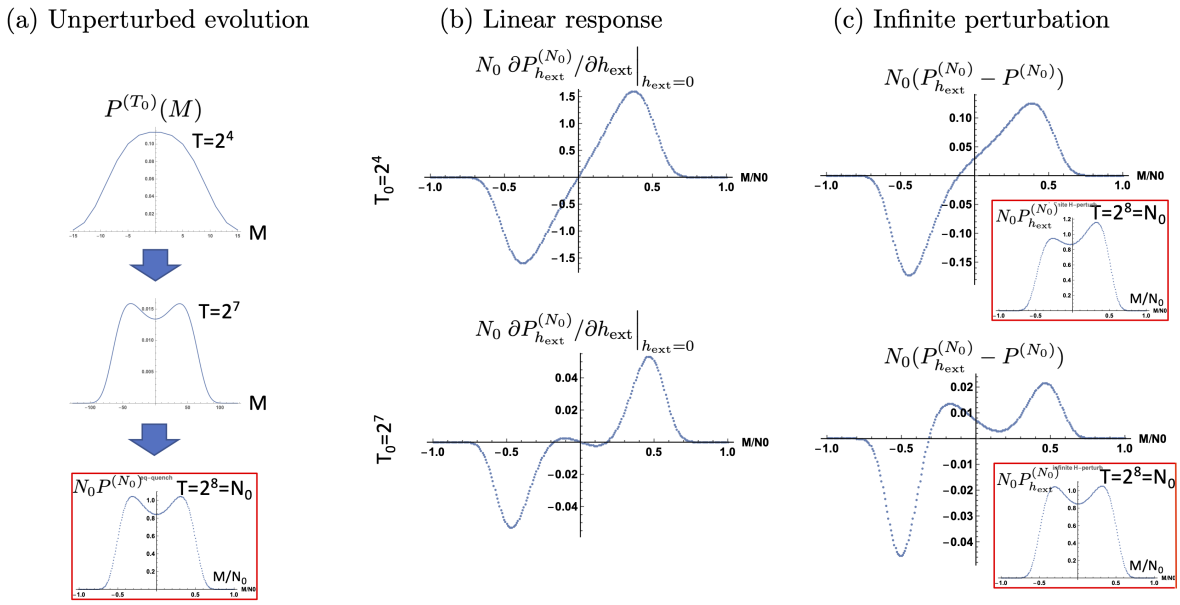

Figure 3.3: (a) The unperturbed evolution of the probability of the total fixed magnetization, M, at three different numbers of fixed spins, $T = 2^4, 2^7$ and $T = 2^8 = N_0$. (b) The linear response of the final distribution $P^{(N_0)}$ to the infinitesimal perturbations given at the different stages, $T_0 = 2^4$ (top) and 2^7 (bottom). The system size scales the horizontal axis. (c) The response of the final distribution $P^{(N_0)}_{h_{\rm ext}}$ to the infinite perturbation given at the different stages, $T_0 = 2^4$ (top) and 2^7 (bottom). The insets show the final perturbed distributions.

response reflect the distribution at the stage when the perturbations have been applied: If a perturbation is given when the unperturbed distribution of M is still unimodal (i.g. $T_0 = 2^4$), the density response in the final magnetization resembles the M-derivative of the unimodal distribution at the stage-T_0. (Notice, however, that the width of the distribution is "magnified" from $|M| \le T_0 (= 16)$ to the final one ranging over $|M| \lesssim 0.7 \times N_0 (\simeq 180)$.) Similarly, if the perturbation is given in the late stage (e.g., $T_0 = 2^7$), the final response resembles the M-derivative of the bimodal distribution at T_0. This trend (ii) suggests an underlying mechanism by which the individual realization of PQ keeps the memory of the stage when the perturbation is given. As noted in Sec.3.4.1, the possibility of first-order transition is excluded. We will see later in Sec.3.5.1 (especially Eq.(3.21)) that the origin of the memory is the (hidden) martingale property of $m^{(\rm eq)}_{T,\hat{M}_T}$.

3.5 Martingale analysis

3.5.1 Mean response of the final magnetization, $\mathbb{E}[\hat{M}_{N_0}]$

We study the mean response of the total spin at the final stage, $\mathbb{E}[\hat{M}_{N_0}]$, when an infinite perturbing field ($h_{\rm ext} = +\infty$) is applied at the stage-$(T_0 - 1)$, just before fixing the T_0-th spin. While this mean value $\mathbb{E}[\hat{M}_{N_0}]$ can be calculated through (3.17), here we will take

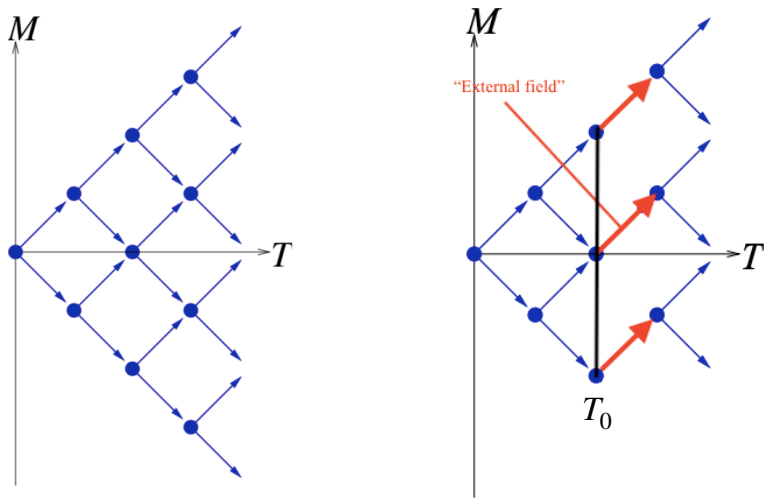

Figure 3.4: (Left) Unperturbed (T, M_T) network. (Right) Network where the infinite-field perturbation is applied towards the $+1$ direction at stage T_0.

a different approach;

$$\mathbb{E}[\hat{M}_{N_0}] = \sum_{M=-T_0}^{T_0} \mathbb{E}[\hat{M}_{N_0}|M_{T_0} = M] P_{h_{\rm ext}}^{(T_0)}(M), \tag{3.20}$$

where $\mathbb{E}[\hat{M}_{N_0}|M_{T_0} = M]$ is the conditional expectation. By $(\mathbf{W}_{h_{\rm ext}}^{(T_0 \leftarrow T_0-1)})_{M+1,M}$, which is described in the last paragraph of Sec.3.4.3, $P_{h_{\rm ext}}^{(T_0)}(M)$ is the shifted copy of the previous stage, that is, $P^{(T_0)}(M+1) = P^{(T_0-1)}(M)$ for $|M| \leq T_0 - 1$ and $P^{(T_0)}(-T_0) = 0$. Therefore, for T_0 not very large ($\ll N_0$) the calculation of $P_{h_{\rm ext}}^{(T_0)}(M)$ is a relatively light calculation. As for the conditional expectation $\mathbb{E}[\hat{M}_{N_0}|M_{T_0} = M]$, if we use the martingale property of $m_{T,\hat{M}_T}^{(\rm eq)}$ for the unperturbed process $T_0 \leq T \leq N_0$ (Eq.(3.9)), we can show the compact result:

$$\mathbb{E}[\hat{M}_{N_0}|M_{T_0} = M] = M + (N_0 - T_0) m_{T_0,M}^{(\rm eq)}. \tag{3.21}$$

Therefore, (3.20) reads finally

$$\mathbb{E}[\hat{M}_{N_0}] = \mathbb{E}[\hat{M}_{T_0}] + (N_0 - T_0)\mathbb{E}[m_{T_0,\hat{M}_{T_0}}^{(\rm eq)}]. \tag{3.22}$$

Note that (3.22) does not require the calculation of transfer matrices beyond the stage-T_0.

The relation (3.21) comes out from a more general statement about the mean increment rate of $\hat{M}_T$:

$$\mathbb{E}[\frac{\hat{M}_T - M_{T_0}}{T - T_0}|M_{T_0} = M] = m_{T_0,M}^{(\rm eq)} \tag{3.23}$$

for $T_0 < T \leq N_0$. The derivation is given in a dedicated section below (3.5.2), where we use the martingale property of $m_{T,\hat{M}_T}^{(\rm eq)}$. The relation (3.21) tells us that the impact of perturbation is directly transmitted by the martingale observable, $m_{T,\hat{M}_T}^{(\rm eq)}$. This opens the

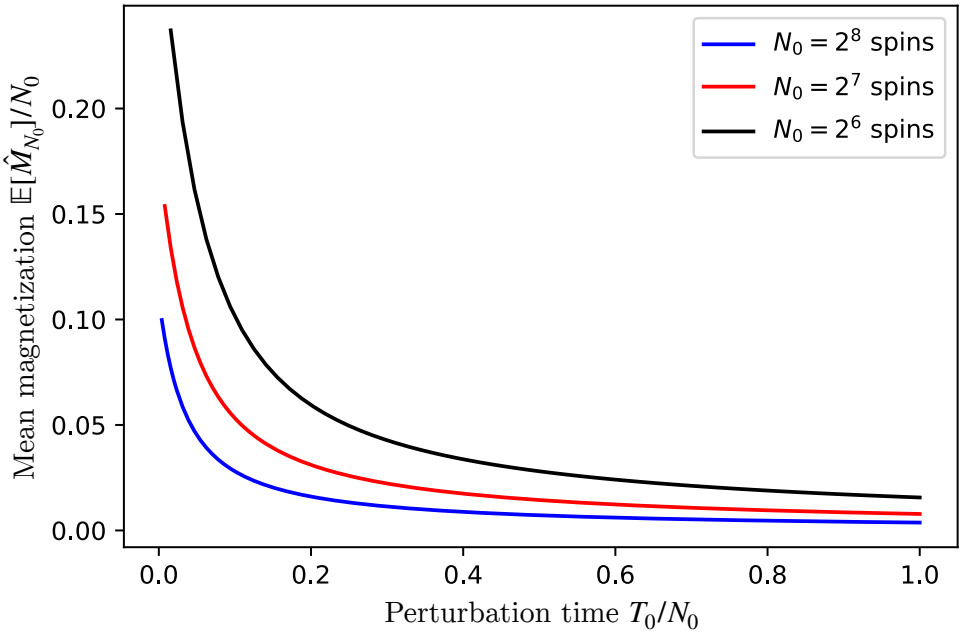

Figure 3.5: Mean response of the magnetization, $\mathbb{E}[\hat{M}_{N_0}]$, to the perturbation $h_{\rm ext} = +\infty$ applied at the stage-T_0.

possibility to predict approximately the final distribution $P^{(N_0)}(M_{N_0})$ from the data at the stage-T_0 when the perturbation is given (see Sec.3.5.3 below) and then to understand better the result of Sec.3.4.3. Because it is only in the expectation the mean increment rate, $\frac{\hat{M}_T - M_{T_0}}{T - T_0}|_{M_{T_0}=M}$, is kept constant over $T_0 < T \leq N_0$, we call it the *stochastic conservation*.

In Fig. 3.5 we plot the mean values of the final magnetization, $\mathbb{E}[\hat{M}_{N_0}]$, The different curves in Fig. 3.5 correspond to the different system sizes, $N_0 = 2^6, 2^7$, and 2^8. Both axes are rescaled by the system sizes. The formula Eq.(3.22) reproduces $\mathbb{E}[\hat{M}_{N_0}]$ so well that the deviation from the full numerical results using $P^{(N_0)}_{h_{\rm ext}}(M)$ is within the thickness of the curves. That the mean response of the frozen spin, $\mathbb{E}[\hat{M}_{N_0}]/N_0$ decreases with the system size N_0 is consistent with our previous observation in Sec.3.4.3, especially Fig.3.3(c).

3.5.2 Derivation of Eq.(3.21)

The total fixed spins $\hat{M}_T$ at the stage-T with $T_0 < T \leq N_0$ reads $\hat{M}_T = \hat{M}_{T_0} + \sum_{j=T_0+1}^{T} \hat{s}_j$, where $\hat{s}_j$ is the value of the spin, which is fixed in the j-th quenching. Taking the expectation of the above formula, i.e.,

$$\mathbb{E}[\hat{M}_T | \hat{M}_{T_0} = M_{T_0}] = M_{T_0} + \sum_{j=T_0+1}^{T} \mathbb{E}[\hat{s}_j | \hat{M}_{T_0} = M_{T_0}], \tag{3.24}$$

we will focus on $\mathbb{E}[\hat{s}_j|\hat{M}_{T_0} = M_{T_0}]$. For $T_0 < T \leq N_0$ the last quantity can be transformed as

$$\begin{aligned}\mathbb{E}[\hat{s}_T|\hat{M}_{T_0} = M_{T_0}] &= \mathbb{E}\Big[\mathbb{E}[\hat{s}_T|\hat{M}_{T-1}]\,|\hat{M}_{T_0} = M_{T_0}]\Big] \\ &= \mathbb{E}\Big[m^{(\mathrm{eq})}_{\hat{M}_{T-1}}|\hat{M}_{T_0} = M_{T_0}\Big] \\ &= m^{(\mathrm{eq})}_{\hat{M}_{T_0}}, \end{aligned} \tag{3.25}$$

where, in order to go to the last line, we have used (3.10) with (T', T) there being replaced by (T, T_0) here, respectively. By choosing $T = N_0$ we arrive at Eq.(3.21). Equation (3.25) can also be derived with approximation, using the approached stopping time theorem given by Eq.(3.11).

3.5.3 Hidden martingale property predicts final distribution

The fluctuation property of $m^{(\mathrm{eq})}_{T,\hat{M}_T}$ adds something on top of (3.21) when the system is large enough in the sense of $N_0 \gg T_0$. Starting from the condition $\hat{M}_{T_0} = M$, the final magnetization $\hat{M}_{T_0}$ should scatter around $\mathbb{E}[\hat{M}_{N_0}|M_{T_0} = M]$, but its standard deviation should to be $\mathcal{O}((N_0)^{\frac{1}{2}})$, therefore, less dominant than the mean part, $(N_0 - T_0)m^{(\mathrm{eq})}_{T_0,M} = \mathcal{O}(N_0)$. This estimation of the standard deviation, $\mathcal{O}((N_0)^{\frac{1}{2}})$, is related to the so-called martingale central-limit theorem (see, for example, Sec.3.3 of [64]) together with the fact that $m^{(\mathrm{eq})}_{T,\hat{M}_T}$ is non-extensive quantity of $\mathcal{O}(1)$. With the tolerance of $\mathcal{O}({N_0}^{\frac{1}{2}})$ errors, Eq.(3.21) leads, therefore, to a sort of geometrical optics approximation ([65]):

$$\hat{M}_{N_0}\Big|_{M_{T_0}=M} = M + (N_0 - T_0)\, m^{(\mathrm{eq})}_{T_0,M} + \mathcal{O}({N_0}^{\frac{1}{2}}). \tag{3.26}$$

This estimation, in turn, allows us to reconstruct the final probability distribution $P^{(N_0)}_{h_{\mathrm{ext}}}(M)$ versus M, see Appendix 3.5.4 for the detailed protocol. In Fig.3.6, we compare the final distributions of $\hat{M}_{N_0}$, one by the geometrical optics approximation and the other by the total numerical calculation of transfer matrix products. Naturally, the former method gives a narrower distribution because this approximation ignores the broadening by the standard deviation, $\sim (256)^{\frac{1}{2}} \simeq 16$. Amazingly, the geometrical optics approximation can nevertheless predict the positions of bimodal peaks very well from the data of unimodal distribution at the stage-T_0. When N_0 and T_0 constitute the double hierarchy $1 \ll T_0 \ll N_0$, our methodology will serve as a fine tool for numerical asymptotic analysis. We have chosen the coupling j_0 at the critical one, $j_{0,\mathrm{crit}}$ because the predictability of bimodal distribution from the unimodal stage looks impressive. Nevertheless, given the tenacious memory, Eq.(3.26) and the predictability as its consequence also hold for the weaker coupling with which the final distribution is unimodal.

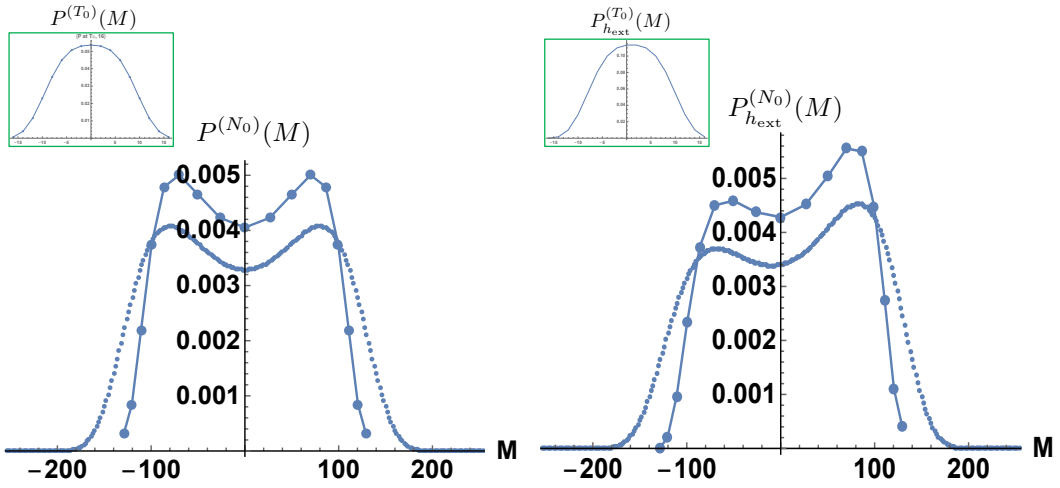

Figure 3.6: Comparison between the final distributions of M_{N_0} predicted by the hidden martingale property (joined T_0+1 dots) with those by full numerical solution (dense dots) for $h_{\rm ext} = 0$ (left) and for $h_{\rm ext} = \infty$ (left) with $T_0 = 2^4$ and $N_0 = 2^8$. The probability densities are rescaled in the figures so that their integral over M is normalized to unity. The figures in inset show the probabilities $P^{(T_0)}$ (left) and $P^{(T_0)}_{h_{\rm ext}}$ (right), respectively. Both are singly peaked, but the latter is almost translocated by $\Delta M = +1$.

3.5.4 Construction of final distribution from early stage one using martingale conditional expectation

For the simplicity of notations, we introduce (see (3.26))

$$\begin{aligned} \mu_i &= -T_0 + 2i \\ m_i &= m^{(\rm eq)}_{T_0,\mu_i} \\ x_i &= \mu_i + (N_0 - T_0)\, m_i, \qquad \text{with } i = 0, 1, \ldots, T_0 \end{aligned} \tag{3.27}$$

We will make up the final probability density $p(x)$ so that its normalization is $\int_{x_0}^{x_{T_0}} p(x)dx = 1$. We suppose that $p(x)$ is piecewise linear whose joint-points are $\{x_i, p(x_i)\}$. The normalization condition then reads

$$\begin{aligned} 1 &= \sum_{i=0}^{T_0-1} \frac{p(x_i) + p(x_{i+1})}{2}(x_{i+1} - x_i) \\ &= p(x_0)\frac{x_1 - x_0}{2} + \sum_{i=1}^{T_0-1} p(x_i)\frac{x_{i+1} - x_{i-1}}{2} + p(x_{T_0})\frac{x_{T_0} - x_{T_0-1}}{2}. \end{aligned} \tag{3.28}$$

Then we define $p(x_i)$ through

$$\begin{aligned} p(x_0)\frac{x_1 - x_0}{2} &= P^{(T_0)}_{h_{\rm ext}}(m_0), \\ p(x_i)\frac{x_{i+1} - x_{i-1}}{2} &= P^{(T_0)}_{h_{\rm ext}}(m_i) \qquad i = 1, \ldots, T_0 - 1 \end{aligned}$$

$$p(x_{T_0})\frac{x_{T_0}-x_{T_0-1}}{2} = P^{(T_0)}_{h_{\rm ext}}(m_{T_0}) \tag{3.29}$$

so that the "ray" of geometrical optics carries the probability from $T = T_0$ to $T = N_0$. The martingale prediction of the probability densities in Fig.3.6 are thus made.

3.6 Conclusion

Using general terminology, let us first summarize the mechanism by which the martingale property gives rise to a tenacious memory of the process. We will use the notation which corresponds to the previous sections, such as $\hat{M}_T$ or $\hat{m}_T$, but we don't rely on the PQ model.

Suppose that $\{\hat{M}_T\}$ $(0 \le T \le N_0)$ is a stochastic process with the discrete time T and has the increment, $\hat{s}_{T+1} \equiv \hat{M}_{T+1} - \hat{M}_T$. We assume that the probabilistic characteristics of $\hat{s}_{T+1}$ is determined by the history of $\{\hat{M}_t\}$ up to $t = T$, and that its conditional expectation $\hat{m}_T \equiv \mathbb{E}[\hat{s}_{T+1}|\mathcal{F}_T]$ is completely determined by the history up to T, denoted by $\mathcal{F}_T$. With only these settings we can verify that $\hat{R}_T \equiv \sum_{t=0}^{T-1}(\hat{s}_{t+1} - \hat{m}_t)$ is martingale, i.e., $\mathbb{E}[\hat{R}_{T+1}|\mathcal{F}_T] = R_T$, the fact which is known as Doob-Lévy decomposition theorem [66, 46]. The martingale of our concern, however, is not this one, but we add another layer; we suppose that $\{\hat{m}_T\}$ is again martingale, that is, $\mathbb{E}[\hat{m}_{T+1}|\mathcal{F}_T] = \hat{m}_T$. This is why the latter is denoted by "hidden martingale". The outcome is that we have

$$\mathbb{E}[\hat{M}_T|\mathcal{F}_{T_0}] = \hat{M}_{T_0} + (T - T_0)\hat{m}_{T_0}, \quad T > T_0, \tag{3.30}$$

which we can verify by following the same argument as in Sec. 3.5.2.

Eq.(3.30) tells how the hidden martingale property of $\{\hat{m}_T\}$ transmits the memory of the past data without exponential or power-low decay. This relation is the general outcome of the hidden martingale and has nothing to do with the origin of the hidden martingale. Especially in our PQ model, the relation Eq.(3.21) represents the tenacious memory whether the distribution $P^{(N_0)}(M)$ is unimodal or bimodal.

For completeness, we also write down the continuous-time counterpart: Suppose that $\{\hat{M}_t\}$ $(0 \le t \le t_0)$ is a stochastic process with the continuous time t and we denote the increment by $d\hat{M}_t \equiv \hat{M}_{t+dt} - \hat{M}_t$. We assume that the probabilistic features of $d\hat{M}_t$ is determined by the history of $\{\hat{M}_\tau\}$ up to $\tau = t$ and its conditional expectation $\hat{m}_t\,dt \equiv \mathbb{E}[d\hat{M}_t|\mathcal{F}_t]$ is completely determined by the history up to t, denoted by $\mathcal{F}_t$. Then by Doob-Lévy decomposition theorem [66, 46], and the martingale central-limit theorem (see, for example, Sec.3.3 of [64]) allow us to represent the stochastic evolution of $\hat{M}_t$ in the form of stochastic differential equation

$$d\hat{M}_t = \hat{m}_t\,dt + \hat{b}_t \cdot d\hat{W}_t, \tag{3.31}$$

where the second term on the r.h.s. is an Itô integral with a Wiener process, $\hat{W}_t$. Now if we further suppose that $\{\hat{m}_t\}$ is martingale, then we have

$$\mathbb{E}[\hat{M}_t|\mathcal{F}_{t_0}] = M_{t_0} + (t - t_0)\hat{m}_{t_0}, \quad t > t_0 \tag{3.32}$$

because $\mathbb{E}[d\hat{M}_t|\mathcal{F}_{t_0}] = \mathbb{E}[\hat{m}_t|\mathcal{F}_{t_0}]dt = \hat{m}_{t_0}dt$ holds for $t > t_0$.

Moreover, we may compare the PQ with some of the "linear voter models" that may exhibit martingale properties; see [67] for an introduction. In a typical example, the binary ($[1, 0]$) site (say x_i) and its neighbor (say $x_i + n_i$) are chosen at random at each discrete time step and the state of x copies the state of $x + n$. In that model, $M_t := \sum_{i=1}^{N_0} x_i(t)/N$, where N is the system size, is deemed to be either 1 or 0, according to the so-called martingale convergence theorem (see, for example, [68] Sec. 11.2). At the same time, the mean of M_∞ is M_0/N by the martingale property of M_t. If we compare such a model with our PQ of spins, a difference is that M_t of the voter model eventually goes only to 1 or 0, unlike our PQ, while the similarity is that (i) both models have a martingale observable, and (ii) the individual realization tends to be polarized due to the interaction with the environment with a long memory.

Appendix: Simple summary of Malliavin weighting

In this Appendix, we explain the Malliavin weighting introduced by Warren and Allen [61] following the work of Berthier [60]. The evolution of the probability distribution from the initial one to the final one is given as the matrix-vector product like (3.16) or (3.17) in the main text. These products can be regarded as discrete path integrals because the different paths to reach the final state $\hat{M}_{N_0}$ form the initial one $\hat{M}_0(=0)$ are mutually exclusive and each path $[M]$ contributes to the path integral by the transfer weight,

$$\mathcal{W}[M] := \prod_{T=0}^{N_0-1} \mathbf{W}^{(T+1\leftarrow T)}_{M_{j_{T+1}},M_{j_T}}. \tag{3.33}$$

The so-called Malliavin weighting is the path functional which gives the relative, or log, sensitivity of this path weight to the infinitesimal external field:

$$q[M] \equiv \left.\frac{\partial \log \mathcal{W}[M]}{\partial h_{\rm ext}}\right|_{h_{\rm ext}=0}. \tag{3.34}$$

Below we will show that the average linear sensitivity of any path-functional $\mathcal{A}[M]$ reads

$$\left.\frac{\partial}{\partial h_{\rm ext}}\mathbb{E}[\mathcal{A}[M]]\right|_{h_{\rm ext}=0} = \mathbb{E}[q[M]\mathcal{A}[M]]|_{h_{\rm ext}=0}. \tag{3.35}$$

Using the formal linear expansion;

$$\mathcal{W}[M] = \mathcal{W}[M]_{h_{\rm ext}=0}(1 + q[M]h_{\rm ext} + \mathcal{O}({h_{\rm ext}}^2)), \tag{3.36}$$

we find

$$\begin{aligned}\frac{\partial \mathbb{E}[\mathcal{A}[M]]}{\partial h_{\rm ext}} &= \lim_{h_{\rm ext}\to 0}\sum^{[M]}\mathcal{A}[M]\frac{\mathcal{W}[M]-\mathcal{W}[M]_{h_{\rm ext}=0}}{h_{\rm ext}}P_0^{(0)}(M_0)\\ &= \sum^{[M]}\mathcal{A}[M]q[M]\mathcal{W}[M]_{h_{\rm ext}=0}P_0^{(0)}(M_0),\end{aligned} \tag{3.37}$$

where the last line on the r.h.s. is the expectation of $\mathcal{A}[M]q[M]$.

To calculate $q[M]$ we recall the form $\mathcal{W}[M] := \prod_{T=0}^{N_0-1}\mathbf{W}^{(T+1\leftarrow T)}_{M_{j_{T+1}},M_{j_T}}$. Using the additivity of the log of product, we have

$$q[M] = \sum_{0\le T\le N_0-1}^{[M]} \left.\frac{\partial \log W^{(T+1\leftarrow T)}_{M_{T+1},M_T}}{\partial h_{\rm ext}}\right|_{h_{\rm ext}=0}, \tag{3.38}$$

where the sum is taken along the history $[M]$. Therefore, the weight $q[M]$ can be calculated cumulatively along the process M. Especially when the perturbation is given uniquely at the stage-(T_0-1), as in the main text, the relative sensitivity is reduced to $q[M] = \partial \log[W^{(T_0\leftarrow T_0-1)}_{M_{T_0},M_{T_0-1}}]/\partial h_{\rm ext}|_{h_{\rm ext}=0}$. If we regard the r.h.s. of Eq.(3.19) as a path integral, the contribution of the path $[M]$ reads $\mathcal{W}[M]q[M]$.

Chapter 4

Local invariance and Canonicity: Static and Dynamic approaches

4.1 Introduction

In the present chapter, we further explore the consequences of the martingale property in the framework of PQ. The mean equilibrium spin for Ising spins ultimately determines the next quenched spin's probability. When the mean equilibrium spin is a martingale, the Markovian evolution of the total quenched magnetization is found to have a local invariance in its probabilistic path weight. There are two significant consequences, both of which were - at least for us - unexpected and were first recognized through numerical simulations. Our first finding is that, given the number of quenched spins T, the probability distribution for the quenched magnetization M can be expressed as a Boltzmann factor containing a "path-weight potential" and a "path-counting entropy" defined on the (T, M)-space. This result will be described in Section 4.2.3 and used to describe the bimodality of the distribution of M in Sec. 4.2.4. Then, in Sec. 4.2.6, the canonical structures compatible with the long-term memory of the present PQ model are described. Section 4.3 focuses on PQ starting from complete thermal equilibrium without constraints. We show that the probability distribution under a given number of quenched spins can also be obtained as the stable limit distribution of a different process that we call Recycled Quenching (RQ). The latter process consists of the alternative application of single-step unquenching and single-step quenching of randomly chosen quenched spin and unquenched spin, respectively. The detail of RQ is described in Section 4.3.1 followed by the analysis of the limit-cycle distribution in Sec. 4.3.3. Finally, in Sec. 4.3.4, the connection to PQ through the martingale is given. We then extend our analysis to understand the conditions under which the canonical characteristics of the whole ensemble (both quenched and unquenched) are conserved along the PQ process and how important is the Markovian assumption on the stochastic evolution for the martingale and underlying canonical structure. In Section 4.4 we introduce the "two-story ensemble" and argue that the detailed balance and the Markovian dynamics are required for this ensemble to be canonical (4.4). Although based on a particular model, our results show what the martingale can bring beyond its original definition in terms of conditional expectation. It is currently unknown to what extent our results can be generalized. More discussion is given in Section 4.7.

The first half of this chapter is extracted from our 2022 article [3] (up until Section 4.4). The rest is extracted from our 2023 preprint [4].

4.2 Martingale property as a local invariance and its consequence in PQ

4.2.1 Fock-like space of probability distributions

We recall that the statistical quantity of main interest is the probability distribution of quenched magnetization, $\{P(T,M)\} \equiv \{P(T,-T), P(T,-T+2), \ldots, P(T,T)\}$ at each stage T. Such distribution can be treated as a vector $\vec{P}(T)$ in the $(T+1)$-dimensional Euclidean space. Because of the normalization condition, this vector spans a T-dimensional simplex. When we consider the evolution of the probability distribution from $T=0$ where $P(0,0)=1$, up to $T=N_0$, we effectively use a kind of Fock space in which $\vec{P}(T)$ is found in the T-th sector. The process of PQ is a linear mapping between adjacent sectors from, for example, $\vec{P}(T)$ to $\vec{P}(T+1)$ through a transfer matrix. We have shown in the previous chapters that under the critical coupling $j = j_{crit}(N_0)$ the distribution $\vec{P}(T)$ undergoes a unimodal to bimodal transition for some T, whose value depends on N_0.

4.2.2 Local invariance of the path weight

The martingale property of ${m^{(\mathrm{eq})}}_{T,M}$ induced by the Markovian process $\{M_T\}$ reads :

$$E[{m^{(\mathrm{eq})}}_{T+1,M_{T+1}}|M_T] = {m^{(\mathrm{eq})}}_{T,M_T} \tag{4.1}$$

As $M_T - M_{T-1}$ takes the Ising spin variable, the conditional probabilities in (4.1) are given in terms of ${m^{(\mathrm{eq})}}_{T,M_T}$, and we have

$$\begin{aligned} {m^{(\mathrm{eq})}}_{T-1,M_{T-1}} &= {m^{(\mathrm{eq})}}_{T,M_{T-1}+1}\frac{1+{m^{(\mathrm{eq})}}_{T-1,M_{T-1}}}{2} &(4.2)\\ &+ {m^{(\mathrm{eq})}}_{T,M_{T-1}-1}\frac{1-{m^{(\mathrm{eq})}}_{T-1,M_{T-1}}}{2}, &(4.3)\end{aligned}$$

where, for later convenience, we have shifted the time T by one. Using the identity

$$2c - a(1+c) - b(1-c) = (1+c)(1-a) - (1-c)(1+b), \tag{4.4}$$

Eq.(4.2) can be rewritten in the form of a *local invariance of path-weight* for the stochastic process M.

$$\left(\frac{1+{m^{(\mathrm{eq})}}_{T-1,M}}{2}\right)\left(\frac{1-{m^{(\mathrm{eq})}}_{T,M+1}}{2}\right) = \left(\frac{1-{m^{(\mathrm{eq})}}_{T-1,M}}{2}\right)\left(\frac{1+{m^{(\mathrm{eq})}}_{T,M-1}}{2}\right) \tag{4.5}$$

where M_{T-1} has been simply denoted by M. Schematically (4.5) implies that the path weight is invariant under a local change between $(T-1,M) \to (T,M+1) \to (T+1,M)$ and $(T-1,M) \to (T,M-1) \to (T+1,M)$, see Fig.4.1(a).

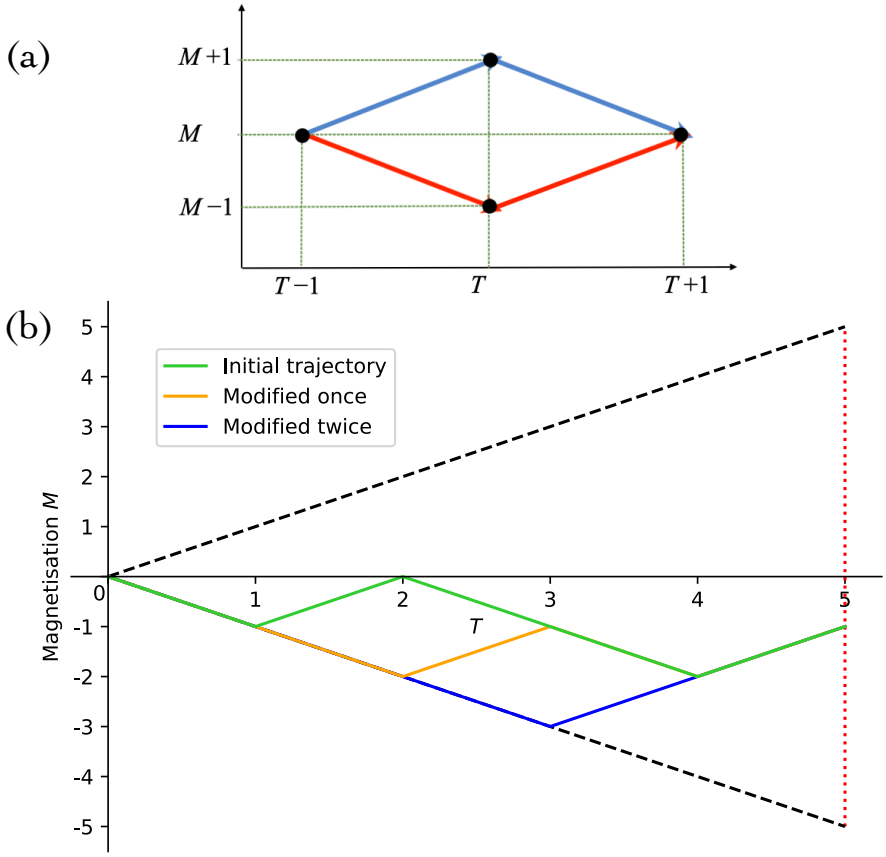

Figure 4.1: (a): Local invariance of the path weight as a consequence that the mean equilibrium spin ${m^{(\mathrm{eq})}}_{T,M}$ is martingale. The upper (blue) and lower (red) paths are weighted, respectively, by the l.h.s. and r.h.s. of Eq.(4.5).
(b): Three representative paths connecting $(T, M) = (0, 0)$ and $(5, -1)$. All the three paths have the same probability weight due to the local invariance relation Eq.(4.5).

The local invariance shown in Fig.4.1(a) significantly reduces the number of independent transition probabilities to an extensive one that only depends on the start and end points of the path considered. In fact, the $\frac{T(T-1)}{2}$ plaquettes [69] like Fig.4.1(a) between $T = 0$ ant $T = T$ impose as many constraints on ${m^{(\mathrm{eq})}}_{T',M}$ with $0 \le T' \le T-1$. As the latter counts $\frac{T(T+1)}{2}$ values, the difference makes T. Moreover, the symmetry with respect to $\pm M$ reduces the freedom among $\{{m^{(\mathrm{eq})}}_{M,T}\}$ down to $\lfloor \frac{T}{2} \rfloor$, where $\lfloor x \rfloor$ is the floor function. The reduction of independent weight may reflect the persistent memory we have found before [2].

4.2.3 Probability distributions of PQ

The new property of the martingale ${m^{(\mathrm{eq})}}_{T,M}$ in (4.5) reveals a "thermodynamic" structure in the evolution of $\vec{P}(T)$. In general, the probability $P(T, M)$ is the sum of the path weight over all paths arriving at (T, M) from $(0, 0)$. However, the relation (4.5) in the present system implies the degeneracy of all such path weights. For illustration Fig.4.1(b) shows the three paths among those reaching $(T, M) = (5, -1)$ from $(0, 0)$. The green (top) path

can be represented as a binary sequence, 01001, where 1 [0] means, respectively, to quench $+1$ $[-1]$ spin. The relation (4.5) means that the path weight is unchanged if we exchange any pair of neighboring bits. Therefore, the orange (middle) path, 00101, and then the blue (bottom) path, 00011, have the same path weight as the green (top) one.

The immediate consequence is that all the paths connecting the origin $(0,0)$ to a certain destination (T,M) through PQ have the same weight, which only depends on the number of 1 [0] bits, or equivalently, on (T,M), see Fig. 4.1(b). We shall denote such weight by $e^{-\tilde{\beta}\mathcal{E}(T,M)}$, where $\tilde{\beta}\equiv 1$ and the function $\mathcal{E}(T,M)$ gives a "path-weight potential" landscape on the (T,M) plane. Having known the individual path weight, the sum of the path weight is obtained by counting the number of distinct paths connecting $(0,0)$ and (T,M), which is the binomial coefficient $\binom{T}{\frac{M+T}{2}}$. We shall denote this number by $e^{\mathcal{S}}$, where $\mathcal{S}$ represents a "path-counting entropy". The latter is analogous to the conformational entropy of a one-dimensional random walk or free polymer chain. If we regard (T,M) as the mesoscopic "state variable" of PQ, the associated microstates (i.e., the paths reaching (T,M)) satisfy equipartition.

In summary the probability $P^{(PQ)}(T,M)$ is given by the Boltzmann factor of a "path free energy", $\mathcal{E}-\frac{1}{\tilde{\beta}}\mathcal{S}$, so that

$$P^{(PQ)}(T,M)=e^{\mathcal{S}(T,M)-\tilde{\beta}\mathcal{E}(T,M)}, \tag{4.6}$$

where

$$e^{\mathcal{S}(T,M)}=\binom{T}{\frac{M+T}{2}} \tag{4.7}$$

$$\begin{aligned} e^{-\tilde{\beta}\mathcal{E}(T,M)} &= \prod_{0\le i<(T-M)/2}\left(\frac{1-m^{(eq)}_{i,-i}}{2}\right) \\ &\times \prod_{1\le i\le(T+M)/2}\left(\frac{1+m^{(eq)}_{T-i,M-i}}{2}\right) \end{aligned} \tag{4.8}$$

This is the first of our main results. Remarkably, the structure of Eq.(4.7) corresponds to a constrained canonical equilibrium with identical entropic factors. The latter is calculated in Section 4.2.5.1. By this matching, we also have the equality between $\tilde{\beta}\mathcal{E}(T,M)$ and the canonical energy, which justifies our designation.

In Fig.4.2, the solid (red) curve shows $\tilde{\beta}\mathcal{E}-\mathcal{S}$ for $T=N_0=256$, while the red-dotted one represents $\log P(T,M)$ which is directly calculated by solving the master equation for the distribution. In Section 4.3.4 we will find Eq. (4.6) by a completely different approach: the "recycled quenching".

As a natural extension of the above argument of the path-weight potential and path-counting entropy, we can also have the compact expression of the propagator $P^{(PQ)}(T,M;T_0,M_0)$ with $0\le T_0\le T\le N_0$, which gives the conditional probability for $M_T=M$ to occur at the stage-T given the initial condition $P^{(PQ)}(T_0,M;T_0,M_0)=\delta_{M,M_0}$. Following the same argument as (4.6) and (4.7) the value of $P^{(PQ)}(T,M;T_0,M_0)$ can be given in terms of $\mathcal{E}(T,M;T_0,M_0)$ and $\mathcal{S}(T,M;T_0,M_0)$, whose detailed account may not be necessary to repeat.

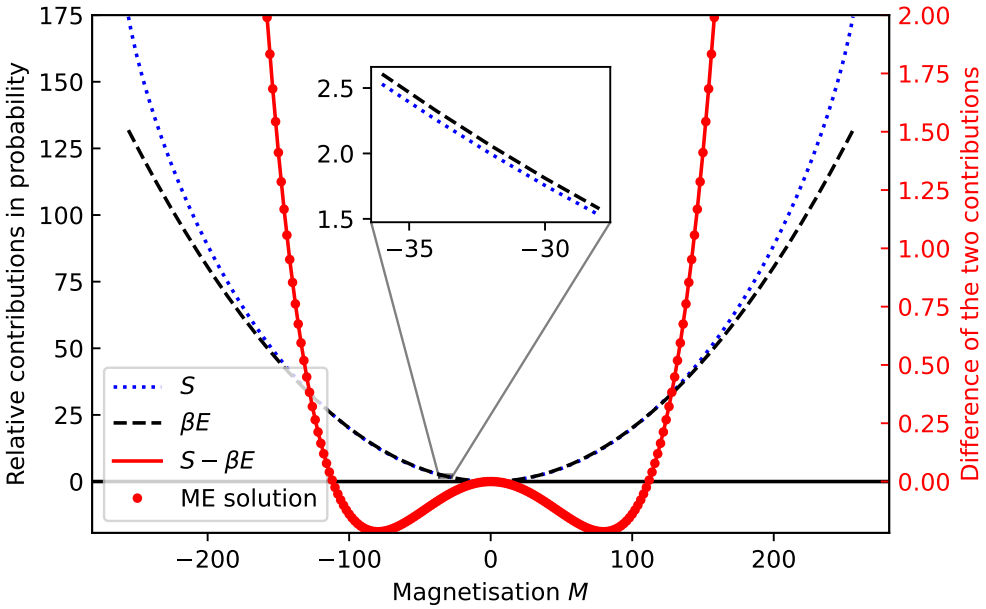

Figure 4.2: *Dashed and dotted curves, left ordinate*: $(-\tilde{\beta}\mathcal{E})$ (dashed black) and $(-\mathcal{S})$ (dotted blue) versus M. The value of each curve at $M = 0$ is adjusted vertically so that they share a unique origin. These two curves crosses $(\tilde{\beta}\mathcal{E} = \mathcal{S})$ at some finite $|M| > 0$. *Solid red curve, right ordinate*: The "path free energy", $\tilde{\beta}\mathcal{E} - \mathcal{S} = (-\log P(T, M))$ $(\tilde{\beta} \equiv 1)$, versus M (abscissa) for $T = N_0 = 256$. The large-dotted curve also represents $(-\log P(T, M))$ but is directly calculated by the master equation (ME), that is, by the repeated multiplication of the transfer matrix of PQ.

4.2.4 Origin of the bimodality as "potential-entropy" trade-off

We have encountered bimodal distributions for M during PQ even if the coupling j/N_0 is not in the ferromagnetic regime. The symmetry breaking does not occur for a finite size N_0, and the propensity of non-zero M should not be taken as the equilibrium phase transition. The above "thermodynamic" decomposition allows us to understand how the bimodality of the probability distribution can arise. We may constitute the following qualitative argument: When the total magnetization M is non-zero, the molecular field, $(j/N_0)M$, on the unquenched spins makes non-zero mean equilibrium spin, $m^{(eq)}_{T,M}$. This causes the biased probability of subsequently quenched spin, reinforcing the non-zero magnetization M as positive feedback. This is the scenario for the instability of $\tilde{\beta}\mathcal{E} - \mathcal{S}$ around $M = 0$. By contrast, the path-counting entropy factor becomes highly diminished for $|M| \sim T$, reflecting the limited availability of paths. This explains the high rise of $\tilde{\beta}\mathcal{E} - \mathcal{S}$ for $|M| \sim T$. The competition between these two factors can give rise to the bimodal distribution. At the early stages, $T \ll N_0$, however, the entropy factor prevails, and the distribution is unimodal [2].

While the above "thermodynamic" picture explains the qualitative origin of bimodality, a more subtle question would be whether such an aspect persists in the limit of large systems, $N_0 \to \infty$, especially when j is chosen to be at the extrapolated Curie point (see

Sec. 2.3.3). The short answer is yes, and we expect that $P(T = N_0; M)$ has maxima at $M = \pm M^\circ(N_0)$, where $M^\circ(N_0) \sim (N_0)^{1-\frac{\nu}{2}}$ with $\nu \simeq 0.933$ being the finite-size scaling exponent such that $j_{crit}(N_0) = 1 + c(N_0)^{-\nu}$. The detailed calculations are developed below in the next section.

4.2.5 Bimodality in the asymptotic limit

We argue that the distribution $P(T = N_0, M)$ remains bimodal in the asymptotic limit $N_0 \to \infty$. Even though the split is of order close to $(\sqrt{N_0})$ the limit distribution is not Gaussian.

4.2.5.1 Canonical sub-distribution

First of all let us write the canonical distribution of globally-coupled Ising spins under the constrain that T of these spins add up to a certain magnetization M.

Let us denote by $\sigma_{0,0}$ all the configurations of the Ising spins, $\{s_1, \ldots, s_{N_0}\}$, and by $\sigma_{T,M}$ the sub-ensemble of spin configurations under the constraints, $s_1 = \ldots = s_{\frac{T+M}{2}} = +1$ and $s_{\frac{T+M}{2}+1} = \ldots = s_T = -1$. Then we define the sub-partition function $Z(\sigma_{T,M}) \equiv \sum_{\{s_1,\ldots,s_{N_0}\} \in \sigma_{T,M}} e^{-H}$ (we have taken the unit of energy such that $\beta = (k_{\rm B}T)^{-1} = 1$). By definition, $Z(\sigma_{0,0})$ is the full partition function. Now the canonical probability $P^{(can)}(T, M)$ of observing that $\sum_{i=1}^{T} s_i = M$ is $\sigma_{T,M}$ among $\sigma_{T,M}$ reads

$$\begin{aligned} P^{(can)}(T, M) &= \binom{T}{\frac{T+M}{2}} \frac{Z(\sigma_{T,M})}{Z(\sigma_{0,0})} \\ &= \text{cst.} \binom{T}{\frac{T+M}{2}} \int_{-\infty}^{+\infty} e^{-\frac{j}{2N_0}(y^2 - M^2)} \left(2 \cosh \left[\frac{j}{N_0}(y + M) \right] \right)^{N_0 - T} dy \\ &= \text{cst.} \binom{T}{\frac{T+M}{2}} \sum_{k=0}^{N_0 - T} \binom{N_0 - T}{k} e^{\frac{j}{2N_0}(2k - N_0 + T + M)^2} \end{aligned} \tag{4.9}$$

where the Hubbard-Stratonovich transformation [37] has been used to do the sum over the allowed spin configurations, and "cst." is a constant independent of T and M. Especially the result is simple and well-known for $T = N_0$, where

$$P^{(can)}(N_0, M) = \text{cst.} \binom{N_0}{\frac{N_0+M}{2}} e^{\frac{j}{2N_0} M^2}. \tag{4.10}$$

We will use this last result below.

4.2.5.2 Bimodality of Distribution under Critical Coupling

Preparation of $m^{(\rm eq)}{}_{T,M}$: The basic quantity is the mean equilibrium spin $m^{(\rm eq)}{}_{T,M}$ which is defined by $m^{(\rm eq)}{}_{T,M} = \frac{\partial}{\partial h}\left(\frac{\log Z}{N}\right)$, where Z is the partition function for the $N = N_0 - T$ Ising spins with the pair coupling $\frac{j}{N_0}$ and under the "molecular field" $h \equiv \frac{j}{N_0} M$.

Using the Hubbard-Stratonovich transformation, it reads $Z \propto \int e^{N\psi(m)} dm$, where

$$\psi(m) := -\frac{j_{\rm eff}}{2} m^2 + \log[\cosh(h + j_{\rm eff} m)] \tag{4.11}$$

$$j_{\rm eff} := \frac{N}{N_0} j = \Big(1 - \frac{T}{N_0}\Big) j. \tag{4.12}$$

We will use the saddle-point approximation for the integral in Z, which is valid for T such that $\mathcal{O}(\frac{N}{N_0}) = 1$ and also $\mathcal{O}(\frac{T}{N_0}) = 1$.

$$\int e^{N\psi(m)} dm \simeq e^{N\psi(m^*)} \sqrt{\frac{2\pi}{N|\psi''(m^*)|}} \tag{4.13}$$

$$m^* = \tanh(h + j_{\rm eff} m^*) \tag{4.14}$$

where the second equation defining m^* originates from $\psi'(m^*) = 0$. Using the standard identities of the tanh function, we can show several formulas such as : $\frac{\partial \psi(m^*)}{\partial h} = m^*$, $\psi''(m^*) = -j_{\rm eff} + (j_{\rm eff})^2[1 - (m^*)^2]$, $\frac{\partial m^*}{\partial h} = \frac{1-(m^*)^2}{1-j_{\rm eff}(1-(m^*)^2)}$. Combining these, we arrive at a closed set of equations yielding ${m^{(\rm eq)}}_{T,M}$:

$$\begin{aligned} {m^{(\rm eq)}}_{T,M} &= m^* - \frac{1}{2N} \frac{\frac{jN}{N_0} m^*[1 - (m^*)^2]}{\Big(1 - \frac{jN}{N_0}[1 - (m^*)^2]\Big)^2}, \\ m^* &= \tanh\left(\frac{jM}{N_0} + \frac{jN}{N_0} m^*\right) \end{aligned} \tag{4.15}$$

The condition $\mathcal{O}(\frac{T}{N_0}) = 1$ is also necessary when j is close to the critical value, which is 1 for $N_0 \to \infty$. Since j appears through $j_{\rm eff} = jN/N_0$, the denominator of the second term on the r.h.s. of the first equation in (4.15) can become very small for small values of T, invalidating (4.15). In assuming both $\mathcal{O}(\frac{N}{N_0}) = 1$ *and* $\mathcal{O}(\frac{T}{N_0}) = 1$, we will ignore this term as $\mathcal{O}(N_0^{-1})$. In short, in (4.15) the $\mathcal{O}(N^{-1})$ term serves only for detecting its validity limit.

Split of the maxima of probability, $M^\circ(T)$. The extrema $M = M^\circ(T)$ of the probability distribution $P(T, M)$ is found from Eq. (14) such that $P(T, M^\circ - 1) = P(T, M^\circ + 1)$. The result reads

$${m^{(\rm eq)}}_{T,M^\circ(T)} = \frac{M^\circ(T)}{T + 2}. \tag{4.16}$$

(We generalize this condition for non-integer M° because $M^\circ \gg 1$ for large N_0.) $M^\circ(T) = 0$ is always the solution for symmetry reasons. Besides, if $M^\circ > 0$ exists, $(-M^\circ)$ does also. Using (4.15) with ignoring the second term on the r.h.s. of the first equation, (4.16) becomes we have

$$\frac{M^\circ(T)}{T + 2} = \tanh\left[j(1 + \frac{2}{N_0}) \frac{M^\circ(T)}{T + 2}\right]. \tag{4.17}$$

It tells that $M^\circ(T)/(T + 2)$ is independent of T. This linearity, $M^\circ(T) \propto (T + 2)$ for $\mathcal{O}(\frac{N}{N_0}) = 1$ and $\mathcal{O}(\frac{T}{N_0}) = 1$, is verified by direct calculation of the distributions. Anticipating that $M^\circ(T)/(T + 2) \ll 1$ for $N_0 \gg 1$ we can use $\tanh z \simeq z - \frac{1}{3} z^3$. Especially,

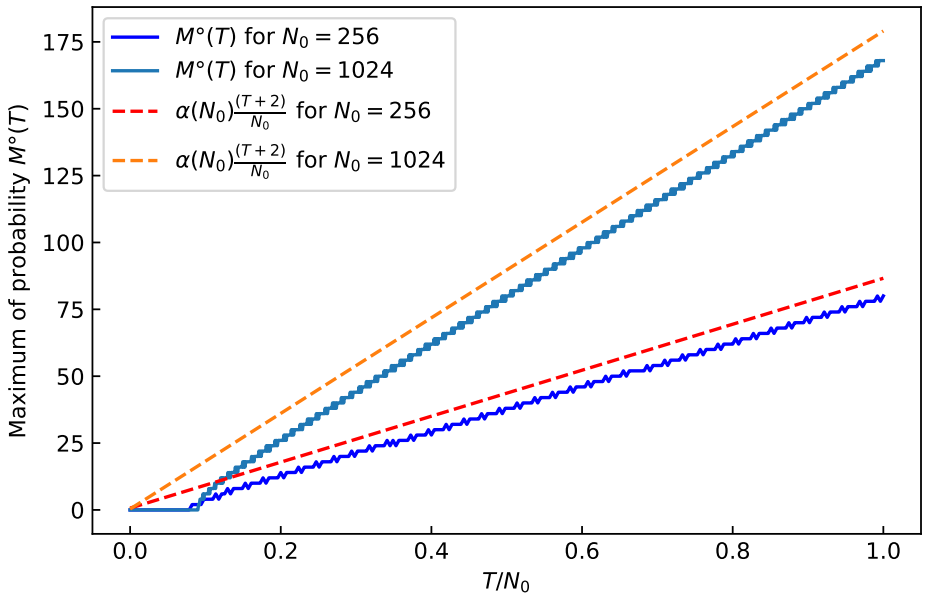

Figure 4.3: Position of the bimodal peak of $P^{[\infty]}(T, M)$ versus $\frac{T}{N_0}$ for $N_0 = 256$ (bottom curve) and $N_0 = 1024$ (top) obtained numerically (*solid curves*). The *dashed red curves* show the respective asymptotic formula Eq.(4.18).

when $0 < j - 1 \ll 1$ we have

$$\frac{M^\circ(T)}{T+2} \simeq \sqrt{3\Big(\frac{2}{N_0} + j - 1\Big)} \tag{4.18}$$

and the result is consistent, i.e., $M^\circ(T)/(T+2) \ll 1$.

If we use j at the "critical value," $j_{\rm crit}(N_0) \simeq 1 + \frac{c}{(N_0)^\nu}$ with $c = 5.06$ and $\nu = 0.933$ according to [1], the above approximation expects $M^\circ(T) \simeq \alpha(N_0)\frac{T+2}{N_0}$ with $\alpha(N_0) = \sqrt{3(2 + cN_0^{1-\nu})}N_0^{\frac{1}{2}}$. In Fig.4.3 we show the numerical result for $M^\circ(T)$ vs $\frac{T}{N_0}$ for different sizes, N_0, without the saddle-point approximation. What we observed so far is that, once the bimodality appears at some stage of progressive quenching, $T = T_0 (< N_0)$, it remains for any T with $T_0 \le T \le N_0$. Admitting this as a fact, we conclude that the bimodality of $P(T = N_0, M)$ remains and we expect $M^\circ(N_0) \simeq \sqrt{3c}N_0^{\frac{2-\nu}{2}}$. This claim is consistent with the claim that $\vec{P}^{(PQ)}(T)$ that started from the condition $\vec{P}^{(PQ)}(0) = \{1\}$ is the canonical weight for the sub-distribution $\vec{P}^{(can)}(T)$. In fact for $T = N_0$ such canonical weight (4.9) is analytically tractable and read for $N_0 \gg 1$ as follows:

$$P^{(can)}(N_0, M) = \text{cst.}\binom{N_0}{\frac{N_0+M}{2}} e^{\frac{j}{2N_0}M^2} \simeq \sqrt{\frac{2}{\pi(1-\mu^2)}}e^{-N_0\phi(\mu;j)} \tag{4.19}$$

with $\mu = \frac{M}{N_0}$ and $\phi(\mu; j)$ being the rate function of the large deviation principle given by

$$\phi(\mu; j) = \frac{j}{2}\mu^2 - \frac{1+\mu}{2}\log(1+\mu) - \frac{1-\mu}{2}\log(1-\mu) \simeq \frac{1-j}{2}\mu^2 + \frac{\mu^4}{12}. \tag{4.20}$$

This also gives $\frac{M^\circ}{N_0} \simeq \sqrt{3(j-1)}$ in the limit $N_0 \to \infty$, being consistent with (4.18). Because $1 - j_{\rm crit}(N_0) \to 0$ under $N_0 \to \infty$, the PQ makes the distribution approach to the critical one $P^{(\rm can)}(\infty, M)$ as limit of bimodal distribution.

As for small values of T, the full numerical results show the unimodal-bimodal transition with T, see Fig.4.3 (thick curves).

4.2.6 Constrained canonical statistics by PQ

One might wonder if the equilibrium canonical distribution lies behind the "thermodynamic" structure of (4.6). The answer is yes, but under constraints: If, and only if, the PQ starts from the unbiased initial condition, $M_{T=0} = 0$ with probability one, does the probability $P^{(PQ)}(T, M)$ have the canonical equilibrium weight for the event that the group of spins $\{s_1, \ldots, s_T\}$ has the magnetization $\sum_{i=1}^T s_i = M$. By contrast, if T_0 spins have already been quenched with their magnetization being M_0, the later probability for $T \geq T_0$, or the propagator $P^{(PQ)}(T, M; T_0, M_0)$ of Section 4.2.3 retains a persistent memory and the distribution coincides with a *constrained* canonical weight for the event that the group of spins $\{s_1, \ldots, s_T\}$ has the magnetization, $\sum_{i=1}^T s_i = M$, *under the constraint* that its subset, $\{s_{i_1}, \ldots, s_{i_{T_0}}\} \subset \{s_1, \ldots, s_T\}$, has the magnetization M_0. The fact that this function has a strict support (of causality) $|M - M_0| > T - T_0$ along the M axis is consistent with the above constraint.

Altogether, the two facets of PQ, the neutrality of quenching hitherto equilibrated spins on the one hand and the persistence of memory in quenched spins on the other hand, are compatible in the form of the constrained canonical distribution.

Below, we argue that the mechanism behind this compatibility is the close relationship between the conditional probability and the act of quenching a spin. Let us denote by $P^{(\rm eq)}(s_i|s_{i-1}, \ldots s_1)$ the conditional probability that the i-th spin s_i takes the specified value (± 1) in a canonical equilibrium ensemble of N_0 spins, $\{s_1, \ldots, s_{N_0}\}$, given that the spins $\{s_1, \ldots, s_{i-1}\}$ are found to take the specified values. Also let us denote by $P^{(\rm PQ)}(s_i|s_{i-1}, \ldots s_1)$ the conditional probability that the i-th spin s_i takes the specified value (± 1) upon quenching in a *constrained* canonical equilibrium ensemble of $N_0 - (i-1)$ spins, $\{s_i, \ldots, s_{N_0}\}$, given that the other spins $\{s_1, \ldots, s_{i-1}\}$ have already been frozen to take the specified values. We may then expect the following equality,

$$P^{(\rm PQ)}(s_i|s_{i-1}, \ldots s_1) = P^{(\rm eq)}(s_i|s_{i-1}, \ldots s_1). \tag{4.21}$$

On the other hand, if the first spin s_1 has been quenched when the whole system $\{s_1, \ldots, s_{N_0}\}$ was in equilibrium, the probability of the quenched spin $P^{(\rm PQ)}(s_1)$ should be equal to the equilibrium one:

$$P^{(\rm PQ)}(s_1) = P^{(\rm eq)}(s_1). \tag{4.22}$$

We then have the equality of the joint probabilities,

$$P^{(\rm PQ)}(s_n, \ldots s_1) = P^{(\rm eq)}(s_n, \ldots s_1), \tag{4.23}$$

for $2 \leq n \leq N_0$ because of the general chain rule, which is valid for both $P^{(\rm PQ)}$ and $P^{(\rm eq)}$

:

$$\begin{aligned} P(s_n, \dots s_1) = & \prod_{i=2}^{n} \left(\frac{P(s_i, \dots, s_1)}{P(s_{i-1}, \dots, s_1)} \right) P(s_1) \\ = & \left(\prod_{i=2}^{n} P(s_i | s_{i-1}, \dots, s_1) \right) P(s_1). \end{aligned} \tag{4.24}$$

Said differently, freezing spins one by one quasi-statically gives the same result as freezing them all together as a snapshot.

While (4.21) seems to hold for the quasi-equilibrium quenching with any choice of $\{s_{i-1}, \dots, s_1\}$, the last result (4.23) holds only with the equilibrium starting point (4.22). If the PQ starts from $P^{(\mathrm{PQ})}(s_1)$ other than $P^{(\mathrm{eq})}(s_1)$ or from some prefixed spins $\{s_{n_0}, \dots, s_1\}$, the progression of PQ carries non-volatile memory, preventing the relaxation to the canonical weight.

4.3 Recycled Quenching (RQ)

4.3.1 Single-step unquenching S and single-step quenching K

Let us leave momentarily from the analysis of the progressive operation of quenching (PQ) and instead consider the cyclic operation of a single-step quenching and un-quenching (recycled quench, or RQ for short). See Fig.4.4. We propose the following process: Take again a system of N_0 Ising spins on a complete network, like our globally-coupled model. Suppose T spins are quenched with a total quenched magnetization M while the $N_0 - T$ remaining spins are thermalized with a bath. We then randomly select a quenched spin and allow it to be unquenched (operation $\boldsymbol{S}$). Subsequently, after reaching thermal equilibrium once again, we apply a single step of quenching step (similar to Sec. 2.2) (operation $\boldsymbol{K}$). While the number of quenched spin returns from $T-1$ to T, the updated state of the system may have its quenched magnetization either set to M or $M \pm 2$.

By applying alternatively the unquenching ($\boldsymbol{S}$) and quenching ($\boldsymbol{K}$), we generate a series of probability distributions, which may be written as follows:

$$\dots \xrightarrow{\boldsymbol{S}} \vec{Q}^{[\ell]}(T-1) \xrightarrow{\boldsymbol{K}} \vec{P}^{[\ell]}(T) \xrightarrow{\boldsymbol{S}} \vec{Q}^{[\ell+1]}(T-1) \xrightarrow{\boldsymbol{K}} \vec{P}^{[\ell+1]}(T) \xrightarrow{\boldsymbol{S}} \dots \tag{4.25}$$

where $\vec{P}$ and $\vec{Q}$ denote the probability vectors of having a specific magnetization after a step K or S, respectively, and the superfix $[\ell]$, etc. merely counts the number of iterated operations, and the number of fixed spins, T, is no more the 'time'.

If we focus on $\vec{P}(T)$'s, a single application of this *recycling* process can be seen as transformation over the probability vector $\vec{P}(T)$ by two operators : $\boldsymbol{S}$ then $\boldsymbol{K}$, leading to

$$\vec{P}^{[\ell+1]}(T) = (\boldsymbol{KS})\vec{P}^{[\ell]}(T). \tag{4.26}$$

Alternatively, if we focus on $\vec{Q}(T-1)$'s, we can think of an adjoint process, where the two steps are reversed in order, i.e., $\boldsymbol{K}$ then $\boldsymbol{S}$, leading to

$$\vec{Q}^{[\ell+1]}(T-1) = (\boldsymbol{SK})\vec{Q}^{[\ell]}(T-1). \tag{4.27}$$

In either point of view, the recycling process retains the number of quenched spins. Al-

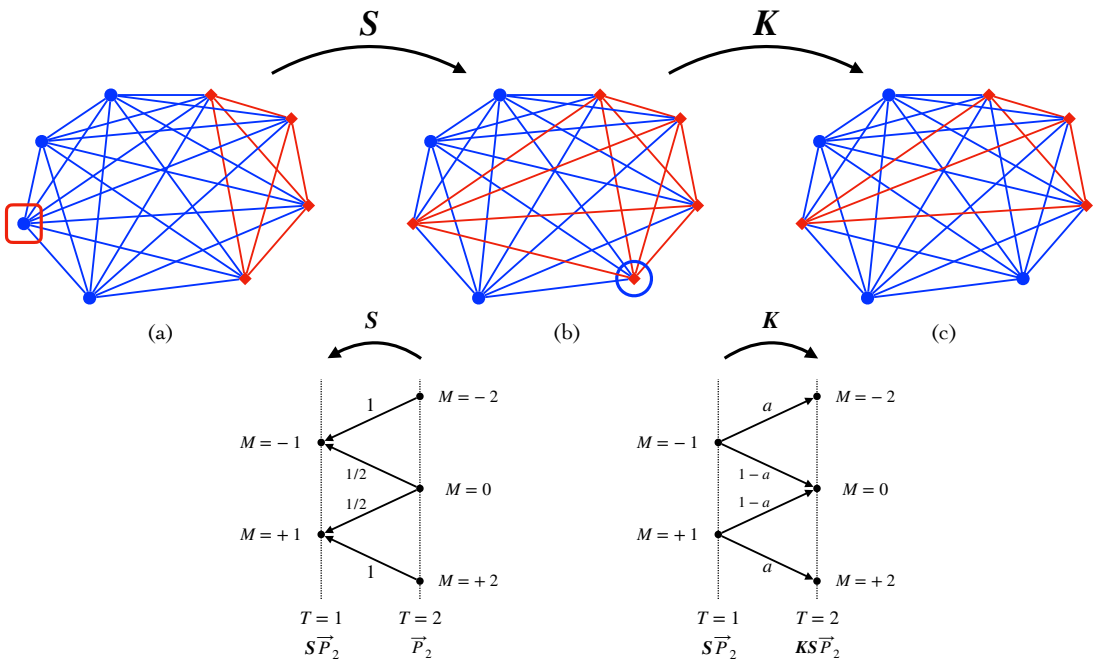

Figure 4.4: *Top row:* Schematic representation of the recycled quenching process. (a): Step $\boldsymbol{S}$: A quenched spin - blue circle (darker gray) and squared in red (lighter gray) - is picked at random and is unquenched. (b): Step $\boldsymbol{K}$: A unquenched spin (red square circled in blue) is quenched as in the Progressive Quenching. (c): Updated state of the system after operating $\boldsymbol{S}$. then $\boldsymbol{K}$. *Bottom row:* Probability tree of the operation of $\boldsymbol{S}$ *(left)* and $\boldsymbol{K}$ *(right)* over distributions for the stages $T = 1$ and $T = 2$.

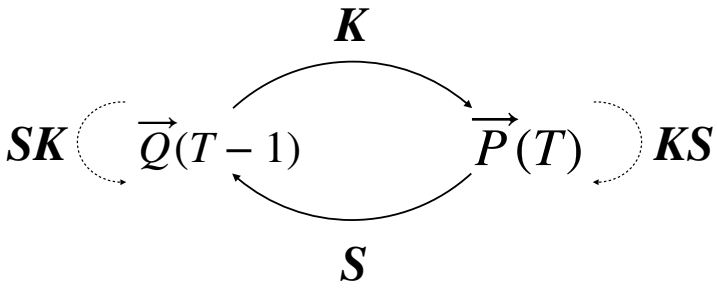

Figure 4.5: Symbolic representation of the action of the recycling operators over the distributions $\vec{P}(T)$ and $\vec{Q}(T-1)$.

together, we can schematize the operation of unquenching and quenching in the form of Fig.4.5. The detailed action of $\boldsymbol{K}$ and $\boldsymbol{S}$ over a probability distribution are detailed below:

4.3.2 Calculation of transfer matrices under $\boldsymbol{K}$, $\boldsymbol{S}$, $\boldsymbol{KS}$ and $\boldsymbol{SK}$

In this section, we derive the transfer matrix elements for the probability vector under the operation of progressive quench $\boldsymbol{K}$, unquenching of randomly selected spin $\boldsymbol{S}$, as well as their combinations $\boldsymbol{KS}$ and $\boldsymbol{SK}$.

We will use the symbol $\delta(\,)$ for the Kronecker's delta, i.e., $\delta(n)$ with $n \in \mathbb{Z}$ takes the value 1 for $n = 0$ and 0 otherwise. We also write the conditional expectation using the symbol E, such as $E[X|Y]$ for the expectation of X given the knowledge of Y. When Y is a random variable, $E[X|Y]$ does also. The component $P(T, M)$ of the probability vector $\vec{P}(T)$ reads

$$P(T, M) = E[\delta(M - \hat{M}_T)]. \tag{4.28}$$

We will abuse the operators $\boldsymbol{K}$ and $\boldsymbol{S}$ to act both on the quenched magnetization $\hat{M}_T$ when T spins are fixed and also on the probability vector $\vec{P}(T)$, i.e., on the ensemble of systems having different M_T according to the given weights. When $\boldsymbol{L}$ stands for the operators, $\boldsymbol{K}$, $(\boldsymbol{KS})$, etc.,

$$\begin{aligned} E[\delta(M - \boldsymbol{L}\hat{M}_T)|\hat{M}_T] &= \sum_k \delta(M - (\hat{M}_T + k))a_{T,k}(\hat{M}_T) \\ &= \sum_k \delta((M-k) - \hat{M}_T)a_{T,k}(M-k), \end{aligned} \tag{4.29}$$

where $a_{T,k}(\,)$ are the weights, can be translated into the usual representation in terms of the transfer matrix elements as

$$\boldsymbol{L}P(T, M) = \sum_k P(T, M-k)a_{T,k}(M-k), \tag{4.30}$$

Operation of $\boldsymbol{K}$: As described above, $\boldsymbol{K}\hat{M}_T$ means the quenched magnetization after an unquenched spin out of $N_0 - T$ ones has been quenched. The system then has $T + 1$

quenched spin. The conditional distribution of the resulting magnetization reads,

$$\begin{aligned} E[\delta(M-\boldsymbol{K}\hat{M}_T)|\hat{M}_T] &= \delta(M-(\hat{M}_T+1))\frac{1+m^{(\mathrm{eq})}{}_{T,\hat{M}_T}}{2} \\ &+ \delta(M-(\hat{M}_T-1))\frac{1-m^{(\mathrm{eq})}{}_{T,\hat{M}_T}}{2} \\ &= \delta(M-1-\hat{M}_T)\frac{1+m^{(\mathrm{eq})}{}_{T,M-1}}{2} \\ &+ \delta(M+1-\hat{M}_T)\frac{1-m^{(\mathrm{eq})}{}_{T,M+1}}{2} \end{aligned} \tag{4.31}$$

We rewrite (4.31) with $T \to T-1$ for later convenience.

$$\begin{aligned} E[\delta(M-\boldsymbol{K}\hat{M}_{T-1})|\hat{M}_{T-1}] = \\ \delta(M-1-\hat{M}_{T-1})\frac{1+m^{(\mathrm{eq})}{}_{T-1,M-1}}{2} \\ +\delta(M+1-\hat{M}_{T-1})\frac{1-m^{(\mathrm{eq})}{}_{T-1,M+1}}{2} \end{aligned} \tag{4.32}$$

or, using the general relationship (4.29) we find $\boldsymbol{K}\vec{P}(T-1)$ as the probability vector in the T-sector with the component,

$$\begin{aligned} (\boldsymbol{K}\vec{P}(T-1))_M &= P(T-1,M-1)\frac{1+m^{(\mathrm{eq})}{}_{T-1,M-1}}{2} \\ &+ P(T-1,M+1)\frac{1-m^{(\mathrm{eq})}{}_{T-1,M+1}}{2} \end{aligned} \tag{4.33}$$

Operation of $\boldsymbol{S}$: We denote by $\boldsymbol{S}\hat{M}_T$ the quenched magnetization after a quenched spin out of T ones has been unquenched. The system has $T-1$ quenched spins and N_0-T+1 unquenched spins. The conditional distribution of the resulting magnetization reads:

$$\begin{aligned} E[\delta(M-\boldsymbol{S}\hat{M}_T)|\hat{M}_T] &= \delta(M-(\hat{M}_T-1))\frac{1+\frac{\hat{M}_T}{T}}{2} + \delta(M-(\hat{M}_T+1))\frac{1-\frac{\hat{M}_T}{T}}{2} \\ &= \delta(M+1-\hat{M}_T)\frac{1+\frac{M+1}{T}}{2} + \delta(M-1-\hat{M}_T)\frac{1-\frac{M-1}{T}}{2}. \end{aligned} \tag{4.34}$$

Operation of $\boldsymbol{KS}$: $\boldsymbol{K}(\boldsymbol{S}\hat{M}_T)$ means to unquench randomly a spin among T quenched ones then quench randomly a spin among $N_0-(T-1)$ thermalized spins. Replacing in (4.32) $\hat{M}_{T-1}$ by $\boldsymbol{S}\hat{M}_T$, where $\boldsymbol{S}\hat{M}_T$ is given in (4.34), the result reads :

$$
\begin{aligned}
E[\delta(M-\boldsymbol{K}(\boldsymbol{S}\hat{M}_T))|\hat{M}_T] = {} & \delta(M-\hat{M}_T)\frac{1+\frac{\hat{M}_T}{T}}{2}\frac{1+{m^{(\mathrm{eq})}}_{T-1,\hat{M}_T-1}}{2} \\
& + \delta(M-2-\hat{M}_T)\frac{1-\frac{\hat{M}_T}{T}}{2}\frac{1+{m^{(\mathrm{eq})}}_{T-1,\hat{M}_T+1}}{2} \\
& + \delta(M+2-\hat{M}_T)\frac{1+\frac{\hat{M}_T}{T}}{2}\frac{1-{m^{(\mathrm{eq})}}_{T-1,\hat{M}_T-1}}{2} \\
& + \delta(M-\hat{M}_T)\frac{1-\frac{\hat{M}_T}{T}}{2}\frac{1-{m^{(\mathrm{eq})}}_{T-1,\hat{M}_T+1}}{2}
\end{aligned}
\tag{4.35}
$$

By taking the expectation over $\hat{M}_T$, i.e. the weighted summation $\sum_{M_T=-T}^{T} P(M_T,T)$, we have the evolution of $\vec{P}$ after a single cycle of operation, $\boldsymbol{KS}$. The fixed point equation (4.41) is obtained by requiring $(\boldsymbol{KS})\vec{P}(T)=\vec{P}(T)$. Rewriting this into the form of (4.41) is very close to the transformation from (4.2) to (4.5). The close relationship between the martingale and the harmonic function has long been known [70].

Operation of $\boldsymbol{SK}$: $\boldsymbol{S}(\boldsymbol{K}\hat{M}_T)$ means to quench randomly a spin among the N_0-T thermalized ones then unquenching randomly a spin among $T+1$ quenched ones. Like the case of operating $\boldsymbol{KS}$, the result reads

$$
\begin{aligned}
E[\delta(M-\boldsymbol{S}(\boldsymbol{K}\hat{M}_T))|\hat{M}_T] = {} & \left(\frac{1+{m^{(\mathrm{eq})}}_{T,M_T}}{2}\right) \\
& \times \left[\delta(M-M_T-2)\left(\frac{1-\frac{M_T+1}{T+1}}{2}\right)+\delta(M-M_T)\left(\frac{1+\frac{M_T+1}{T+1}}{2}\right)\right] \\
& + \left(\frac{1-{m^{(\mathrm{eq})}}_{T,M_T}}{2}\right) \\
& \times \left[\delta(M-M_T)\left(\frac{1-\frac{M_T-1}{T+1}}{2}\right)+\delta(M-M_T+2)\left(\frac{1+\frac{M_T-1}{T+1}}{2}\right)\right]
\end{aligned}
\tag{4.36}
$$

By taking the expectation over $\hat{M}_T$, i.e., the weighted summation $\sum_{M_T=-T}^{T} P(M_T,T)$, we have the evolution of $\vec{Q}$ upon after a single cycle of operation, $\boldsymbol{SK}$. The fixed point equation (13) in the main text is obtained by requiring $(\boldsymbol{SK})\vec{Q}(T)=\vec{Q}(T)$.

4.3.3 Stationary distributions

Case studies: Because the number of quenched spins remains the same after the action of $\boldsymbol{KS}$ and $\boldsymbol{SK}$, these combined operations are the transfer matrix on the vectors $\vec{P}$ and $\vec{Q}$, respectively. Applying the Perron-Frobenius theorem to those matrices ensures the existence of the non-degenerate maximum eigenvalue which is unity. Thus, we expect the presence of unique *stable* stationary distributions, $\vec{P}^{[\infty]}(T)$ and $\vec{Q}^{[\infty]}(T-1)$, respectively. We consider the cases $T=2$ and 3 below to understand the stability or convergence intuitively.

$T = 2$ **case:** Fig.4.4 (bottom left) indicates the transfer probabilities assigned to $\boldsymbol{S}$ acting on $\vec{P}_2$, where $\vec{P}_2 = (P(2,-2), P(2,0), P(2,+2))^t$, and Fig.4.4 (bottom right) indicates the transfer probabilities assigned to $\boldsymbol{K}$ acting on $\boldsymbol{S}\vec{P}_2$, where $a \equiv \frac{1+m_{1,+1}^{(eq)}}{2} = \frac{1-m_{1,-1}^{(eq)}}{2}$. The transfer matrix $\boldsymbol{KS}$ is, in this case :

$$\boldsymbol{KS} = \begin{pmatrix} a & \frac{a}{2} & 0 \\ 1-a & 1-a & 1-a \\ 0 & \frac{a}{2} & a \end{pmatrix} \tag{4.37}$$

A simple induction gives an explicit formula for $(\boldsymbol{KS})^N$ and its convergence:

$$\begin{aligned} (\boldsymbol{KS})^N &= \begin{pmatrix} \frac{a}{2} + \frac{a^N}{2} & \frac{a}{2} & \frac{a}{2} - \frac{a^N}{2} \\ 1-a & 1-a & 1-a \\ \frac{a}{2} - \frac{a^N}{2} & \frac{a}{2} & \frac{a}{2} + \frac{a^N}{2} \end{pmatrix} \\ &\stackrel{N\to\infty}{\longrightarrow} \begin{pmatrix} \frac{a}{2} & \frac{a}{2} & \frac{a}{2} \\ 1-a & 1-a & 1-a \\ \frac{a}{2} & \frac{a}{2} & \frac{a}{2} \end{pmatrix} \end{aligned} \tag{4.38}$$

Therefore, from whatsoever distribution $\vec{P}_2$ the result of RQ cycle, $(\boldsymbol{KS})^N\vec{P}(2)$, converges to the stationary distribution: $\vec{P}^{[\infty]}(2) = (\frac{a}{2}, 1-a, \frac{a}{2})^t$. We notice that this stationary distribution coincides with the one obtained by the progressive quenching from $P^{(PQ)}(0,0) = 1$, that is $\vec{P}^{(PQ)}(2) = \vec{P}^{[\infty]}(2)$ (see below).

$T = 3$ **case:** We can make the scheme similar to Fig.4.4 (bottom) to find the transfer matrix $\boldsymbol{KS}$. We then obtain :

$$\boldsymbol{KS} = \begin{pmatrix} b & \frac{b}{3} & 0 & 0 \\ 1-b & \frac{2-b}{3} & \frac{1}{3} & 0 \\ 0 & \frac{1}{3} & \frac{2-b}{3} & 1-b \\ 0 & 0 & \frac{b}{3} & b \end{pmatrix}, \tag{4.39}$$

where $b \equiv \frac{1+m_{2,+2}^{(eq)}}{2} = \frac{1-m_{2,-2}^{(eq)}}{2}$. Expression for $(\boldsymbol{KS})^N$ is rather cumbersome but we know the convergence of $(\boldsymbol{KS})$ by its eigenspectrum, $\{1, \frac{2b+1}{3}, \frac{2b}{3}, 0\}$, where we have $1 > (2b+1)/3 > 2b/3 > 0$ because $0 < b < 1$. The normalized eigenvector corresponding to the steady state is : $\vec{P}^{[\infty]}(3) = (\frac{b}{2(3-2b)}, \frac{3(1-b)}{2(3-2b)}, \frac{3(1-b)}{2(3-2b)}, \frac{b}{2(3-2b)})^t$. To compare, the distribution obtained by the progressive quenching reads $\vec{P}^{PQ}(3) = (\frac{ab}{2}, \frac{1-ab}{2}, \frac{1-ab}{2}, \frac{ab}{2})^t$ with b just defined and $a \equiv \frac{1+m_{1,1}^{(eq)}}{2}$ already defined above. This apparently different distribution is, in fact, identical to the former, $\vec{P}^{[\infty]}(3)$, because the martingale (4.2) - or the local invariance (4.5) - imposes the relation, $a = \frac{1}{3-2b}$.

General case: Altogether, from the previous case studies we admit that the iterative operation of $(\boldsymbol{KS})$ or $(\boldsymbol{SK})$ on a probability vector of the T-sector brings about the convergence to $\vec{P}^{[\infty]}(T)$ and $\vec{Q}^{[\infty]}(T)$, respectively, as stable fixed points:

$$(\boldsymbol{KS})\vec{P}^{[\infty]}(T) \;=\; \vec{P}^{[\infty]}(T)$$

$$(\boldsymbol{SK})\vec{Q}^{[\infty]}(T) \;=\; \vec{Q}^{[\infty]}(T) \tag{4.40}$$

These fixed points are also the eigenvectors of these operators with the maximum eigenvalue (= 1). Using the concrete expressions for the action of $(\boldsymbol{KS})$ and $(\boldsymbol{SK})$ the equations in (4.40) can be rewritten as follows, where we use the notations, $p_M = P^{[\infty]}(T, M)$ and $q_M = Q^{[\infty]}(T, M)$:

$$\begin{aligned} 0 = {} & p_{M-2}\Big(1 - \frac{M-2}{T}\Big)\Big(1 + {m^{(\mathrm{eq})}}_{T-1,M-1}\Big) \\ & - p_M\Big(1 + \frac{M}{T}\Big)\Big(1 - {m^{(\mathrm{eq})}}_{T-1,M-1}\Big) \\ & - \Big[p_M\Big(1 - \frac{M}{T}\Big)\Big(1 + {m^{(\mathrm{eq})}}_{T-1,M+1}\Big) \\ & - p_{M+2}\Big(1 + \frac{M+2}{T}\Big)\Big(1 - {m^{(\mathrm{eq})}}_{T-1,M+1}\Big)\Big] \end{aligned} \tag{4.41}$$

and similarly :

$$\begin{aligned} 0 = {} & q_{M-2}\Big(1 - \frac{M-1}{T+1}\Big)\Big(1 + {m^{(\mathrm{eq})}}_{T,M-2}\Big) \\ & - q_M\Big(1 + \frac{M-1}{T+1}\Big)\Big(1 - {m^{(\mathrm{eq})}}_{T,M}\Big) \\ & - \Big[q_M\Big(1 - \frac{M+1}{T+1}\Big)\Big(1 + {m^{(\mathrm{eq})}}_{T,M}\Big) \\ & - q_{M+2}\Big(1 + \frac{M+1}{T+1}\Big)\Big(1 - {m^{(\mathrm{eq})}}_{T,M+2}\Big)\Big] \end{aligned} \tag{4.42}$$

Since $[\cdots]$ in the second lines are simply shifted by $+2$ for the variable M with respect to the first lines, the "first integrals" are

$$\begin{aligned} & p_M\Big(1 - \frac{M}{T}\Big)\Big(1 + {m^{(\mathrm{eq})}}_{T-1,M+1}\Big) \\ & - p_{M+2}\Big(1 + \frac{M+2}{T}\Big)\Big(1 - {m^{(\mathrm{eq})}}_{T-1,M+1}\Big) = c_+ \end{aligned} \tag{4.43}$$

and

$$\begin{aligned} & q_M\Big(1 - \frac{M+1}{T+1}\Big)\Big(1 + {m^{(\mathrm{eq})}}_{T,M}\Big) \\ & - q_{M+2}\Big(1 + \frac{M+1}{T+1}\Big)\Big(1 - {m^{(\mathrm{eq})}}_{T,M+2}\Big) = c_-, \end{aligned} \tag{4.44}$$

where $c_\pm$ are independent of T. Moreover, it is only for $c_+ = 0$ $[c_- = 0]$ that p_{T+2} $[q_{T+2}]$ or p_{-T-2} $[q_{-T-2}]$ are not generated. Therefore, $c_\pm = 0$. We then have

$$\frac{p_{M+2}}{p_M} = \frac{\Big(1 - \frac{M}{T}\Big)\Big(1 + {m^{(\mathrm{eq})}}_{T-1,M+1}\Big)}{\Big(1 + \frac{M+2}{T}\Big)(1 - {m^{(\mathrm{eq})}}_{T-1,M+1})} \tag{4.45}$$

and

$$\frac{q_{M+2}}{q_M} = \frac{\Big(1 - \frac{M+1}{T+1}\Big)\Big(1 + {m^{(\mathrm{eq})}}_{T,M}\Big)}{\Big(1 + \frac{M+1}{T+1}\Big)(1 - {m^{(\mathrm{eq})}}_{T,M+2})}. \tag{4.46}$$

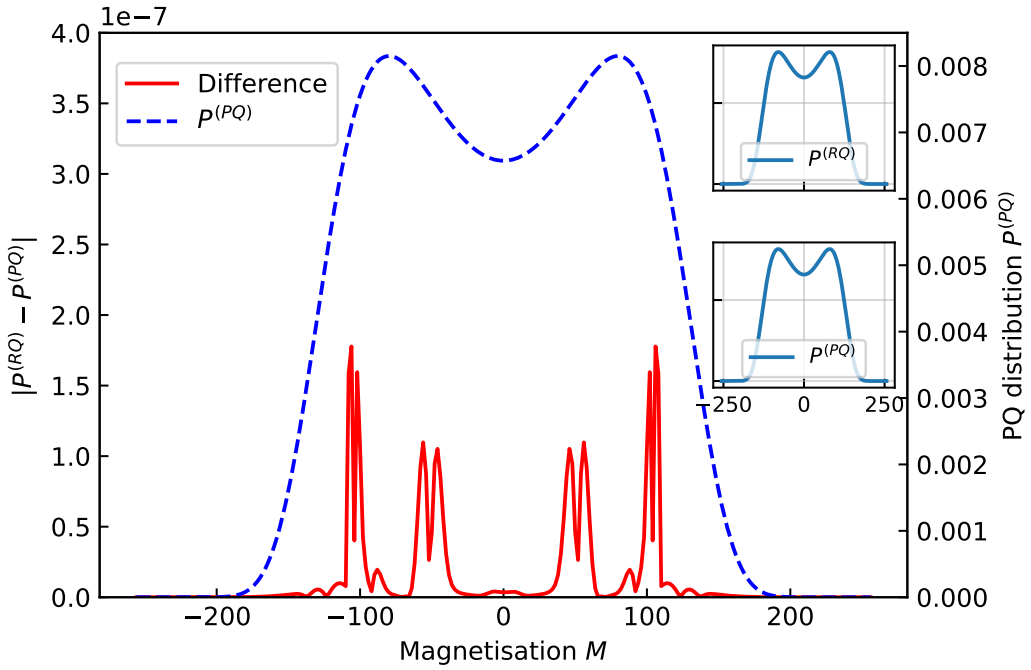

Figure 4.6: For $N_0 = T = 256$ the distribution of PQ, $\vec{P}_T^{(PQ)}$ *(lower inset)* and the stationary distribution of RQ, $\vec{P}^{[\infty]}(T)$ *(upper inset)* are compared (*solid curve and the left ordinate* in unit of 10^{-7}). The *dashed curve and the right ordinate* shows $\vec{P}_T^{(PQ)}$.

With the aid of the normalization conditions, the iterative conditions (4.45) and (4.46) should give the stationary distributions $\vec{P}^{[\infty]}(T)$ and $\vec{Q}^{[\infty]}(T)$, respectively.

4.3.4 Martingale connects stationary distributions of RQ to PQ

Numerical comparisons : Having characterized $\vec{P}^{[\infty]}(T)$ and $\vec{Q}^{[\infty]}(T)$ with any value of T as the stable fixed distributions of $(\boldsymbol{KS})$ and $(\boldsymbol{SK})$, respectively, we evaluated numerically these distributions for different T and for N_0. It is done by seeking the eigenvectors corresponding to the largest eigenvalue (= 1). To our surprise, our analysis shows that the two stationary distributions, $\vec{P}^{[\infty]}(T)$ and $\vec{Q}^{[\infty]}(T)$, are extremely similar, and the similitude increases with the number of spins in the entire system N_0. Moreover, they are also almost identical to the distribution of the Progressive Quenching, $\vec{P}_T^{(PQ)}$, when $N_0 \gg 1$. Fig.4.6 shows the comparison between $\vec{P}^{(RQ)}(T) \equiv \vec{P}^{[\infty]}(T)$ *(upper inset)* and $\vec{P}^{(PQ)}(T)$ *(lower inset)*. The difference of order 10^{-7} *(solid curve in red)* is much smaller than the probability distribution, which is of order 10^{-2} *(dashed curve in blue)* in the case of $N_0 = T = 256$.

Implication of martingale : The key to understanding the above-mentioned "coincidence" is the martingale. The local invariance (4.5), which is equivalent to the martingale property of $m^{(\mathrm{eq})}{}_{T,\hat{M}_T}$, Eq.(4.1), assures that the r.h.s. of (4.45) and that of (4.46) are the same. To show this we have also used the identity, $\left(1 - \frac{M}{T}\right)/\left(1 + \frac{M+2}{T}\right) =$

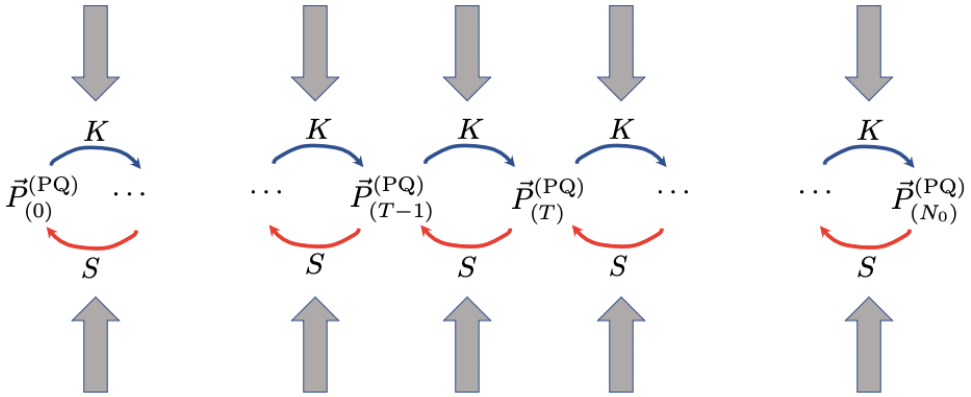

Figure 4.7: While the progressive quenching (the symbol $\boldsymbol{K}$ and blue arrows) generates $\vec{P}^{(PQ)}(T)$ from $\vec{P}^{(PQ)}(T-1)$, the random unquenching of quenched spins (the symbol $\boldsymbol{S}$ and red arrows) generates $\vec{P}^{(PQ)}(T-1)$ from $\vec{P}^{(PQ)}(T)$ as the "on-shell" reverse operation. At the same time, the family of these distributions $\{\vec{P}^{(PQ)}(T)\}_{T=0}^{N_0}$ are the attractor of the Recycling Quenching, $\boldsymbol{KS}$ *and* $\boldsymbol{SK}$ (the upward and downward thick arrows).

$\left(1-\frac{M+1}{T+1}\right)/\left(1+\frac{M+1}{T+1}\right)$. Under the normalization condition, these two equations, therefore, define the unique distribution: $\vec{P}^{[\infty]}(T)=\vec{Q}^{[\infty]}(T)$. The consequence of this equality is profound if we recall (4.25) with $\ell=\infty$, because the latter implies

$$\boldsymbol{K}\vec{P}^{[\infty]}(T-1)=\vec{P}^{[\infty]}(T) \tag{4.47}$$

$$\boldsymbol{S}\vec{P}^{[\infty]}(T)=\vec{P}^{[\infty]}(T-1) \tag{4.48}$$

Eq.(4.47) tells that the whole family of stationary distributions of Recycled Quenching, $\{\vec{P}^{[\infty]}\}_{T=0}^{N_0}$, is generated by the Progressive Quenching one after another starting from the initial one, $\vec{P}^{(PQ)}(0)=1$.

$$\vec{P}^{[\infty]}(T)=\vec{Q}^{[\infty]}(T)=\vec{P}^{(PQ)}(T). \tag{4.49}$$

This is the second of our main results. This fact, a kind of envelope relation, can also be verified by directly "integrating" (4.45) and comparing with (4.6) and (4.7) (the details not shown). Eq.(4.48) tells that the random unquenching of a spin by $\boldsymbol{S}$ allows to step back the distribution of the Progressive Quenching. Schematically, we may represent these by Fig.4.7.

We note that this is an "on-shell" property, which concerns only the stationary distributions of RQ. In a sense "off-shell," the family $\{\vec{P}_T^{(PQ)}\}_{T=0}^{N_0}$ constitutes a set of stable attractors of the RQ operations, $\boldsymbol{KS}$ and $\boldsymbol{SK}$.

4.4 Canonicity upon PQ in two-story ensemble

In the *Note added in proof* of our paper [3], we predicted a further description about the origin of canonical distribution of the final quenched magnetization, $M_{T=N_0}$, in fact with the implicit assumption of Markovian dynamics. The main questions are:

(i) A problem of combinatorics (Sec. 4.4.1): How the quenched ensemble is compatible with the canonical statistics upon the consecutive quenching operations where the unquenched spins are in constrained equilibrium ?
(ii) A problem of dynamics (Sec. 4.5): At the level of discrete spins - and even more microscopic - how is the operation of quenching compatible with the reversible evolution, given the apparent Deborah number, that is the dimensionless ratio of the relaxation time of the system and the observation period, exceeding unity? Indeed, the quenching process physically implies rendering towards zero the transition rate for the flipping of the spin in question.

4.4.1 Combinatorial approach

First, we introduce the notion of *two-story ensemble*, the way of characterizing the statistics of N_0 spins, which is convenient for the PQ. We separate those N_0 spins into two groups, $\{s_1, \ldots, s_T\}$, and the remainder, $\{s_{T+1}, \ldots, s_{N_0}\}$ (keeping the quenched/free spins distinction in mind) and we introduce the sub-totals of spins through $M_T = \sum_{i=1}^{T} s_i$ and $\mu_T = \sum_{j=T+1}^{N_0} s_j$. The joint probability $P_{QF}(M_T, \mu_T)$ satisfies

$$P_{QF}(M_T, \mu_T) = P_{F|Q}(\mu_T|M_T) P_Q(M_T), \tag{4.50}$$

where $P_Q(M_T)$ is the marginal and $P_{F|Q}(\mu_T|M_T)$ is the conditional probability.[1] We interpret this identity in the way that $P_Q(M_T)$ characterizes the *families* of spin configurations in the quenched part, $\{s_1, \ldots, s_T\}$, while $P_{F|Q}(\mu_T|M_T)$ reflects the sub-ensemble of the spin configuration, $\{s_{T+1}, \ldots, s_{N_0}\}$, in each family member. The configurations in the same family are realized ergodically, while those belonging to a distinct quenched family are non-ergodic in the two-story ensemble. (In our model on the complete lattice, we further replaced $\{s_1, \ldots, s_T\}$ by M_T as a collective tag of the family.)

The above is for a particular two-story ensemble. The different values of T define the distinct construction of two-story ensembles. In the context of PQ, however, we introduce a particular form of connection between a two-story ensemble $\{P_Q(M_T), P_{F|Q}(\mu_T|M_T)\}$ and its "neighbor" ensemble, $\{P_Q(M_{T+1}), P_{F|Q}(\mu_{T+1}|M_{T+1})\}$. This connection is schematically explained in Fig.4.8, where $N_\pm$ and $n_\pm$ denote the numbers of ± 1 spins in the quenched and free parts. All the spins are initially unquenched ($T = 0$ and $M = 0$) and thought to be in equilibrium without an external field. The probability for μ_0, denoted by $P_F^{(can)}(\mu_0)$ reads:

$$P_F^{(can)}(\mu_0) = \mathcal{N}_{0,0} \binom{N_0}{\frac{N_0+\mu_0}{2}} e^{\frac{j}{N_0}\mu_0^2}, \tag{4.51}$$

where the normalization constant $\mathcal{N}_{0,0}$ is such that $\sum_{\mu=-N_0}^{N_0\,(mod\,2)} P_F^{(can)}(\mu_0) = 1$. We further assume that, upon the quenching of the $(T+1)$-th spin, the (N_0-T) free spins have already been re-equilibrated under the given fixed magnetization, M_T. In Appendix 4.4.2 we show by induction that the joint probabilities, $P_{QF}(M_T, \mu_T)$ for all T, obey the canonical statistics if the initial weight $P_F(\mu_0)$ obeys the canonical statistics and that the PQ fixes the value of any one of the free spins under constrained canonical equilibrium. Regarding the statistics of quenched spins, the above result implies that at any stage, for example,

[1] For the simplicity of notations we suppressed the index T as the number of quenched spins. For example, it is understood that $P_{QF}(M_T, \mu_T)$ is for the T quenched spins.

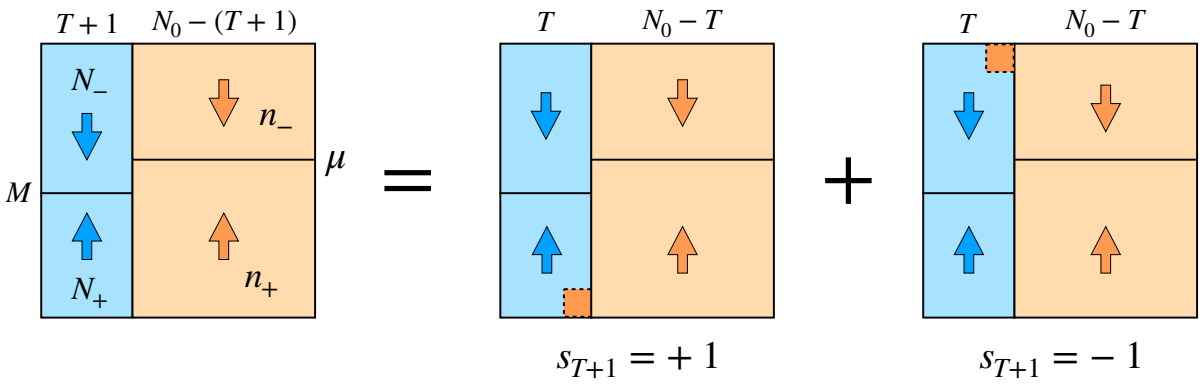

Figure 4.8: Schematic representation of the process of updating the two-story ensemble. The blocks represent the partition of the spins into the quenched part (the left column in blue) and the free part (the right column in red). According to the sign of spins, each column is subdivided: $N_+ + N_- = T + 1$ and $n_+ + n_- = N_0 - (T + 1)$ while $N_+ - N_- = M(= M_{T+1})$ and $n_+ - n_- = \mu(= \mu_{T+1})$.

the T-th stage, their magnetization M_T is distributed as if the T spins were randomly sampled from an equilibrium ensemble of N_0 spins.

Relation to martingale : In light of the canonicity underlying the two-story ensemble of quenched and free spins, the mechanism that allowed the "martingality" of $m^{(\mathrm{eq})}{}_{T,M_T} \equiv E[s_{T+1}|M_T]$ is easily understood: While $E[s_{T+1}|M_T]$ originally meant the expectation of the spin s_{T+1} upon quenching in the presence of the magnetization M_T due to the T already fixed spins, the underlying canonicity allows to map it to the equilibrium expectation of s_{T+1} when the spins $\{s_1, \ldots, s_T\}$ have the magnetization M_T. Together with the homogeneity among the free spins, $\{s_{T+1}, \ldots, s_{N_0}\}$, we finally regard $m^{(\mathrm{eq})}{}_T$ as the canonical expectation $E^{(can)}[s_{N_0}|M_T]$. The "M_T-martingality" for the latter follows directly from the tower rule applied to $m_T \equiv E[z|s_1, \ldots, s_T]$, see Section 3.2.2, where z stands for any random variable belonging to the above canonical ensemble. In this viewpoint, we can better understand the effect of Recycled Quenching (RQ) mentioned above. After applying the RQ infinitely many times, the probability $P_Q(M_T)$ of having the quenched magnetization M_T over T quenched spins in fact obeys the canonical marginal distribution, $\sum_{\mu_T} P^{(can)}(\mu_T, M_T)$, where $P^{(can)}(\mu_T, M_T)$ is the joint canonical distribution of the spins when T randomly chosen spins have the magnetization M_T.

The picture of the two-story ensemble and the underlying canonical statistics should apply to systems other than the Ising spins on a complete lattice. See, as an example, Appendix 4.7 for the $q = 3$ Potts model. Note that the equivalence between the martingale and the local invariance is, however, specific to the Ising spin model.

4.4.2 Details of the two-story ensemble calculations

We show the canonicity of $P_{F,Q}(\mu_T, M_T)$ through proof by induction. The key combinatorial identity is the following:

$$\begin{aligned}\binom{T+1}{N_+}\binom{N_0-(T+1)}{n_+} &= \frac{n_++1}{N_0-T}\binom{T}{N_+-1}\binom{N_0-T}{n_++1} \\ &+ \frac{N_0-T-n_+}{N_0-T}\binom{T}{N_+}\binom{N_0-T}{n_+},\end{aligned} \tag{4.52}$$

where, as noted in the main text, $N_+ = \frac{1}{2}(T + M_{T+1} + 1)$ and $n_+ = \frac{1}{2}(N_0 - (T+1) + \mu_{T+1})$ are the number of $(+1)$ spins in the quenched part and unquenched part, respectively. When T spins have been quenched, we put the hypothesis:

$$\begin{aligned}P_{F,Q}(\mu_T, M_T) &= P^{(can)}_{F,Q}(\mu_T, M_T) \\ &\equiv \mathcal{N}_T \binom{T}{\frac{T+M_T}{2}}\binom{N_0-T}{\frac{(N_0-T)+\mu_T}{2}} e^{\frac{j}{2N_0}(\mu_T+M_T)^2},\end{aligned} \tag{4.53}$$

where $\mathcal{N}_T$ is the normalization constant such that $\sum_{\mu=-(N_0-T)}^{N_0-T\,(mod\,2)} \sum_{M=-T}^{T\,(mod\,2)} P_{F,Q}(\mu_T, M_T) = 1$. According to Fig. 4.8, we combine the case of $s_{T+1} = 1$ and $s_{T+1} = -1$ as the newly quenched spin with appropriate weight. With the above identity (4.52) we can show that the joint probability after the $(T+1)$-th quench, $P_{F,Q}(\mu_{T+1}, M_{T+1})$ is again canonical :

$$\begin{aligned}P^{(can)}_{F,Q}(\mu_{T+1}, T+1) &= \frac{N_0-T+\mu_{T+1}+1}{2(N_0-T)} P^{(can)}_{F,Q}(\mu_{T+1}+1, T), \\ P^{(can)}_{F,Q}(\mu_{T+1}, M_{T+1}) &= \frac{N_0-T+\mu_{T+1}+1}{2(N_0-T)} P^{(can)}_{F,Q}(\mu_{T+1}+1, M_{T+1}-1) \\ &+ \frac{N_0-T-\mu_{T+1}+1}{2(N_0-T)} P^{(can)}_{F,Q}(\mu_{T+1}-1, M_{T+1}+1) \\ P^{(can)}_{F,Q}(\mu_{T+1}, -(T+1)) &= \frac{N_0-T-\mu_{T+1}+1}{2(N_0-T)} P^{(can)}_{F,Q}(\mu_{T+1}-1, -T),\end{aligned} \tag{4.54}$$

where the first and the last lines apply, respectively, for $\mu_{T+1} \geq -(N_0-T)+1$ and $\mu_{T+1} \leq (N_0-T)-1$, while the middle line applies for $-T \leq M_{T+1} \leq T$. Because $P_{F,Q}(\mu_0, M_0 = 0) = P^{(can)}_{F,Q}(\mu_0, M_0 = 0)$ by definition,the proof by induction is completed. Once we establish $P_{F,Q}(\mu_T, M_T) = P^{(can)}_{F,Q}(\mu_T, M_T)$ for all T, the marginal $P_Q(M_T)$ is given through $P_Q(M_T) = \sum_{\mu_T} P^{(can)}_{F,Q}(\mu_T, M_T)$.

4.5 Dynamical approach - Finite time reversible operation

At the level of discrete spins, Glauber's algorithm [71, 72] is a representative model of continuous-time Markovian evolution. In this model the flipping of the Ising spin s_i in

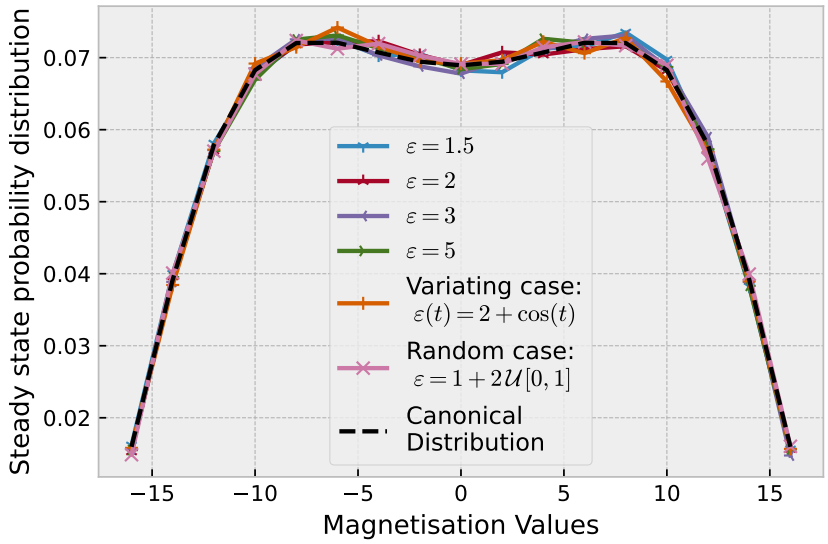

Figure 4.9: Invariance of the steady state distribution of Glauber algorithm with different values of ε, either fixed with time, variating, or chosen randomly at each time step. $\mathcal{U}[0,1]$ stands for a uniform random variable over the interval $[0,1]$.

the presence of the interacting energy,

$$E_i(t) = j \sum_{k(\neq i)} s_k(t), \tag{4.55}$$

is characterized by the transition rate of the single-spin flip:

$$P[s_i(t+dt) = -s_i(t)] = \frac{dt}{2\varepsilon_i(t)}(1 - s_i(t)\tanh(\beta E_i(t))), \tag{4.56}$$

where the characteristic time $\varepsilon_i(t)$ may depend on the time t. In this context the operation of quenching the spin s_{T+1} is to render $\varepsilon_{T+1}(t)$ to $+\infty$. On the other hand, we know that if the time constants $\{\varepsilon_i\}$ are static, the above algorithm can establish the canonical distribution as a steady state. While the latter does not immediately imply that the quenching, or general time-dependent modulation of ε_i's, allows the canonicity to be kept intact against the dynamic perturbation. It is assured by the fact that the Kullback-Leibler divergence,

$$D_{\mathrm{KL}}(P\|P^{can}) = -\sum_{\{s_i\}} P(\{s_i\},t) \ln \frac{P(\{s_i\},t)}{P^{can}(\{s_i\})}, \tag{4.57}$$

is a Lyapunov functional of the Markovian evolution of $P(\{s\},t)$ whether or not $\{\varepsilon_i\}$ are time-dependent[2]. Figure 4.9 demonstrates that the Glauber model keeps the canonicity whatsoever the choice of characteristic times $\{\varepsilon_i\}$, either static or dynamic.

Below the Ising-spin scale, the individual spin may be visualized as a state point in

[2]Into the generic inequality, $D(\mathsf{K}P\|\mathsf{K}Q) \leq D(P\|Q)$ for the probability vectors P and Q with a transfer matrix K, we substitute $P = P_t$, $Q = P^{can}$ and $\mathsf{K} = \mathbf{1} + dt\,\mathsf{R}$, where R is the rate matrix. Then we have $D(P_{t+dt}\|P^{can}) \leq D(P_t\|P^{can})$.

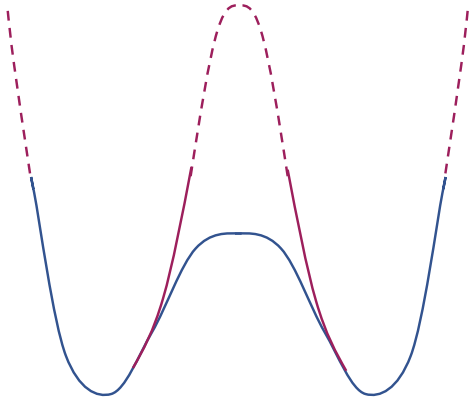

Figure 4.10: A double-well potential as a microscopic model of single-spin quenching. The dashed parts of the curves are those inaccessible by thermal activation with the experimental time.

a double-well potential. A well-known example is the bit-memory analyzed by Landauer [73]. The potential is generally asymmetric and fluctuating in the presence of an external field or interactions with other spins. It is, therefore, generally impossible to raise the barrier of a double-well potential strictly reversibly in a finite time. It is, nevertheless, instructive to quantify the irreversibility. The (partial) excess entropy production [74, 75, 76, 77] may be fitted for this purpose. If we approximately discretize the coordinate x of the double-well potential (Figure 4.10), the mean excess entropy production associated with the (nearby) transitions $x' \to x$ denoted by $\dot{S}^{ex}_{x,x'}$ reads

$$\dot{S}^{ex}_{x,x'} = R_{xx'}p_{x'} \ln \frac{R_{xx'}p_{x'}}{R_{x'x}p_x} + R_{x'x}p_x - R_{xx'}p_{x'}, \tag{4.58}$$

where p_x is the probability and $R_{x',x}$ is the transition rate from x to x' and we assumed that the time-reversed state of x is x itself. When the potential is modified sufficiently slowly relative to the microscopic timescale, the probability flows, $R_{xx'}p_{x'} - R_{x'x}p_x$, with x and x' within the same valley, remain effectively zero through the detailed balance, with the only exception around the barrier top. In the next section, we demonstrate that, by focusing on the barrier top, this framework gives the famous Landauer's entropic loss by $\ln 2$ upon the erasure process of a bit memory. By contrast, in the present context, the quenching of a spin is made so that the DB is observed *including* at the vicinity of the barrier top. Then the local entropy production $\dot{S}_{x,x'}$ in (4.58) vanishes everywhere. With more than one spin, the above argument should be lifted to a high-dimensional phase space and the associated continuous transition networks.

4.6 Excess entropy production applied to Landauer's bit memory

Let us use once again the excess entropy production [78] and apply it to Landauer's entropic loss by $\ln 2$ upon the erasure of bit memory. After that, we modify this result to

show the absence of entropy production when a spin is quenched slowly.

Using the stochastic entropy introduced by Seifert [8] and following the classification in [51] the excess entropy production rate of a memory bit and the attached heat bath

$$\dot{S}^{ex} = \sum_x \dot{p_x} \ln \frac{q_x}{p_x}, \tag{4.59}$$

where p_x is the probability density at time t while q_x is the steady state probability satisfying the detailed balance (DB),

$$R_{xy} q_y = \tilde{R}_{\tilde{y}\tilde{x}} q_x, \tag{4.60}$$

with $\tilde{x}$ being the time reversed state of x (when the velocity is included in x) and $R_{xy} = W_{x \leftarrow y}$ for $y \neq x$, and $R_{xx} = -\sum_{y(\neq x)} W_{y \leftarrow x}$ being the minus of the escape rate. By definition, $\sum_x R_{xy} = 0$. By substituting into (4.59) the master equation,

$$\partial_t p_x = \sum_y R_{xy} p_y \tag{4.61}$$

and using the DB condition (4.60) the mean excess entropy production $\dot{S}^{ex}_{x,y}$ specifically associated with the state transition between x and y is given by [78]:

$$\dot{S}^{ex}_{x,y} := R_{xy} p_y \ln \frac{R_{xy} p_y}{\tilde{R}_{\tilde{y}\tilde{x}} p_x} + \tilde{R}_{\tilde{y}\tilde{x}} p_x - R_{xy} p_y. \tag{4.62}$$

Here $\dot{S}_{x,y}$ is non-negative because of the generic inequality, $a \ln \frac{a}{b} + b - a \geq 0$.

When the above framework is applied to the double-minimum potential as a model of memory bit, the spatial coordinate x is finely discretized, and the probability density p_x is supposed to be quasi-equilibrium within each valley: $p_x = \theta_t q_x$ for $x < 0$ and $p_x = (2 - \theta_t) q_x$ for $x > 0$. When a memory stocked by this potential is erased through the symmetric lowering of the barrier separating the two valleys, we take $\theta_{t=0} = 2$ and $\theta_{t=\infty} = 1$.

If we substitute these hypotheses into (4.59) and integrate over time from 0 to ∞,, we already have the expected result, $\ln 2$. The advantage of the partial entropy production is that (4.62) allows us to pinpoint where this increment occurs along the potential surface. Except for the vicinity of the barrier top of the potential ($x = 0$), the detailed balance (4.60) is effectively established, and $\dot{S}^{ex}_{x,y}$ vanishes, where we supposed the time-reversal symmetry, $\tilde{x} = x$ and $\tilde{R}_{\tilde{y}\tilde{x}} = R_{yx}$. The only transition that can be irreversible is between $x = 0-$ and $x = 0^+$. More concretely,

$$\frac{\dot{S}^{ex}_{0^-,0^+}}{k_{\mathrm{B}}} = R_{0^-,0^+} \theta_t q_0 \ln \frac{\theta_t}{2 - \theta_t} + R_{0^+,0^-}\, p(0^-) - R_{0^-,0^+}\, p(0^+) \tag{4.63}$$

$$\frac{\dot{S}^{ex}_{0^+,0^-}}{k_{\mathrm{B}}} = R_{0^+,0^-} (2 - \theta_t) q_0 \ln \frac{2 - \theta_t}{\theta_t} + R_{0^-,0^+}\, p(0^+) - R_{0^+,0^-}\, p(0^-), \tag{4.64}$$

and the sum of these two gives

$$\frac{\dot{S}^{ex}_{0^-,0^+}}{k_{\rm B}} + \frac{\dot{S}^{ex}_{0^+,0^-}}{k_{\rm B}} = [R_{0^-,0^+}\theta_t q_0 - R_{0^+,0^-}(2-\theta_t)q_0] \ln \frac{\theta_t}{2-\theta_t}. \tag{4.65}$$

Here the quantity in the square bracket on the r.h.s. is the net probability flow from the left to the right valley. We, therefore, can write $[R_{0^-,0^+}\theta_t q_0 - R_{0^+,0^-}(2-\theta_t)q_0] = \frac{1}{2}|\dot{\theta}_t|$. With this estimation, the time integral of $\dot{S}^{ex}_{0^-,0^+} + \dot{S}^{ex}_{0^+,0^-}$ from $\theta_0 = 2$ to $\theta_\infty = 1$, where $|\dot{\theta}_t| = -\dot{\theta}_t$, yields finally

$$\int_{t=0}^{\infty} dt[\frac{\dot{S}^{ex}_{0^-,0^+}}{k_{\rm B}} + \frac{\dot{S}^{ex}_{0^+,0^-}}{k_{\rm B}}] = \int_0^{\infty} (-\frac{1}{2}\dot{\theta}_t) \ln \frac{\theta_t}{2-\theta_t} dt = \ln 2. \tag{4.66}$$

Therefore, only the excess entropy production at the top of the potential barrier is responsible for all the entropy loss.

When we retrace the above reasoning in our Progressive Quenching (PQ) case, the total entropy production should also be concentrated at the barrier top, $x = 0^{\pm}$, where the barrier height is raised to well above $k_{\rm B}T$. If the DB is maintained during the operation of PQ, the current $[R_{0^-,0^+}\theta_t q_0 - R_{0^+,0^-}(2-\theta_t)q_0]$ vanishes, unlike the case of Landauer, and the production, $\dot{S}_{0^-,0^+} + \dot{S}_{0^+,0^-}$, also does. In conclusion, when the potential barrier is raised slowly enough on the microscopic scale, the operation of PQ is reversible, and, as a result, the two-story canonical distribution is maintained.

4.7 Conclusion and Discussion

In this chapter, we showed that the PQ process has a local invariance induced by the hidden martingale. This new symmetry allowed us to derive an exact probability formula corresponding to the canonical one under unbiased conditions. By introducing a new operation: the single-spin unquenching, we described a new stochastic process - Recycled Quenching - whose stable stationary distribution is associated with the PQ through the local invariance.

Progressive Quenching, though the operator $\boldsymbol{K}$, is an operation by which the partition between the system and its environment is updated. In contrast, the unquenching, through $\boldsymbol{S}$, is a kind of its inverse. In our model, this dichotomy between the system (here, the unquenched spins) and the environment (the quenched ones) subsystems is explicitly made. The quenching operation drives a spin in an out-of-equilibrium state while the unquenched part remains at equilibrium under the updated constraint. Such flexibility of partition opens a niche where we may find new concepts. The evolution of Progressive Quenching from an unbiased initial condition generates the family of stable, steady states for the Recycled Quenching process, the alternation of single-step quenching ($\boldsymbol{K}$) and single-step unquenching of a randomly chosen spin ($\boldsymbol{S}$). That family of steady distributions plays the role of a stable manifold in the space of distributions with multi-sectors. There are several questions that we still need to exploit and left for future study. We have yet to address the kinetic aspects of RQ, which might bring more information about this new realm of flexible System-Environment partition.

The two-story ensemble allowed us to understand how the Boltzmann-like structure

of Eq.(4.6) arose, and how important the Markov property and detailed balance are for the PQ to keep the canonical distribution. Under these conditions, the canonicity is conserved even without allowing the unquenched spins to reach a quasi-equilibrium before the subsequent fixation of spins as far as the system starts with a canonical thermal ensemble. (cf. When we go down to a more microscopic scale, the detailed balance may become incompatible with the quenching operation.) When the two-story canonical structure is assured, the hidden martingale holds through the tower-rule applied to the conditional canonical expectations. Applying the Glauber algorithm made us realize that kinetics actually do not play any role, as surprising as it may have sound to us only a couple of years ago. Moreover, we may now see the act of quenching a degree of freedom as a particular potential barrier transformation with 0 entropy production.

Following those results, we will extend the and generalize our framework to general Markov Chains, and see if the detailed-balance bears an important role as much as it does for our spin systems. This will be the subject of the next chapter.

Appendix: PQ for the 3-Potts model

The picture of the two-story ensemble and the underlying canonical statistics should apply to systems other than the Ising spins on a complete lattice. The $q = 3$ Potts model on the complete lattice is an example. Below, we describe the model in some detail.

Energy and entropy of the $q = 3$ Potts model on a complete lattice

The energy of the $q = 3$ Potts model on a complete lattice reads

$$H = -\frac{J_0}{N_0} \sum_{1 \le i < j \le N_0} e_i \cdot e_j = -\frac{J_0}{2N_0} \left\| \sum_{1 \le i \le N_0} e_i \right\|^2 + \frac{J_0}{2}, \tag{4.67}$$

where e_i is the state of the i-th Potts element, etc. To be concrete, we represent the three states of the Potts' element on the plane: $e^{(1)} = (0, 1)^t$, $e^{(2)} = (\frac{\sqrt{3}}{2}, -\frac{1}{2})^t$, and $e^{(3)} = (-\frac{\sqrt{3}}{2}, -\frac{1}{2})^t$. The quenching process is performed by keeping the same update rule. At stage T, the mean value of the next quenched Potts spin e_{T+1} holds:

$$\mathbb{E}[e_{T+1} | e_1, \ldots, e_T] = \langle e_i \rangle^{(\mathrm{eq})}_{i \in \{T+1, \ldots, N_0\}} \tag{4.68}$$

When T of N_0 spins have been quenched, their repartition of orientation is denoted by $n^{(i)}$ for the state $e^{(i)}$. We note $n^{(1)} + n^{(2)} + n^{(3)} = T$ and $n^{(1)}e^{(1)} + n^{(2)}e^{(2)} + n^{(3)}e^{(3)} = M_T$, together with $e^{(1)} + e^{(2)} + e^{(3)} = 0$. The distribution of the T spins can then be characterized by the two parameters: $\nu^{(1)} = n^{(1)} - n^{(3)}$ and $\nu^{(2)} = n^{(2)} - n^{(3)}$. By noticing $\nu^{(1)} + \nu^{(2)} = T - 3n^{(3)}$, all $n^{(i)}$ are specified by $\nu^{(1)}$ and $\nu^{(2)}$;

$$\begin{aligned} n^{(1)} &= \frac{1}{3}(T + 2\nu^{(1)} - \nu^{(2)}) \\ n^{(2)} &= \frac{1}{3}(T - \nu^{(1)} + 2\nu^{(2)}) \\ n^{(3)} &= \frac{1}{3}(T - \nu^{(1)} - \nu^{(2)}) \end{aligned} \tag{4.69}$$

With these in mind, the energy of the whole system reads;

$$H = -\frac{J_0}{2N_0} \| M_T + \sum_{T+1 \le i \le N_0} e_i \|^2 + \frac{J_0}{2}, \tag{4.70}$$

where $M_T = \nu^{(1)}e^{(1)} + \nu^{(2)}e^{(2)}$, and the entropy of quenched part $S(n^{(1)}, n^{(2)}, n^{(3)})$ (with $k_{\mathrm{B}} \equiv 1$) reads

$$e^{S(n^{(1)}, n^{(2)}, n^{(3)})} = \frac{T!}{n^{(1)}!n^{(2)}!n^{(3)}!}, \tag{4.71}$$

Consequences of martingality of mean equilibrium spin

When each node of the complete network has a q-state Potts spin with $q > 2$, the homogeneity of the unquenched Potts spins allows, as in the Ising ($q = 2$) case, the tower-rule-based martingale of the mean equilibrium unquenched spin, which in turn justifies

the underlying two-story canonical statistics. Unlike the $q = 2$ case [3], the martingale does not imply the Boltzmann-type weight for the path probability *per se.* Nevertheless, certain constraints are imposed by this martingale property, as will be shown below.

By ${m^{(\mathrm{eq})}}_T \equiv \sum_{s_{T+1}} s_{T+1} P_T(s_T|M_T)$, the martingale relationship, $E[{m^{(\mathrm{eq})}}_{T+1}|M_T] = {m^{(\mathrm{eq})}}_T$ reads

$$\sum_{s_{T+2}} \sum_{s_{T+1}} (s_{T+2} - s_{T+1}) P_{T+1}(s_{T+2}|M_T + s_{T+1}) P_T(s_{T+1}|M_T) = 0, \tag{4.72}$$

where we have made use of the identity, $\sum_{s_{T+2}} P_{T+1}(s_{T+2}|M_T + s_{T+1}) = 1$, with any T and M_T. This is valid for any $q \geq 2$ and any symmetric spin-spin interactions such as clock, Potts, etc. If $q = 2$, this equality immediately goes back to the local invariance because the summation contains only those terms with $(s_{T+2}, s_{T+1}) = (-1, 1)$ and $(1, -1)$. For $q = 3$, those processes which quench the two Potts elements of the same state consecutively drop out from the summation, and the above relationship (4.72) is reduced to an 2D equality, that is, starting from a common frozen spin, $M_T = \sum_{i=1}^{T} s_i$, there are the two constraints on the local path probabilities of M_t:

$$\begin{aligned} P_{T+1,T}(e^{(2)}, e^{(1)}|M_T) - P_{T+1,T}(e^{(1)}, e^{(2)}|M_T) &= P_{T+1,T}(e^{(3)}, e^{(2)}|M_T) - P_{T+1,T}(e^{(2)}, e^{(3)}|M_T) \\ &= P_{T+1,T}(e^{(1)}, e^{(3)}|M_T) - P_{T+1,T}(e^{(3)}, e^{(1)}|M_T). \end{aligned} \tag{4.73}$$

Each line in the above should represent a common function of M_T.

Chapter 5

Generalization to Markovian Transition Networks

5.1 Introduction

Markov chains have been studied in depth for more than a century now, whose fields of application are broad and diverse [79, 80, 81, 82]. It is especially the case of stochastic physics [83, 6, 10]. Some studies concern the effect of change of the parameters of the Markov chain, that is, the topology of the transition network and the rates associated with the jump on it [84, 85, 86, 87]. It turns out that Progressive Quenching (PQ) belongs to this category of studies.

In this Chapter, we aim to understand the importance of the Markovian assumption on the stochastic evolution of the martingale and its underlying canonical structure. We will discuss separately the Markovian (in this Chapter) and non-Markovian cases (Chapter 6), as well as distinguish the dynamics with or without the detailed balance.

The contents are extracted from our 2023 preprint [4], with Section 5.4 being original to this manuscript.

5.2 PQ viewed in the transition network

Returning to the discrete description of spins, we aim to extend the PQ to the Markovian transition networks (TN) context. This subsection is a preparation for that purpose, where we translate the PQ of a spin system in the language of TN. The extension will be discussed in Section 5.2.1.

We consider a system with N degrees of freedom denoted by $\{x_1, x_2, \ldots, x_N\}$. The set of possible values of x_i is denoted by A_i. For example, $A_i = \{-1, 1\}$ for an Ising spin s_i. The state space A then reads $A \equiv \bigotimes_{i=1}^{N} A_i$. Any state $\alpha \in A$ can then be described by a set of degrees of freedom, $\{x_1, x_2, \ldots, x_N\}$. Inversely, any variable x_i is the function of the state, $x_i(\alpha)$. The transition network in A is such that (i) if we exclude the simultaneous change of more than one variable, the topology of transition edges is hyper-rectangle, and (ii) if any one variable, e.g. x_i, is quenched, the network is divided into two groups, losing the ergodicity. Fig 5.1(b) illustrates (i) and (ii), where an initial TN graph is divided into non-connected subgraphs.In this section we will consider continuous-time processes,

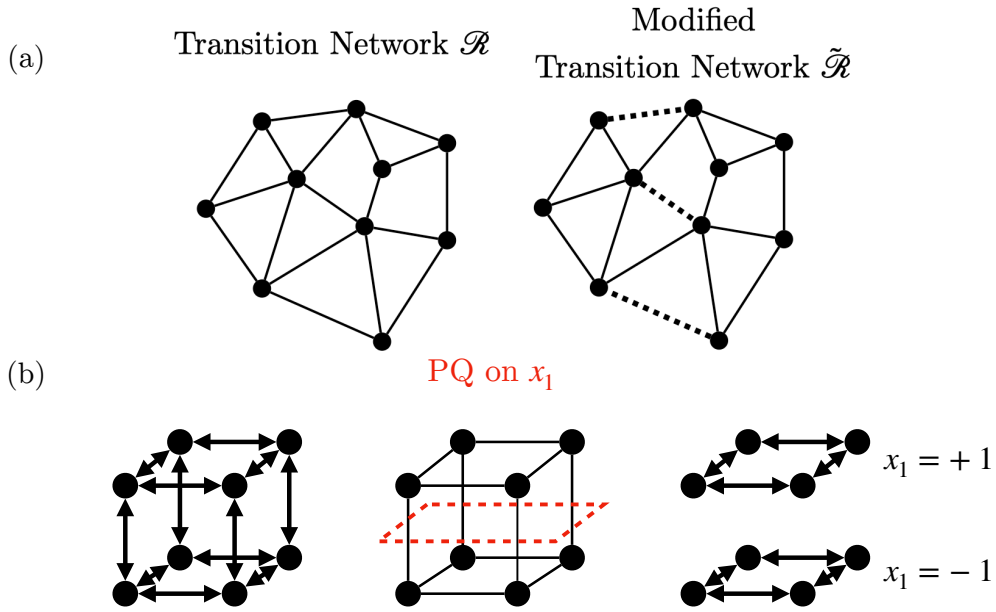

Figure 5.1: Progressive Quenching on Transition Networks. (a) Schematic illustration of the network transformation (Eqs. (5.3) and (5.4)). Some edges with no net probability flow are removed (dashed line). (b)Schematic illustration of a cubic Markov transition network modulated by PQ (in the case of three Ising spins, for example). After quenching the first degree of freedom denoted by x_1, the cubic network is separated into two square disconnected subnetworks.

therefore we denote by t the continuous time, not to be confused with the "quenching" index T which denotes the number of quenched degrees of freedom.

Let $\boldsymbol{\mathcal{R}}$ be the rate matrix of the master equation for the network on A:

$$\frac{d\vec{P}}{dt} = \boldsymbol{\mathcal{R}}\vec{P}, \tag{5.1}$$

and let $\vec{P}^{\rm st}$ be the steady state distribution; $\boldsymbol{\mathcal{R}}\vec{P}^{\rm st} = \vec{0}$. We also introduce the net probability current from α to α' through

$$J_{\alpha' \leftarrow \alpha} \equiv \mathcal{R}_{\alpha' \leftarrow \alpha} P_\alpha - \mathcal{R}_{\alpha \leftarrow \alpha'} P_{\alpha'}. \tag{5.2}$$

When the detailed balance (DB) is established for the steady state, $\vec{P}^{\,st}$, we have $J_{\alpha' \leftarrow \alpha} = 0$ for all the pair of states, (α, α').

Having the progressing quenching in mind, we introduce the class-Kronecker delta, $\delta^{(T)}_{\alpha,\alpha'} (= \delta^{(T)}_{\alpha',\alpha})$ through

$$\delta^{(T)}_{\alpha,\alpha'} = \begin{cases} 1 & : \quad \wedge_{i=1}^{T} \{x_i(\alpha) = x_i(\alpha')\} \\ 0 & : \quad \text{otherwise} \end{cases}, \tag{5.3}$$

that is, it picks up those pair of states that belongs to the same quenched degrees of freedom, $\{x_1, \ldots, x_T\}$. The notation $\wedge_{i=1}^{T}$ denotes the conditions that need to be fulfilled simultaneously. When the progressive quenching has fixed $\{x_1, \ldots, x_T\}$ but leaves the

other variables free to fluctuate, the modified rate matrix, which we denote by $\tilde{\mathcal{R}}_{T,\alpha'\leftarrow\alpha}$ is given as

$$\tilde{\mathcal{R}}_{T,\alpha'\leftarrow\alpha} = \delta^{(T)}_{\alpha,\alpha'}\mathcal{R}_{\alpha'\leftarrow\alpha} \tag{5.4}$$

for $\alpha \neq \alpha'$, and $\tilde{\mathcal{R}}_{T,\alpha\leftarrow\alpha} = -\sum_{\beta(\neq\alpha)}\tilde{\mathcal{R}}_{T,\beta\leftarrow\alpha}$ for the diagonal element to satisfy the normalization conditions, $\sum_{\alpha'}\tilde{\mathcal{R}}_{T,\alpha'\leftarrow\alpha} = 0$ for $\forall\alpha$. Eq. (5.4) simply means the state transition is possible only when $\delta^{(T)}_{\alpha,\alpha'} = 1$.

A simple but important observation is that if the steady state of the unquenched system, $\vec{P}^{\rm st}$, satisfies the detailed balance, then we have a trivial rewriting for every pair (α, α'),

$$\begin{aligned} 0 &= J_{\alpha'\leftarrow\alpha} \\ &= \mathcal{R}_{\alpha'\leftarrow\alpha}P^{\rm st}_{\alpha} - \mathcal{R}_{\alpha\leftarrow\alpha'}P^{\rm st}_{\alpha'} \\ &= \delta^{(T)}_{\alpha,\alpha'}\left(\mathcal{R}_{\alpha'\leftarrow\alpha}P^{\rm st}_{\alpha} - \mathcal{R}_{\alpha\leftarrow\alpha'}P^{\rm st}_{\alpha'}\right) \\ &= \tilde{\mathcal{R}}_{\alpha'\leftarrow\alpha}P^{\rm st}_{\alpha} - \tilde{\mathcal{R}}_{\alpha\leftarrow\alpha'}P^{\rm st}_{\alpha'}. \end{aligned} \tag{5.5}$$

This means that $\vec{P}^{\rm st}$ satisfies also the DB condition for the quenched system. The steady states of $\widetilde{\boldsymbol{\mathcal{R}}}$ are in general not unique because of the *broken ergodicity* (see Fig 5.1(b). Nevertheless, the canonical distribution, $\vec{P}^{\rm st}$, is among the possible steady states.

5.2.1 PQ of Markovian transition network without detailed balance

When the states space A is not a product space corresponding to multiple degrees of freedom of the system, we may still consider quenching as eliminating a part of bidirectional edges from the transition network (TN). If the detailed balance (DB) condition is not globally satisfied, removing bidirectional edges in a TN generally causes the modification of its steady-state distribution. The inset of Fig 5.2 shows just a simple example where the stationary state has a circulation of probability. Before "quenching" the stationary probability on the three states is $\{p_1, p_2, p_3\} = \left\{\frac{1}{3}, \frac{1}{3}, \frac{1}{3}\right\}$. When we remove the edges between the states 1 and 2, the stationary probability becomes $(r^2 + rr' + r^2)^{-1}\{r'^2, r^2, rr'\}$. The detailed balance holds globally only when $r = r'$, and the stationary distribution remains unchanged by this operation.

When we consider the general TN and ask when the removal of bidirectional edges leaves the steady state probability intact, a rule of thumb is as follows:
When a pair of states, (α, α') realize the vanishing net probability flow, $J_{\alpha'\leftarrow\alpha} = 0$, we can eliminate simultaneously $\mathcal{R}_{\alpha'\leftarrow\alpha}$ and $\mathcal{R}_{\alpha\leftarrow\alpha'}$ without perturbing the stationary distribution. The demonstration follows the idea of (5.5) above. We suppose that the initial TN has a steady state $\vec{P}^{\,(\rm st)}$. We denote by χ_Q all those pairs of states for which the net probability flow vanishes, i.e.,

$$\chi_Q \equiv \left\{(\alpha, \alpha') \,|\, \mathcal{R}_{\alpha'\leftarrow\alpha}P^{(\rm st)}_{\alpha} - \mathcal{R}_{\alpha\leftarrow\alpha'}P^{(\rm st)}_{\alpha'} = 0\right\}. \tag{5.6}$$

Here χ_Q's suffix Q stands for "quenchable". We introduce the "optional"-Kronecker delta,

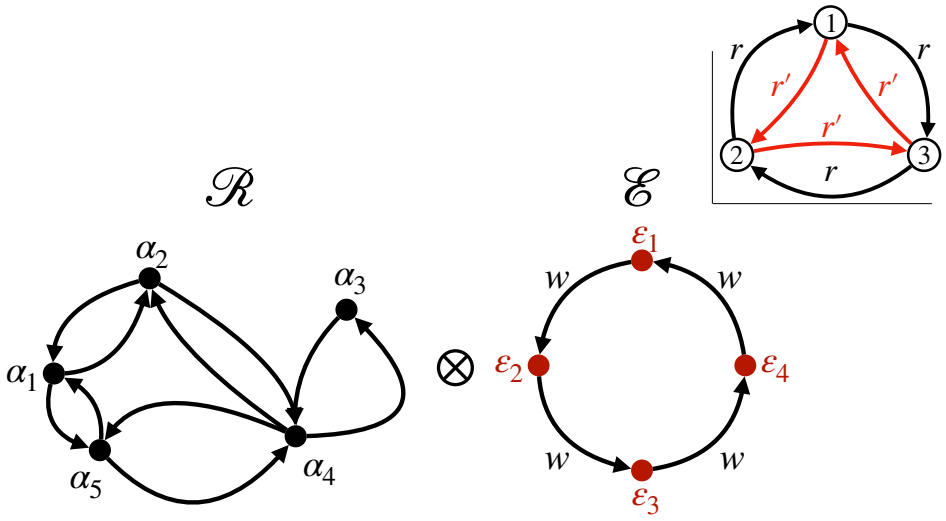

Figure 5.2: An example of a two-layered transition network whose steady state does not verify the detailed balance for any pair of states but has the possibility of a "quench" that leaves the stationary probabilities intact. See the main text (5.2.1) for the details. (inset) A simple example of a stationary Markov chain without detailed balance. If $r \neq r'$, there is a non-zero probability flux, and cutting a link will change the stationary distribution.

$\delta^{(Q)}_{\alpha,\alpha'}$ through

$$\delta^{(Q)}_{\alpha,\alpha'} = \delta^{(Q)}_{\alpha',\alpha} = \begin{cases} 1 \text{ or } 0 \text{ (optional)} & : \quad (\alpha,\alpha') \in \chi_Q \\ 1 & : \quad \text{otherwise} \end{cases}, \tag{5.7}$$

that is, $\delta^{(Q)}$ can vanish only for the pairs whose net steady probability flow is zero. We then "quench" the original TN according to the "optional"-Kronecker delta:

$$\tilde{\mathcal{R}}_{\alpha'\leftarrow\alpha} \equiv \delta^{(Q)}_{\alpha,\alpha'}\mathcal{R}_{\alpha'\leftarrow\alpha}. \tag{5.8}$$

We can check that the "quenched" TN still has $\vec{P}^{\,(\mathrm{st})}$ as the stationary state. In fact, for every α'

$$\begin{aligned} &\sum_\alpha (\tilde{\mathcal{R}}_{\alpha'\leftarrow\alpha}P^{(\mathrm{st})}_\alpha - \tilde{\mathcal{R}}_{\alpha\leftarrow\alpha'}P^{(\mathrm{st})}_{\alpha'}) \\ =&\sum_\alpha \delta^{(Q)}_{\alpha,\alpha'}(\mathcal{R}_{\alpha'\leftarrow\alpha}P^{(\mathrm{st})}_\alpha - \mathcal{R}_{\alpha\leftarrow\alpha'}P^{(\mathrm{st})}_{\alpha'}) \\ =&\sum_\alpha (\mathcal{R}_{\alpha'\leftarrow\alpha}P^{(\mathrm{st})}_\alpha - \mathcal{R}_{\alpha\leftarrow\alpha'}P^{(\mathrm{st})}_{\alpha'}) \\ =&0. \end{aligned} \tag{5.9}$$

Here, to go to the third line, we have used the fact that, whenever the pair (α,α') is $\notin \chi_Q$, we have $\delta^{(Q)}_{\alpha,\alpha'} = 1$ by definition. The last equality is the stationary condition for the original TN. The main part of Fig. 5.2 gives an example in which the TN does not have a global detailed balance, but the "quenching" of TN is possible. The system has two layers, $\mathcal{R}$ and $\mathcal{E}$. The former layer has the Glauber dynamics allowing detailed balance among $\{\alpha_1,\alpha_2,\alpha_3,\alpha_4,\alpha_5\}$. The latter layer $\mathcal{E}$ undergoes the stochastic circulation

among $\{\varepsilon_1, \varepsilon_2, \varepsilon_3, \varepsilon_4\}$. We assume that the four values ε_k $(k = 1, \ldots, 4)$ are the global time constant of the Glauber dynamics for the first layer $\mathcal{R}$. Then, we can quench the bidirectional edges for any pairs of nodes on this layer.

Remark : The modification of the transition rates, $\mathcal{R}_{\alpha' \leftarrow \alpha} \mapsto \tilde{\mathcal{R}}_{\alpha' \leftarrow \alpha}$ and $\mathcal{R}_{\alpha \leftarrow \alpha'} \mapsto \tilde{\mathcal{R}}_{\alpha \leftarrow \alpha'}$ should be realized *pairwise* simultaneously, either instantaneously or gradually, but in keeping the ratio $\tilde{\mathcal{R}}_{\alpha' \leftarrow \alpha}(t)/\tilde{\mathcal{R}}_{\alpha \leftarrow \alpha'}(t)$ constant so as to maintain the flow-free condition, $(\tilde{\mathcal{R}}_{\alpha' \leftarrow \alpha}(t) P_{\alpha}^{(\mathrm{st})} - \tilde{\mathcal{R}}_{\alpha \leftarrow \alpha'}(t) P_{\alpha'}^{(\mathrm{st})}) = 0$.

5.3 A discrete-time version

We consider a *discrete-time* and discrete-state Markov process characterized by the transition probabilities $K(\alpha_i \rightarrow \alpha_j)$. We suppose that this process is stationary, and we denote by $P^{\mathrm{st}}(\alpha)$ the stationary probability. We will show that, if the Detailed-Balance (DB) holds in the stationary ensemble, the Progressive Quenching (PQ) allows $P^{\mathrm{st}}(\alpha_i)$ to remain the stationary distribution.

When a group of degrees of freedom, say $\{a_i\}^Q$, are quenched, certain transitions that involve the change of this variable are prohibited. We introduce $\delta^Q(\alpha, \alpha')$ so that $\delta^Q(\alpha, \alpha') = 1$ [0] if the transitions $\alpha \rightarrow \alpha'$ and $\alpha' \rightarrow \alpha$ are allowed [prohibited], respectively. Then under the condition of quenched variables, $\{a_i\}^Q$, the off-diagonal transition probabilities, that we denote by $K^Q(\alpha_i \rightarrow \alpha_j)$ $(i \neq j)$, should read

$$K^Q(\alpha_i \rightarrow \alpha_j) = \delta^Q(\alpha, \alpha') K(\alpha_i \rightarrow \alpha_j) \tag{5.10}$$

To maintain the normalization condition of the probability, the diagonal element of the transition probability should also be compensated:

$$\begin{aligned} K^Q(\alpha_i \rightarrow \alpha_i) \quad &= 1 - \sum_{j}^{(j \neq i)} K^Q(\alpha_i \rightarrow \alpha_j) \\ &= K(\alpha_i \rightarrow \alpha_i) + \sum_{j}^{(j \neq i)} (1 - \delta^Q(\alpha_i, \alpha_j)) K(\alpha_i \rightarrow \alpha_j) \end{aligned} \tag{5.11}$$

We now ask whether the stationary distribution of the original transition network (TN), $P^{\mathrm{st}}(\alpha_i)$, remains so for the quenched TN if the former TN satisfies the DB. We rewrite the stationarity condition of $P^{\mathrm{st}}(\alpha_i)$:

$$\begin{aligned} P^{\mathrm{st}}(\alpha_i) \quad &= \sum_j P^{\mathrm{st}}(\alpha_j) K(\alpha_j \rightarrow \alpha_i). \\ &= \sum_{j(\neq i)} P^{\mathrm{st}}(\alpha_j) \Big(\delta^Q(\alpha_i, \alpha_j) + [1 - \delta^Q(\alpha_i, \alpha_j)] \Big) K(\alpha_j \rightarrow \alpha_i) \\ &\quad + P^{\mathrm{st}}(\alpha_i) K(\alpha_i \rightarrow \alpha_i) \\ &= \sum_{j(\neq i)} P^{\mathrm{st}}(\alpha_j) K^Q(\alpha_j \rightarrow \alpha_i) \\ &\quad + \sum_{j(\neq i)} [1 - \delta^Q(\alpha_i, \alpha_j)] P^{\mathrm{st}}(\alpha_j) K(\alpha_j \rightarrow \alpha_i) + P^{\mathrm{st}}(\alpha_i) K(\alpha_i \rightarrow \alpha_i) \end{aligned}$$

$$
\begin{aligned}
&= \sum_{j(\neq i)} P^{\rm st}(\alpha_j) K^Q(\alpha_j \to \alpha_i) \\
&\quad + P^{\rm st}(\alpha_i) \sum_{j(\neq i)} [1 - \delta^Q(\alpha_i, \alpha_j)] K(\alpha_i \to \alpha_j) + P^{\rm st}(\alpha_i) K(\alpha_i \to \alpha_i) \\
&= \sum_{j(\neq i)} P^{\rm st}(\alpha_j) K^Q(\alpha_j \to \alpha_i) + P^{\rm st}(\alpha_i) K^Q(\alpha_i \to \alpha_i) \\
&= \sum_{j} P^{\rm st}(\alpha_j) K^Q(\alpha_j \to \alpha_i), \qquad (5.12)
\end{aligned}
$$

where the fourth equality is due to the DB condition of the original TN,

$$P^{\rm st}(\alpha_j) K(\alpha_j \to \alpha_i) = P^{\rm st}(\alpha_i) K(\alpha_i \to \alpha_j). \qquad (5.13)$$

Eq.(5.12) means that $P^{\rm st}(\alpha_i)$ is a stationary distribution of the quenched system, though it may not be the unique one.

5.4 A graph theory formulation

From the schematic view of Fig. 5.1(a) and Eq.(5.9), we may note that two graphs with similar transition probabilities but different topologies can have the same stationary distribution. This difference in topology is essential, as it changes the number of possible paths for the system's evolution. This particular aspect is well represented by the so-called "Markov Chain Tree Theorem", which links the static distribution of a Markov Chain with the spanning-tree-decomposition of its representing graph [85]. This theorem, first derived by Hill in 1968 [88] (with anterior similar methods, such as Bott and Mayberry in 1954 [89] - but not available online) and referred by Schnakenberg in his 1976 review as "Kirchhoff's theorem" [85], was then rigorously proved in 1983 by Leighton and Rivest (first in an internal MIT paper, then published in 1986 in the appendix of [90]). Below, we present this theorem and sketch an analysis of its consequences on our PQ process.

5.4.1 Markov Chain Tree Theorem

Let us consider a physical system whose evolution is described by a stationary Markov Chain, with states α and a transition matrix $\mathcal{R}$, both represented by a graph G as pictured in Fig.5.2. A spanning tree (or maximal tree) of G, denoted by $T(G)$, is a tree subgraph of G that reaches all vertices α of G. More precisely, $T(G)$ is a connected subgraph of G containing no cycles spanning over the entire set of states of G. For an arbitrarily connected graph, the total number of spanning trees $t(G)$ is given by Kirchhoff's matrix-tree theorem [91], known as Cayley's formula in the case of complete graphs. We will denote those trees by $T^{(\mu)}(G)$, with $\mu = 1, 2, \ldots, t(G)$. An example is shown in Figure 5.3 where $t(G) = 8$. Each spanning tree can be directed towards a certain vertex (or state) α by orienting each edge towards this certain state. The now directed spanning tree is denoted $T^\mu_\alpha(G)$. See Fig.5.4 for illustration. Now for each $T^\mu_\alpha(G)$, we define the quantity $A(T^\mu_\alpha(G))$ such that:

$$A(T^\mu_\alpha(G)) = \prod_{(\gamma,\gamma') \in T^\mu_\alpha(G)} \mathcal{R}_{\gamma' \leftarrow \gamma} \geq 0. \qquad (5.14)$$

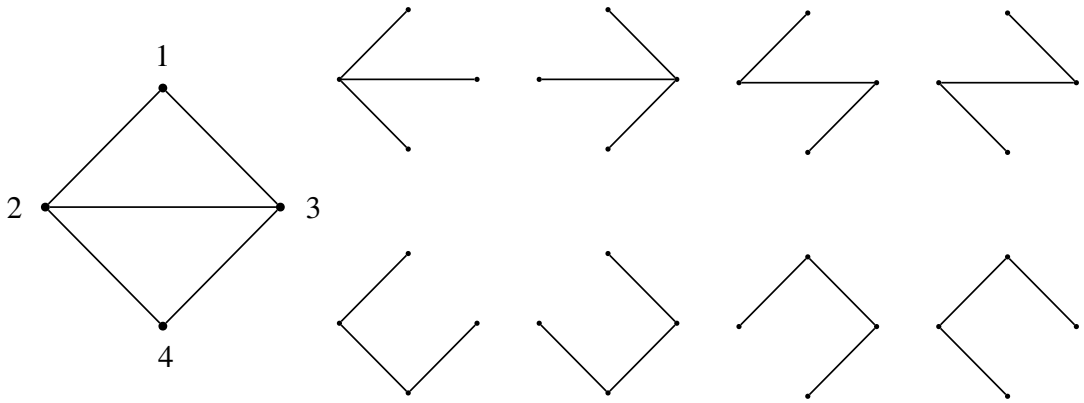

Figure 5.3: A simple undirected graph and all eight possible corresponding spanning trees. Adapted from [85].

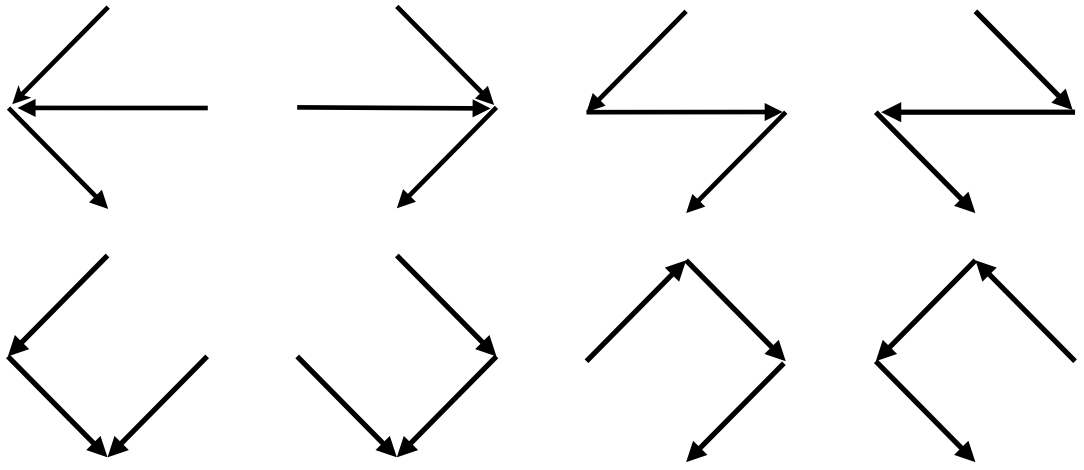

Figure 5.4: All possible T_4^{μ}, i.e spanning trees of Figure 5.3 directed towards $\alpha = 4$

$A(T_\alpha^\mu(G))$ is, therefore, the product of all (directed) transition probabilities $\mathcal{R}_{\gamma' \leftarrow \gamma}$ that occur in $T_\alpha^\mu(G)$. Now for each state α, we define the factors:

$$S_\alpha = \sum_{\mu=1}^{t(G)} A(T_\alpha^\mu(G)) \tag{5.15}$$

and

$$S = \sum_\alpha S_\alpha \tag{5.16}$$

Note that there is the same number of product terms $t(G)$ in all S_α, only the order and orientation of the vertices change. The Markov-Chain tree theorem states that for all α:

$$P^{\text{st}}(\alpha) = \frac{S_\alpha}{S} \tag{5.17}$$

where P^{st} denotes the stationary distribution. Eq.(5.16) ensures that $0 \leq P^{\text{st}}(\alpha) \leq 1$. Therefore, we have a direct link between the graph's topology, through the structure and number of spanning trees, and the system's steady state. Furthermore, since the Progressive Quenching applied to transition networks is equivalent to removing certain edges (or setting their transition rates to 0) of the graph without changing the stationary distribution, we may identify S_α/S as a topological invariant of the graph.

5.4.2 Quenching and spanning trees

Let us consider a pair of states $(\alpha, \alpha') \in \chi_Q(\mathcal{R})$, i.e., so that there is no net probability flux at the steady state between them. We showed earlier that the modified transition network $\tilde{\mathcal{R}}$, where the (α, α') edge has been removed, has the same stationary distribution. If we denote it by $\tilde{P}^{\text{st}}$, we may write for any state γ:

$$P^{\text{st}}(\gamma) = \frac{S_\gamma}{S} = \frac{\tilde{S}_\gamma}{\tilde{S}} = \tilde{P}^{\text{st}}(\gamma) \tag{5.18}$$

where $\tilde{S}$ and $\tilde{S}_\gamma$ correspond to Eqs.(5.15, 5.16) for the graph $\tilde{G}$ of $\tilde{\mathcal{R}}$. This allows for faster enumeration of "relevant" spanning trees, as $t(\tilde{G}) \leq t(G)$. For example, in Fig.5.3, removing the $(2,3)$ edge actually removes the top row of spanning trees. Equivalently, setting $\tilde{\mathcal{R}}_{2 \leftrightarrow 3} = 0$ cancels all corresponding $A(T_\gamma^\mu(\tilde{G}))$, which decreases the number of terms in Eq.(5.15). Furthermore, if we denote by $q(G)$ the indexes' set of spanning trees containing the edge (α, α'), we may write:

$$S_\gamma = \underbrace{\sum_{\mu \notin q(G)} A(T_\gamma^\mu(G))}_{=\tilde{S}_\gamma} + \underbrace{\sum_{\mu \in q(G)} A(T_\gamma^\mu(G))}_{:=U_\gamma} \tag{5.19}$$

$$S = \underbrace{\sum_{\mu \notin q(G)} \sum_\gamma A(T_\gamma^\mu(G))}_{=\tilde{S}} + \underbrace{\sum_{\mu \in q(G)} \sum_\gamma A(T_\gamma^\mu(G))}_{:=U}, \tag{5.20}$$

with U_γ the sum of vanishing contributions and $U = \sum_\gamma U_\gamma$. Then, Eq.(5.18) leads to the following ratio equality for any state γ:

$$\frac{\tilde{S}_\gamma}{U_\gamma} = \frac{\tilde{S}}{U}. \tag{5.21}$$

Therefore, all states γ have the same "remaining-to-vanishing" ratio.

We think it might be possible to prove Eq.(5.18) without referring to Eq.(5.9) via combinatorics of spanning trees and the 0-net probability flow hypothesis, but we have not yet succeeded. Nevertheless, reducing the number of spanning trees to count is of great importance in accelerating pathfinding algorithms [92] or optimizing communication networks [93]. Therefore, if there are reasons to think that the net flow of probability will vanish between two vertices, removing the connecting edge will simplify the topology of the graph without changing the stationary state. This shows how extensive the notion of Progressive Quenching can be, from modeling physical processes to graph topology. However, those results heavily rely on the Markov property. In the next Chapter, we will explore how the non-Markovianity of physical systems changes the stationary distributions of quenched systems.

Chapter 6

Non-Markovian spin systems

The previous results are valid only for Markovian systems. Our study of Progressive Quenching is now extended to non-Markovian systems, whether the detailed balance (DB) is verified (Section 6.1) or not (Section 6.2). The examples are the Ising spin systems studied above but with memory effects.

The contents are extracted from our 2023 preprint [4].

6.1 System with hidden spins satisfying detailed balance

6.1.1 Model, effective coupling and DB

In this part, we recall two known aspects of non-Markovian processes through the case studies under a simple setup. As a model, we consider a chain of N "visible" spins $\{s_i\}$ with ferromagnetic nearest-neighbor coupling J. We suppose also that the neighboring spin pairs, say s_i and s_{i+1} share a "hidden" spin $\sigma_{i+\frac{1}{2}}$, through the coupling K. Fig.6.1 shows the case of a closed chain with three visible spins and three hidden ones. The

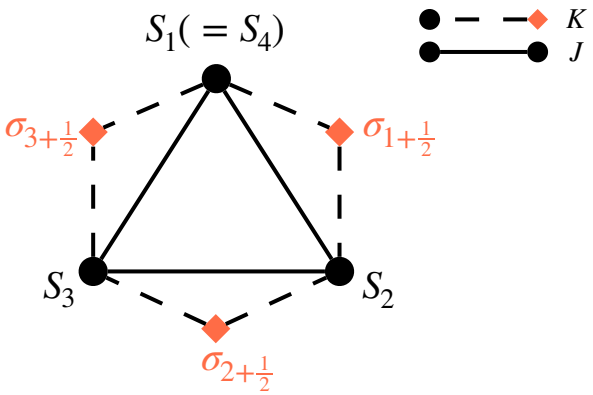

Figure 6.1: Model of non-Markovian spin system consisting of the visible (S_i) and hidden ($\sigma_{i+\frac{1}{2}}$) spins, see Eq.(6.1).

energy of the entire system reads

$$\mathcal{E} = -\sum_{i=1}^{N} J s_i s_{i+1} - K \sum_{i=1}^{N} (s_i + s_{i+1}) \sigma_{i+\frac{1}{2}}, \tag{6.1}$$

where $s_{N+1} \equiv s_1$. After taking the sub-trace over σ's, the effective energy $\tilde{E}_s$ and the effective partition function $\tilde{\mathcal{Z}}$ read:

$$\tilde{\mathcal{Z}} = \sum_{\{s_i\}} e^{-\beta \tilde{E}_s}, \quad \tilde{E}_s = -\sum_{i=1}^{N} \tilde{J} s_i s_{i+1}, \tag{6.2}$$

where the effective, temperature-dependent, coupling constant $\tilde{J}$ is

$$\tilde{J} \equiv J + (2\beta)^{-1} \ln \cosh(2\beta K). \tag{6.3}$$

The visible spins, therefore, follow the canonical statistics with the apparent coupling $\tilde{J}$ as long as the single-time statistics are concerned. If the whole system evolves by a Markovian dynamics such as the Glauber model, the observer who has only access to the visible spins $\{s_i\}$ finds its non-Markovian evolution. The non-Markovian nature in a simple case is demonstrated below. There is no more instantaneous detailed balance (DB) about the visible spins. Nevertheless, if the whole system $\{s, \sigma\}$ obeys a Markovian evolution with DB, the visible spins still satisfy a *trajectory-wise* detailed balance:

$$\mathbb{P}([\{s_i(t)\}_{i=1}^{N}]_{t=0}^{T}) = \mathbb{P}([\{s_i(t)\}_{i=0}^{N}]^{*T}_{t=0}), \tag{6.4}$$

where $[\{s_i(t)\}_{i=0}^{N}]^{*T}_{t=0}$ denotes the time reversal of the forward trajectory, $[\{s_i(t)\}_{i=1}^{N}]_{t=0}^{T}$. The derivation of (6.4) is given in Sec. 6.1.3.

6.1.2 Non-Markovianity of the Hidden-Spin model

Let the system has the energy function,

$$H = -K(s_1 + s_2)\sigma,$$

where $K > 0$ and the variables, s_1, s_2 and σ, are Ising spins. The "hidden" spin σ mediates the interaction between the "observable" spins, s_1 and s_2. We shall use the unit such that the inverse temperature is $\beta = 1$. We assume a Markovian evolution of this system but observe only s_1 and s_2. We introduce a short time step, dt, and focus on the three consecutive instants, $\{t_{k-1}, t_k, t_{k+1}\} = \{(k-1)\,dt, k\,dt, (k+1)\,dt\}$. We also introduce the notations, $\alpha_k = (s_1(t_k), s_2(t_k))$ and $\sigma_k = \sigma(t_k)$. Supposing $dt \ll \epsilon$, we will ignore the errors of $\mathcal{O}((dt)^2)$. Our main concern is the history-conditioned probability, $P(\alpha_{k+1}|\alpha_k, \alpha_{k-1})$, and we claim the general inequality, $P(\alpha_{k+1}|\alpha_k, \alpha_{k-1}) \neq P(\alpha_{k+1}|\alpha_k, \alpha'_{k-1})$ for $\alpha_{k-1} \neq \alpha'_{k-1}$. The Markovian transition probability in terms of the micro-state $\binom{\alpha_k}{\sigma_k}$ is written as $P\left(\begin{matrix}\alpha_{k+1} \\ \sigma_{k+1}\end{matrix}\middle|\begin{matrix}\alpha_k \\ \sigma_k\end{matrix}\right)$. Using this, the conditional probability $P(\alpha_{k+1}|\alpha_k, \alpha_{k-1})$ can be expressed

as

$$P(\alpha_{k+1}|\alpha_k,\alpha_{k-1}) = \frac{P(\alpha_{k+1},\alpha_k,\alpha_{k-1})}{P(\alpha_k,\alpha_{k-1})} = \frac{\sum_{\sigma_{k+1},\sigma_k,\sigma_{k-1}} P\begin{pmatrix}\alpha_{k+1}\\ \sigma_{k+1}\end{pmatrix}\begin{pmatrix}\alpha_k\\ \sigma_k\end{pmatrix} P\begin{pmatrix}\alpha_k\\ \sigma_k\end{pmatrix}\begin{pmatrix}\alpha_{k-1}\\ \sigma_{k-1}\end{pmatrix} P\begin{pmatrix}\alpha_{k-1}\\ \sigma_{k-1}\end{pmatrix}}{\sum_{\sigma'_k,\sigma'_{k-1}} P\begin{pmatrix}\alpha_k\\ \sigma'_k\end{pmatrix}\begin{pmatrix}\alpha_{k-1}\\ \sigma'_{k-1}\end{pmatrix} P\begin{pmatrix}\alpha_{k-1}\\ \sigma'_{k-1}\end{pmatrix}}. \quad (6.5)$$

As for the probability $P\begin{pmatrix}\alpha_{k-1}\\ \sigma_{k-1}\end{pmatrix}$ we assume the canonical weight, $\exp(-H(\begin{smallmatrix}\alpha_{k-1}\\ \sigma_{k-1}\end{smallmatrix}))/Z$ with the partition function, $Z = 4+2e^{2K}+2e^{-2K}$. In the conditional probability $P\begin{pmatrix}\alpha_{k+1}\\ \sigma_{k+1}\end{pmatrix}\begin{pmatrix}\alpha_k\\ \sigma_k\end{pmatrix}$ we ignore the flipping of more than one spin because such an event weights $\mathcal{O}((dt)^2)$. As for the single spin flip, we use the formalism of Bergmann-Lebowitz [94]: The transition rate $W_{b\leftarrow a}$ from the micro-state a to b for $P(b|a) = W_{b\leftarrow a}dt$ takes the form, $W_{b\leftarrow a} = \nu_0 e^{-(\Delta_{[a,b]}-F_a)}$, which assures the (microscopic) Markovian DB. For those transition flipping σ we assign $\Delta_{[a,b]} = \delta$ while for those keeping σ fixed we assign $\Delta_{[a,b]} = \Delta$. The energy value F_a takes among $\{-2K, 0, 2K\}$. Some symbolic calculus tells that, while the transitions from the anti-parallel pair do not reflect the past further than $\mathcal{O}(dt)$[1];

$$\begin{aligned} P((++)|(+-),(++)) &= P((--)|(+-),(++)) \\ &= (\nu_0 dt)e^{-\Delta} \\ P((++)|(+-),(+-)) &= P((--)|(+-),(+-)) \\ &= (\nu_0 dt)e^{-\Delta}, \end{aligned} \quad (6.6)$$

the transition from the parallel pair depends on the further past;

$$\begin{aligned} P((-+)|(++),(-+)) &= P((+-)|(++),(-+)) \\ &= (\nu_0 dt)e^{-\Delta}\cosh(2K) \\ P((-+)|(++),(++)) &= P((+-)|(++),(++)) \\ &= (\nu_0 dt)e^{-\Delta}\mathrm{sech}(2K). \end{aligned} \quad (6.7)$$

[2] Thus we claim the general inequality; $P(\alpha_{k+1}|\alpha_k,\alpha_{k-1}) \neq P(\alpha_{k+1}|\alpha_k,\alpha'_{k-1})$ for $\alpha_{k-1} \neq \alpha'_{k-1}$. Intuitively, Eq.(6.7) means that if the state $(++)$ is realized only during $[(k-1)dt, kdt]$, the transition to $(-+)$ or to $(+-)$ is enhanced by the factor $\coth(2K)$ (>1) as compared with the case in which the state $(++)$ has been maintained before $(k-1)dt$.

6.1.3 Trajectory-wise detailed balance

Suppose a system undergoes a Markovian stochastic process, satisfying the detailed balance (DB). We denote by $\omega_k = (\begin{smallmatrix}\alpha_k\\ \sigma_k\end{smallmatrix})$ the state of the system at time t_k, where α and σ

[1] The notation (+-) means $(s_1, s_2) = (1, -1)$,, etc.

[2] Recall that at most only one spin can flip during dt. Therefore, $\alpha_{k+1} \neq \alpha_k$ implies $\sigma_{k+1} = \sigma_k$.

stand for the visible and hidden variables, respectively. For simplicity the time-reversed state of ω is assumed to be ω. As in Sec. 6.1.2 we use the discretization of time with small interval dt. Then the "instantaneous" DB condition for ω, reads,

$$\mathbb{P}(\omega_{k-1}|\omega_k)P^{eq}_{\omega_k} = \mathbb{P}(\omega_k|\omega_{k-1})P^{eq}_{\omega_{k-1}}. \tag{6.8}$$

In repeatedly using this relation, we have the trajectory-wise DB for the variable ω starting from the canonical state, P^{eq} :

$$\begin{aligned}\mathbb{P}(\{\omega_k\}^{\mathcal{K}}_{k=0}) &= \mathbb{P}(\omega_{\mathcal{K}}|\omega_{\mathcal{K}-\infty})\cdots\mathbb{P}(\omega_2|\omega_1)\mathbb{P}(\omega_1|\omega_0)P^{eq}_{\omega_0}\\ &= P^{eq}_{\omega_{\mathcal{K}}}\mathbb{P}(\omega_{\mathcal{K}-1}|\omega_{\mathcal{K}})\cdots\mathbb{P}(\omega_1|\omega_2)\mathbb{P}(\omega_0|\omega_1)\\ &= \mathbb{P}(\omega_0|\omega_1)\mathbb{P}(\omega_1|\omega_2)\cdots\mathbb{P}(\omega_{\mathcal{K}-1}|\omega_{\mathcal{K}})P^{eq}_{\omega_{\mathcal{K}}}\\ &\equiv \mathbb{P}(\{\omega_k\}^{*\mathcal{K}}_{k=0}).\end{aligned} \tag{6.9}$$

We then focus only on the history of the visible observables, $\{\alpha_k\}^{\mathcal{K}}_{k=0}$. For that purpose we integrate out the hidden part, $\{\sigma_k\}^{\mathcal{K}}_{k=0}$:

$$\mathbb{P}(\{\alpha_k\}^{\mathcal{K}}_{k=0}) = \sum_{\{\sigma_m\}^{\mathcal{K}}_{m=0}} \mathbb{P}(\{\omega_k\}^{\mathcal{K}}_{k=0}),$$

where the sum is taken under the fixed $\{\alpha_k\}^{\mathcal{K}}_{k=0}$. Applying (6.9) to each term on the r.h.s. above, we have

$$l.h.s. = \sum_{\{\sigma_m\}^{*\mathcal{K}}_{m=0}} \mathbb{P}(\{\omega_k\}^{*\mathcal{K}}_{k=0}) \tag{6.10}$$

$$= \mathbb{P}(\{\alpha_k\}^{*\mathcal{K}}_{k=0}). \tag{6.11}$$

Thus, we have the trajectory-wise DB relation.

$$\mathbb{P}(\{\alpha_k\}^{\mathcal{K}}_{k=0}) = \mathbb{P}(\{\alpha_k\}^{*\mathcal{K}}_{k=0}). \tag{6.12}$$

The relation like (6.8) does not hold any more because $\mathbb{P}(\alpha_{k+1},\alpha_k) = \mathbb{P}(\alpha_{k+1}|\alpha_k)P^{eq}_{\alpha_k}$ contains behind many trajectories of ω.

6.1.4 Effects of the PQ

Quenching generally breaks canonicity: In principle, the quenching of a visible spin *can* accompany any actions on the hidden part even though the system starts by the canonical ensemble. For example, we can imagine the case in which the quenching of the visible spin s_i in Fig.6.1 imposes a specific value for the hidden spin $\sigma_{i+\frac{1}{2}}$ at the i-th step of quenching. The general principle mentioned above may have exceptions through deliberately designed actions of the PQ. Two such cases are demonstrated below.

Case of unbroken canonicity upon PQ: We take up again the non-Markovian model shown in Fig. 6.1, with the energy given by Eq.(6.1) wherein the steady state the Detailed-Balance (DB) holds. A Glauber algorithm is used to simulate the dynamics of the whole system, and we progressively quench the visible spins exclusively while the hidden vari-

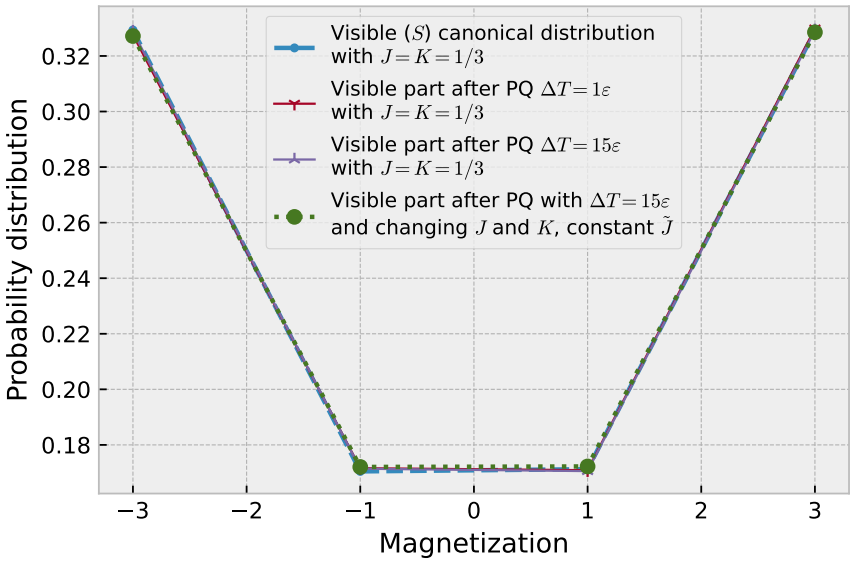

Figure 6.2: Probability distribution of the visible spins $M = S_1 + S_2 + S_3$ after all the visible spins have been fixed. For the solid curves J and K are kept at $(1/3)(k_{\rm B}T)$ with the interval between consecutive quench being $\Delta T/\epsilon = 0, 1$ and 15 respectively. The dashed curve corresponds to variating values of J and K - see the main text for the detailed protocol.

ables remain intact. According to Sec. 5.2, the PQ of that system, particularly the selective quenching of visible spins, should not modify the distribution as the two-story ensemble. Fig. 6.2 (thick curves) verifies this idea, where the probability distribution of the (visible) magnetization, $M \equiv S_1 + S_2 + S_3$, after all these spins have been quenched. Here the quenching of visible spins is progressively done with a regular (dimensionless) interval, $\Delta T/\epsilon = 0, 1$ and 15 (solid curves), where $\Delta T/\epsilon = 0$ is equivalent to the snapshot of the equilibrium ensemble before quench. The distributions are independent of the interval $\Delta T/\epsilon$.

We also examined another *ad hoc* protocol in which the fixation of visible spin accompanies the modification of the coupling parameters, J and K. At every quenching, the value of J is reduced by 50% whole that of K is incremented so that the effective coupling $\tilde{J}$ of Eq.(6.3) remains unchanged. When we monitor the magnetization of visible spins, $M \equiv S_1 + S_2 + S_3$, its distribution after sufficient interval $\Delta T/\epsilon$ recovers the canonical one, by construction (Fig.6.2, dotted curve). Nevertheless, there is a visible transient before the equilibration in M, which we monitor through its variance $\langle M^2 \rangle$, see Fig.6.3 (cf. $\langle M \rangle = 0$). The fluctuations of M are transiently attenuated as a fast response to the reduction of J, then it recovers the canonical level (horizontal dotted line) gradually due to the compensatory increment of K.

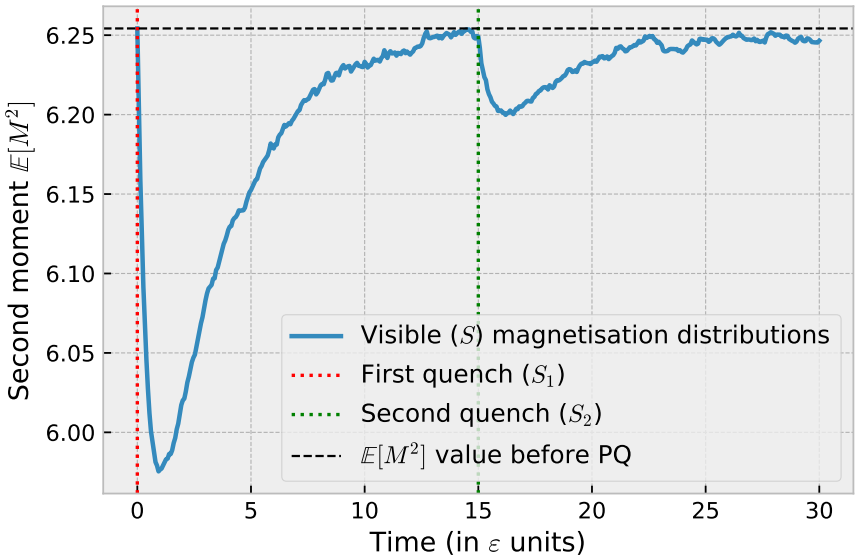

Figure 6.3: Transient processes corresponding to the protocol for the dashed curve in Figure 6.2. The second moment $E[M^2]$ (cf. $E[M] = 0$) of the whole visible magnetization, $M = S_1 + S_2 + S_3$, is plotted against the scaled time, t/ϵ after each quenching. The statistical average is taken over multiple realizations of the process.

6.2 Delayed interactions in spin systems: The Choi-Huberman model

We have seen in the previous subsection (Sec.6.1) that the conservation of the canonicity upon the PQ requires a Markovian evolution rule in addition to the detailed balance in the starting steady state. In the last part of this chapter, we study the effect of PQ on the non-Markovian system whose steady state has been broken from the beginning, i.e., before quenching the system's degrees of freedom, to understand the PQ better.

6.2.1 Original Choi-Huberman model and its steady state

The starting model was introduced by Choi and Huberman in 1985 [95]. In their model, the interactions between spins have a delay τ with respect to the instantaneous ones, i.e., each spin at t "sees" the other spins at $(t - \tau)$. The probability of flipping of the spin s_i reads:

$$P[s_i(t + dt) = -s_i(t)] = \frac{dt}{2\varepsilon} [1 - s_i(t) \tanh(\beta E_i(t - \tau))] \tag{6.13}$$

with E_i being defined by Eq.(4.55). Except for the limit of the Glauber model [71] with $\tau = 0$, the steady state distribution should break the detailed balance because $\tau > 0$ invalidates the time-reversal symmetry. We characterize the irreversibility by the non-dimensionalized parameter, $a \equiv \tau/\varepsilon$. Throughout this section (6.2), the numerical simulation based on (6.13) is done with the time mesh $dt/\varepsilon = 0.1$ for $a \geq 1$ and $dt = 0.05$ for $a < 1$. In the appendix 6.3 of this chapter, we show analytically that the steady state

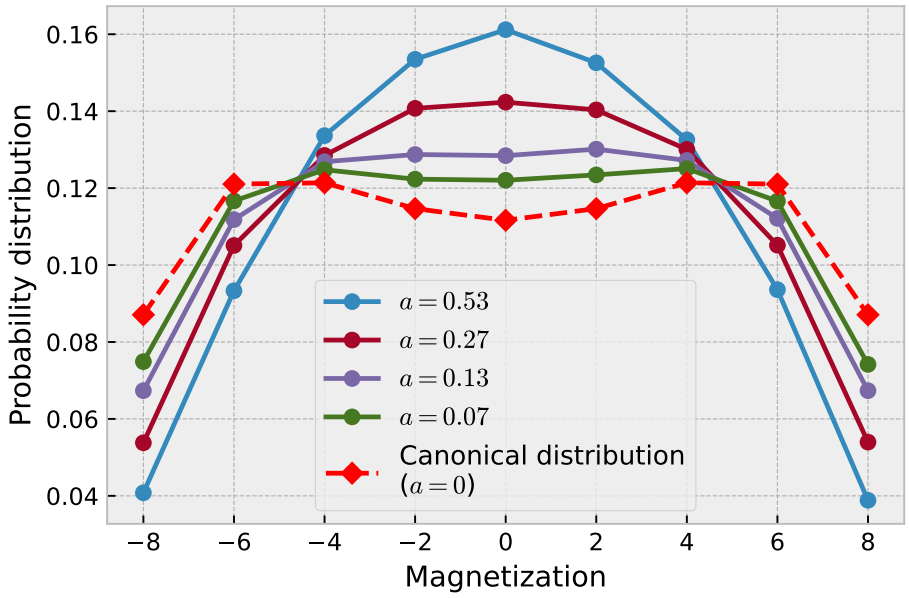

Figure 6.4: Plot of the steady state distribution of the total magnetization, $M = \sum_{i=1}^{N} s_i$ with $N = 8$ in the Choi-Huberman (C-H), for different values of non-dimensionalized delay, $a = \tau/\varepsilon$. The canonical distribution ($\tau = 0$) corresponds to the $a = 0$ case.

depends on the kinetic parameter, ε (via a), for the system with two spins. We recall that the canonical equilibrium, i.e. $a = 0$, is independent of ε. Numerically, we show in Fig.6.4 how the steady state distribution of the system with eight spins depends on the irreversibility parameter a. We see that the larger the value of a, the more paramagnetic (unimodal) the system behaves as compared with the bimodal distribution with Markovian limit, $a = 0$. Intuitively, when the delay τ is augmented, the cooperative fluctuations among the spins are lessened.

6.2.2 Effects of the PQ of the Choi-Huberman model

If we introduce the PQ in the above model of Choi-Huberman, what effect should we expect? First, we studied how the two-story distribution of the total magnetization evolves as a function of the number of quenched spins. The irreversibility parameter a is kept at 1.07 where the intact distribution is unimodal (see Fig.6.4). We have given a large enough time interval ΔT between the consecutive quenching so that $\Delta T/\varepsilon = 15 \gg a$. Leaving the details in section 6.3, we found that the evolution is qualitatively similar to Fig.6.4, where the increment in the number of quenched spins corresponds to the *reduction* of the irreversibility parameter a. This result may be qualitatively understandable because the quenching of the spin s_i amounts to the replacement of ε_i by ∞, or the reduction of a_i to 0 for that spin. When the time interval between the consecutive quenching, ΔT, is not exceedingly larger than either ε or τ, the second dimension-free parameter, $\Delta T/\varepsilon$, comes into play in addition to a. Fig.6.5 shows how the final distribution of the total magnetization, M, depends on the values of $\Delta T/\varepsilon$, where the non-dimensionalized delay

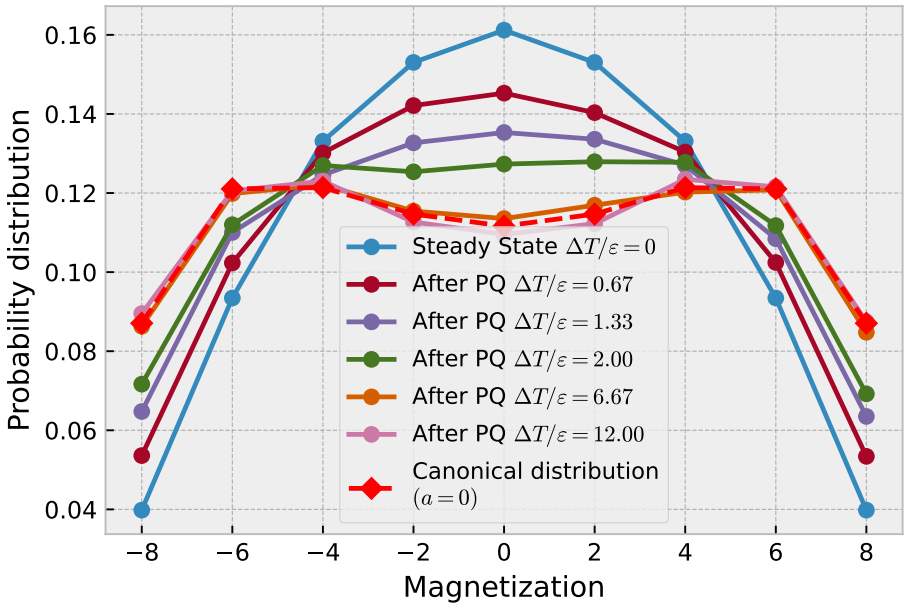

Figure 6.5: The magnetization distribution after the Progressive Quenching has been completed with different values of $\Delta T/\varepsilon$. The steady-state distribution, as well as the canonical distributions, are also plotted for comparison.

a is again fixed at 1.07. Note that with $\Delta T/\varepsilon = 0$, the steady state ensemble of the original Choi-Huberman model is entirely copied by PQ as the quenched ensemble. With increasing the value of $\Delta T/\varepsilon$, the free spins have more time to adapt to the quenched part, and the distribution of M undergoes the change which is a qualitatively similar manner to the case of *decreasing* the value of a. The above results in Figs.6.4 and 6.5 motivate to study the possible synthetic effect of a and $\Delta T/\varepsilon$, or the possible characterization by $(\Delta T/\varepsilon)/a(= \Delta T/\tau)$. Nevertheless, the comparison on the level of the probability distribution of M is too complicated. We, therefore, characterize each distribution by the second moment $\mathbb{E}[M^2]$ standardized by its canonical value (i.e., for $a = 0$ and arbitrary $\Delta T/\varepsilon$), which we denote by $\mathbb{E}_{can}[M^2]$, all knowing that some subtle aspects of the distribution will be lost. For example, the equality, $\mathbb{E}[M^2] = \mathbb{E}_{can}[M^2]$, does not mean that the distribution is identical to the canonical one. Fig.6.6 shows this type of "projection" from the Fig.6.5, being complemented by more data points. Somewhat surprisingly the ratio $\mathbb{E}[M^2]/\mathbb{E}_{can}[M^2]$ exceeds unity for $\Delta T/\varepsilon \gtrsim 8$. The unimodal-bimodal transition of the distribution takes place where $\mathbb{E}[M^2]/\mathbb{E}_{can}[M^2] = 0.9$ approximately (see below).

Fig. 6.7 summarizes the contours of $\mathbb{E}[M^2]/\mathbb{E}_{can}[M^2]$ on the plane of a and $\Delta T/\varepsilon$ for $N_0 = 8$ as the landscape of correlation among quenched spins. $\mathbb{E}[M^2]/\mathbb{E}_{can}[M^2]$ represents rather well the characteristics of the probability distribution of M. Especially the unimodal-bimodal transition of the distribution of M is found to occur where $\mathbb{E}[M^2]/\mathbb{E}_{can}[M^2] \simeq 0.9$ (data not shown). Along the vertical axis with $a = 0$, the model is the reversible canonical one, therefore, $\mathbb{E}[M^2]/\mathbb{E}_{can}[M^2] = 1$ by definition. However, there is another contour of "canonical" level. The zone above this contour is "super-canonical" realizing $\mathbb{E}[M^2]/\mathbb{E}_{can}[M^2] > 1$ although the excess part is quite small. This

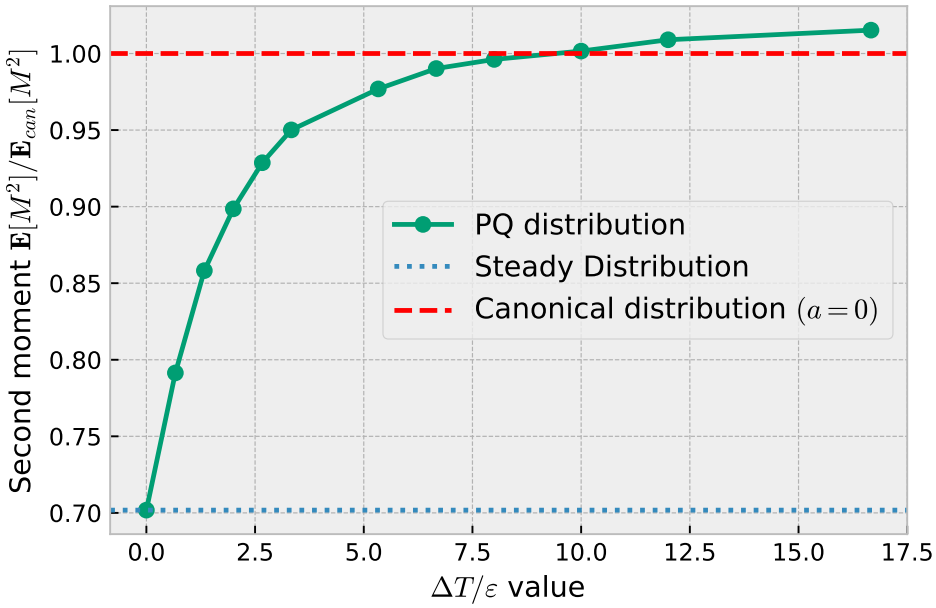

Figure 6.6: Plot of the standardized second moment of the magnetization after PQ, $\mathbb{E}[M^2]/\mathbb{E}_{can}[M^2]$, versus the time interval parameter, $\Delta T/\varepsilon$, where $a = 1.07$ is kept the same as in Figure 6.5 and $N = 8$. The steady-state levels ($\Delta T/\varepsilon = 0$) and the canonical case ($a = 0$) are also shown by dashed horizontal lines.

overreach reveals some synergistic effect of the three characteristic time constants, ε, τ and ΔT. Moreover, the "super-canonical" feature is more enhanced, rather than contrary, for the larger system size N. We can see Fig. 6.6 as a vertical projection of Fig. 6.7 for $a = 1.07$. In the parameter region below the second non-vertical "canonical" contour, $\mathbb{E}[M^2]/\mathbb{E}_{can}[M^2] = 1$, the landscape of $\mathbb{E}[M^2]/\mathbb{E}_{can}[M^2]$ is monotone with respect to both a and $\Delta T/\varepsilon$. This suggests that there is a compensating nature of ΔT for the delay τ. However, near the origin, the perturbation by a dominates over the influence of $\Delta T/\varepsilon$.

6.3 Conclusion

In the non-Markovian process, even when the system realizes a trajectory-wise detailed balance, the quenching may involve uncontrollable/unobservable modifications in the underlying freedoms that constitute the memory of the observable parts, and such changes can cause the breaking of canonicity of the observable part. We also applied the PQ to the system for which the detailed balance is absent even in the unquenched steady ensemble. In the case of PQ on the Choi-Huberman (C-H) model, the operation of PQ can be unambiguously formulated. Monitoring through the variance of the total magnetization, we examined the interplay between the intrinsic non-Markovian parameter τ of the dimension of time and the time interval between the subsequent quenching, ΔT. While the canonical correlation that favored the cooperative fluctuations of spins is attenuated by the non-Markovian delay τ, the operation of quenching reinforces the cooperative fluctuations through ΔT.

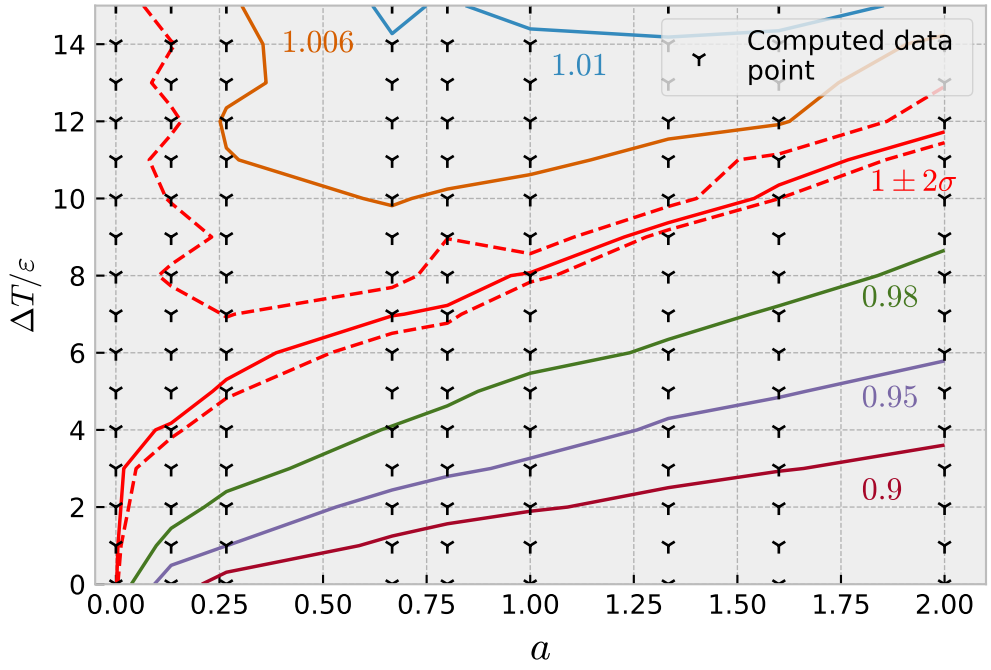

Figure 6.7: Contour plot of the standardized mean square (in a similar way as pictured in Figure 6.6) of the final quenched magnetization, $\mathbb{E}[M^2]/\mathbb{E}_{can}[M^2]$, on the plane of $(a, \Delta T/\varepsilon)$ with $N = 8$. Each tic symbol indicates points where $\mathbb{E}[M^2]$ has been calculated over 6×10^5 samples and the contours are thereby calculated using the ContourPy library. The red dashed lines correspond to the contours of the $\pm 2\sigma$ confidence interval for $\mathbb{E}[M^2] = \mathbb{E}_{can}[M^2]$. The values at which the contours are plotted are indicated next to the corresponding line.

Appendix

Evolution of spin correlations along PQ in the two-story ensemble

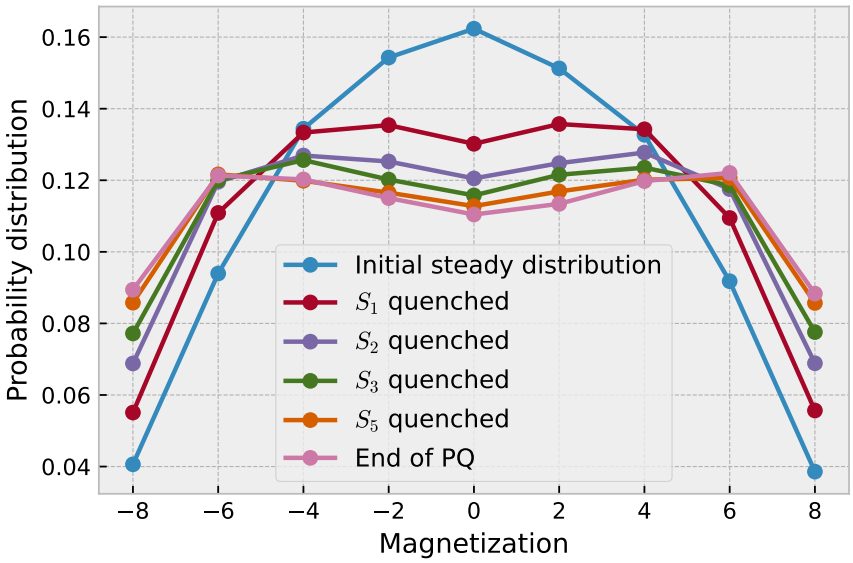

Figure 6.8: The distribution of magnetization at different stages of PQ. The non-dimensionalized delay a and the non-dimensionalized time interval between consecutive quenches, $\Delta T/\varepsilon$, are fixed at $(a, \Delta T/\varepsilon) = (1.07, 15)$.

Fig.6.8 shows how the distribution of the total magnetization evolves with the stages of PQ. Here, it is understood that, when a part of all of the spins are quenched, the total magnetization M is calculated using the two-story ensemble including both quenched spins and thermally fluctuating ones (see Sec.4.4). The kinetic parameters are fixed at $(a, \Delta T/\varepsilon) = (1.07, 15)$. As compared with the CH model without quenching (the unimodal blue points and links), we observe that the progress of quenching enhances the correlation among the spins, as is the case with a decreased delay parameter a observed in Figs.6.4.

Absence of Detailed Balance in the Choi-Huberman model

This Appendix focuses on verifying the non-canonical nature of the steady state of the Choi-Huberman model, the Ising spin system with delayed interaction. The approach is to take up a simplified and discrete-time version of the Choi- Huberman (CH) model applied to the two Ising spins and to show that its steady state depends on the kinetic parameters, which is not the case for the canonical ensemble.

The time is discretized with the unit being unity, and we set the delay of the interaction τ to be equal to this unit, i.e., $\tau = 1$. We denote by $\vec{s}(t) := \begin{pmatrix} s_0(t) \\ s_1(t) \end{pmatrix}$ the polarization of the two spins at time t. Following the CH model, the probability that $s_0(t)$ $[s_1(t)]$ at t are flipped at the time $(t+1)$ depends on the spin state of their (exclusive) neighbors, but

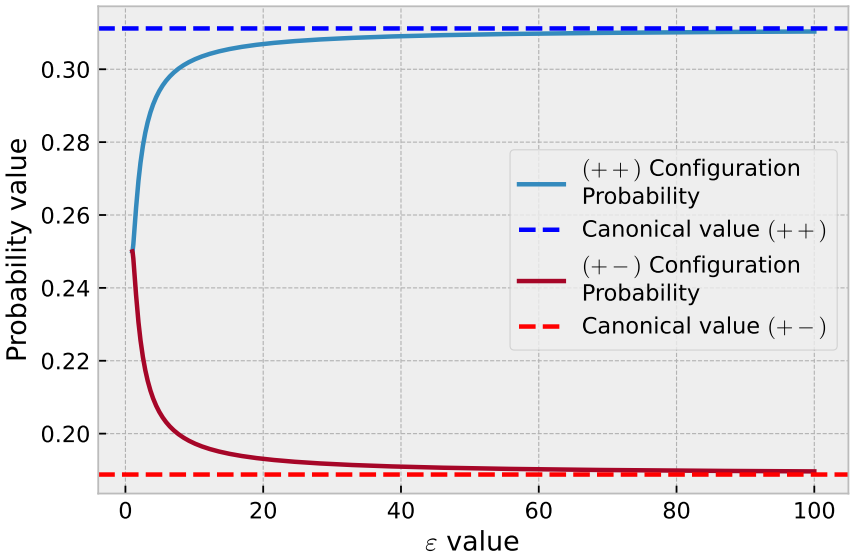

Figure 6.9: Plot of the steady-state probabilities (solid curves): $P^{\rm st}\left[\begin{pmatrix}+1\\+1\end{pmatrix}\right] = P^{\rm st}\left[\begin{pmatrix}-1\\-1\end{pmatrix}\right]$ in blue, and $P^{\rm st}\left[\begin{pmatrix}+1\\-1\end{pmatrix}\right] = P^{\rm st}\left[\begin{pmatrix}-1\\+1\end{pmatrix}\right]$ in red, as functions of $\varepsilon(\geq 1)$. The coupling parameter $\eta = \tanh(\beta j)$ has been set such that $\beta j = 1/4$. Data were drawn using the formula (6.17).

at the time $(t-1)$, that is, on $s_1(t-1)$ $[s_0(t-1)]$. In the spirit of the (discrete-time) Glauber model, we adopt the probabilities,

$$\mathbb{P}\left[s_0(t+1) = -s_0(t)|\vec{s}(t), \vec{s}(t-1)\right] = \frac{1}{2\varepsilon}(1 - s_0(t)s_1(t-1)\eta) \tag{6.14}$$

$$\mathbb{P}\left[s_1(t+1) = -s_1(t)|\vec{s}(t), \vec{s}(t-1)\right] = \frac{1}{2\varepsilon}(1 - s_1(t)s_0(t-1)\eta), \tag{6.15}$$

with $\eta = \tanh(\beta j/2)$, where $j/2$ is the coupling constant for this two spin system, similarly to the Glauber mode. (The factor $1/2$ is merely from the convention on the complete lattice applied to $N = 2$ spins.) For the sake of simplicity, we assume that the flip of the two spins takes place independently for one from the other. Then the probability of $\vec{s}(t+1)$ reads,

$$\begin{aligned}\mathbb{P}\left[\vec{s}(t+1)|\vec{s}(t), \vec{s}(t-1)\right] = \frac{1}{4}&\left[1 + s_0(t+1)s_0(t)\left(1 - \frac{1 - s_0(t)s_1(t-1)\eta}{\varepsilon}\right)\right] \\ &\times \left[1 + s_1(t+1)s_1(t)\left(1 - \frac{1 - s_1(t)s_0(t-1)\eta}{\varepsilon}\right)\right],\end{aligned} \tag{6.16}$$

where, for the discrete-time version, Glauber's elementary time scale, ε, should be no less than unity. To handle the above non-Markovian transition probabilities, we follow the usual technique of Markovianizing the original description by extending the state so that the state involves more than one moment of time. Here we choose as the extended state the

2×2 matrix, $(\vec{s}(t+1),\vec{s}(t)) := \begin{pmatrix} s_0(t+1) & s_0(t) \\ s_1(t+1) & s_0(t) \end{pmatrix}$. Through such redefinition of the state, the transition from $(\vec{s}(t),\vec{s}(t-1))$ to $(\vec{s}(t+1),\vec{s}(t))$ is Markovian. (cf. The redundancy of the description due to the reappearance of $\vec{s}(t)$ does not harm the procedure.) Formally, this Markov chain should be written as a 16 matrix, and the question of the steady state probability is reduced to the search of the eigenvector of this matrix with the unitary eigenvalue. After some symbolic calculus, the steady-state probability $P^{\rm st}(\vec{s})$ is found to be

$$\begin{aligned} P^{\rm st}\begin{pmatrix}+1\\+1\end{pmatrix} &= \frac{(1+\eta)(\varepsilon-\eta)^2(2\varepsilon+\eta-1)}{8\varepsilon^3-4\varepsilon^2\left(3\eta^2+1\right)+8\varepsilon\eta^2+4\eta^2\left(\eta^2-1\right)} \\ &= P^{\rm st}\begin{pmatrix}-1\\-1\end{pmatrix} \qquad (6.17) \\ P^{\rm st}\begin{pmatrix}+1\\-1\end{pmatrix} &= \frac{(1-\eta)(\varepsilon+\eta)^2(2\varepsilon-\eta-1)}{8\varepsilon^3-4\varepsilon^2\left(3\eta^2+1\right)+8\varepsilon\eta^2+4\eta^2\left(\eta^2-1\right)} \\ &= P^{\rm st}\begin{pmatrix}-1\\+1\end{pmatrix}. \qquad (6.18) \end{aligned}$$

Evidently, the steady state depends on the kinetic parameter ε, as a sign of non-canonical ensemble. Figure 6.9 shows the above probabilities as function of $\varepsilon(\geq 1)$. In the limit, $\varepsilon\to+\infty$, the system behaves canonically (the top and bottom dashed lines), whereas in the limit, $\varepsilon\to 1^+$, all the probabilities become 1/4. The theoretical formula (6.17) is also in excellent agreement with numerical simulations.

"Markovianization" of non-Markov problems

Network modification and state replication techniques can be used to perform exact "Markovianization" of non-Markov problems [96]. For example, we consider a 1D chain

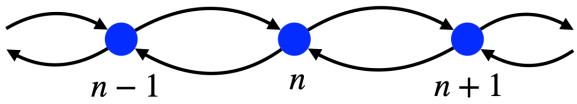

Figure 6.10: Scheme of a 1D chain network on which a non-Markov jump process occurs.

of states with jump probabilities depending on the current state and the previous jump realization. We define the stochastic jump $\hat{X}_k$ that takes the value $+1$ when the walker goes from a state n to the state $n+1$, or the value -1 if the walker goes from n to $n-1$ at stage k. We suppose that the probability of having $\left(\hat{X}_k=\pm 1\right)$ depends on the value of the previous jump. The jump probabilities $\mathbb{P}(\hat{X}_k=\pm 1|X_{k-1}=\pm 1)$ are defined as follows:

Condition	Jump probability	
	k-th jump $=+1$	k-th jump $=-1$
$(k-1)$-th jump $=+1$	$(1-\theta)w$	θw
$(k-1)$-th jump $=-1$	θw	$(1-\theta)w$

We can map this problem to a Markovian transition network, *via* a replica of the whole chain, to allow the conditions on $\hat{X}_{k+1}$ to be taken into account.

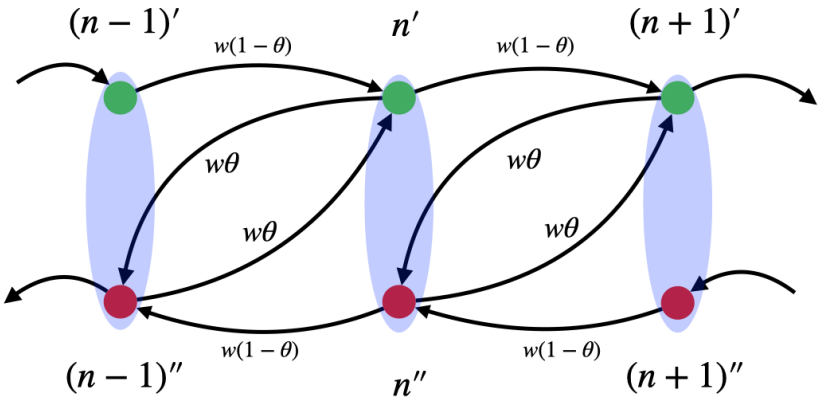

Figure 6.11: Modified transition network derived from Fig.6.10. The non-Markovian process is rendered Markovian thanks to the double chains.

In the example depicted in Fig.6.11, the states $\{n'\}$ are only reached **from the left** to ensure that the previous transition was $+1$. Similarly, the states $\{n''\}$ are reached **from the right**, ensuring that the previous transition was -1. We then link the states with transition rates in accordance with the table to fully describe the Markovian network. We can then apply the previous techniques to obtain, for example, FPT statistics. Note that n' and n'' both describe the same original state n, and their statistics must be added to obtain the original one.

The random walk exhibits a directional persistence when the parameter θ differs from $1/2$. The $0 < \theta < 1/2$ case typically represents the "run and tumble" processes, whereas $1/2 < \theta < 1$ represents turn alterations (typical trajectories are depicted in Fig.6.12). Otherwise, if $\theta = 1/2$, the process is a Markovian random walk. This "fine-graining" method of Markovianization preserves the time resolution of the underlying process instead of coarse-graining methods (discussed above in Sec.1.3.2).

The topology of the TN in Fig.6.11 is isomorphic with that of the run-and-tumble model of an active swimmer [96]. In the latter model, the nodes n' and $n-1''$ in Fig.6.11 is associated to the position n.

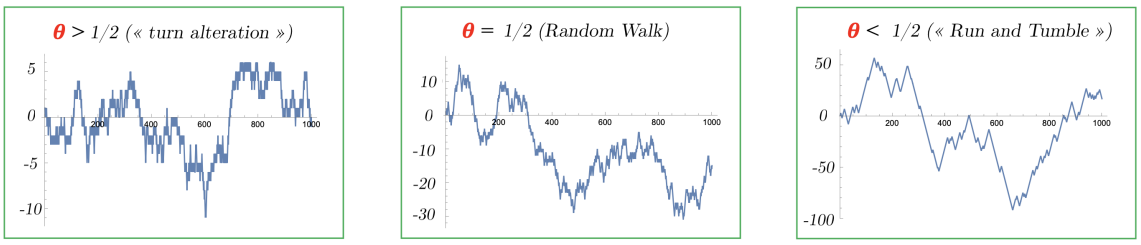

Figure 6.12: Typical trajectories for the three different cases. Note that the smaller θ is, the more spread trajectories are. This effect is explained qualitatively by the diffusion coefficient D dependency with θ (Eq.6.23).

Calculation of the diffusion coefficient We take the period between **consecutive tumbling** as a time unit. (The step displacement of the tumbling will be taken into account later as the first displacement of this period.) Since the **tumbling** transition rate is θw, the probability density of this period is $P(t)dt = (\theta w)e^{-\theta wt}dt$. During this period, a number of forward jump, n, occurs with a Poissonian distribution $P(n|t) = \frac{e^{-(1-\theta)wt}}{n!}[(1-\theta)wt]^n$. The joint probability is then,

$$P(t,n)dt = \frac{e^{-(1-\theta)wt}}{n!}[(1-\theta)wt]^n(\theta w)e^{-\theta wt}dt. \tag{6.19}$$

Note that, using the gamma function identity on natural integers: $\Gamma(n) = \int_0^\infty e^{-x}x^{n-1}dx = (n-1)!$ with $n \in \mathbb{N}^*$, we have :

$$\begin{aligned} P(n) &= \int_0^\infty P(t,n)dt \\ &= \int_0^\infty \frac{e^{-(1-\theta)wt}}{n!}[(1-\theta)wt]^n(\theta w)e^{-\theta wt}dt \\ &= (1-\theta)^n\theta\int_0^\infty \frac{e^{-wt}}{n!}(wt)^n w dt \\ &= (1-\theta)^n\theta\frac{1}{n!}\int_0^\infty e^x x^n dx = (1-\theta)^n\theta \qquad \text{with } x = wt. \end{aligned} \tag{6.20}$$

The run length ℓ_n is given by $\ell_n = n+1$, to account for the initial unit step associated with the tumbling. For the N pairs of periods of forward and backward runs, the total time is $T = (\sum_{k=1}^N t_k^+) + (\sum_{k=1}^N t_k^-)$ and the total displacement is $X = (\sum_{k=1}^N \ell_k^+) - (\sum_{k=1}^N \ell_k^-)$. For each period we apply $P(t_k^\pm, n_k^\pm)$, where $\ell_k^\pm = n_k^\pm + 1$. The quantity of interest is the ratio $\mathbb{E}[X^2]/(2\mathbb{E}[T])$. Since different $\ell_k^\pm$'s are mutually independent,

$$\mathbb{E}[T] = 2N\mathbb{E}[t] \tag{6.21}$$

$$\mathbb{E}[X^2] = 2N(\mathbb{E}[\ell^2] - \mathbb{E}[\ell]^2) = 2N(\mathbb{E}[n^2] - \mathbb{E}[n]^2). \tag{6.22}$$

From $P(n)$ we find $\mathbb{E}[n^2] - \mathbb{E}[n]^2 = \frac{(1-\theta)}{\theta^2}$, while from $P(t)$ we find $\mathbb{E}[t] = \frac{1}{\theta\omega}$. Altogether, the diffusion constant is

$$D = \frac{\mathbb{E}[X^2]}{2\mathbb{E}[T]} = \frac{\mathbb{E}[n^2] - \mathbb{E}[n]^2}{2\mathbb{E}[t]} = \frac{w}{2}\frac{1-\theta}{\theta}. \tag{6.23}$$

Here, w is the total frequency of jumps, either rightward or leftward.

General Conclusion

This manuscript relates the evolution of Progressive Quenching over the course of my three-year thesis in its linearities and branchings. What began as an adaptation to Ising spins of a concept developed for the study of quasicrystals has been generalized and extended to Markov chains and has become a playground for the application of martingale theory in physics. Our focus on the Curie-Weiss model (globally coupled spins) in the first three chapters is restrictive by nature but has nevertheless enabled us to understand how the interactions between the quenched and free parts of the system subjected to Progressive Quenching are articulated.

Chapter 3 enabled us to systematically lay the foundations of the process introduced in the introduction and to understand the influence of the various system parameters. By fixing the temperature β, we have highlighted two limiting cases, namely the limits of zero coupling between spins, leading to unbiased random walks, and infinite coupling, leading to a necessarily polarized system. Therefore, the cases of interest are located at the boundary between these two limits, which we have identified as the critical coupling, i.e., the coupling that maximizes the system's magnetic susceptibility. We were also able to understand how to write the contribution of the fixed part in the Hamiltonian of the system, namely through an effective magnetic field acting on the whole free system. The Curie-Weiss model provides a simple formulation of this contribution.

Chapter 4 focuses on the notion of martingale, which governs the dynamics of system magnetization. This law, which highlights the cyclic relationship between fixed and free systems through characteristic quantities, enables us to understand the temporal evolution of the system. The latter seeks to maintain its average magnetization and thus results in trajectories following the contours of constant magnetization. This martingale law was first derived in an approximate way, but it turned out to be exact. We were keen to retain the approximate derivation, as it also tells us about the compensating mechanisms that enable $m^{(\mathrm{eq})}$ conservation. From this, we were able to conclude that it was possible to estimate the final position of a process, e.g. M_T, because it retains the value of $m^{(\mathrm{eq})}$ on average. We can then project these trajectories onto iso-$m^{(\mathrm{eq})}$ contours in order to estimate their final values. A crucial point is that the later this estimate is made, the more accurate it is. We interpret this property as the system's effective memory. It is the first positions of the trajectory that will globally determine its direction and therefore its final position. We have quantified this dependency by calculating the system's sensitivity. The greater the number of unfixed spins, the more sensitive the system is to perturbations.

We can offer a parallel to these conclusions in terms of social dynamics. When a common choice is made (typically, a referendum in a given population), public debate is primarily driven by the first people to give their opinions. So, in a social group that tends to be homogeneous in terms of opinion (i.e., with typically ferromagnetic interactions), the issues and debates brought to the news are generally dictated by the people giving their opinion first, who are also the people with the most media exposure. This admittedly unscientific parallel nevertheless allows us to justify that when public opinion is not very stable, social interactions are, on average, close to a critical value in the sense of equation 3.

Once the trajectory dynamics or Progressive Quenching realization had been studied, we turned to their overall distribution, i.e. the probability distribution of the final magnetization M_{N_0}. This is the subject of Chapter 5. First, we observed the dependence on the value of the spin-spin coupling j_0 in Chapter 3 and realized that this distribution

coincides with the canonical distribution of the system at thermodynamic equilibrium. First, through Recycled Quenching, an endless process derived from PQ, we were able to understand the origin of this distribution conservation, whereas spin binding is a priori a non-equilibrium process. The fundamental property at play here is the total probability formula, which allows us to establish that choosing the value of N_0 spins one by one or all together does not change the probability of their distribution. Once this equality had been established, we turned our attention to the dynamics of spin balancing and the influence of a quench on this. Using Glauber's dynamic algorithms, we demonstrated that the time between quenches had no influence on the final distribution, even though the systems were by nature frustrated quenches. We then explained this phenomenon from a thermodynamic point of view, with a parallel to Landauer's theory.

We then undertook a generalization of our results, supported by the results obtained with Glauber dynamics. For the latter, whatever the relaxation time of the system, the canonical distribution was the stationary distribution towards which the system tends under the rules of the algorithm. We wondered whether this could be generalized to stationary Markov chains (of which Glauber's algorithm is one). We then formulated Progressive Quenching for any Markov chain through our initial idea of representing a system by its degrees of freedom, which we can then fix. We showed that the condition for the final distribution due to the state of a system after Progressive Quenching was that the states verified between the detailed balance. In other words, when two states exchange balanced probability flows, we can remove the transitions between them without changing the static distribution of the system. For example, Glauber's algorithm verifies the detailed balance by construction, as this is a fundamental aspect of thermodynamic equilibrium on the microscopic scale. In this case, Progressive Quenching will give us the canonical distribution. We then sketched this result as a representation of a topological invariant of the directed graph representative of Markov chains.

The final chapter explores the consequences of Progressive Quenching on non-Markovian systems. We abandon our general Markov chain framework and return to Ising spin systems. We first studied systems with hidden degrees of freedom coupling visible spins together. We were then able to show that this system can be renormalized by integrating the invisible degrees of freedom. The latter modifies the system's equilibrium dynamics, but the equilibrium state of the entire system is not modified by Progressive Quenching. We observe magnetization "overshoots" during quenching, but the equilibrium value of the magnetization remains unchanged. We therefore set out to introduce delay into the spin interactions, following Choi and Huberman's model. The introduction of delay changes the picture entirely, as it makes the equilibrium state of the system dependent on the values of the kinetic coefficients. However, we realized that the action of quenching a spin is equivalent to making its typical response time tend towards $+\infty$. Progressive Quenching thus modifies the system's kinetics and hence its static distribution when its interactions include delay. Using numerical simulations, we were able to "map" the stationary state of the Choi-Huberman model as a function of the time lag between spins and the waiting time between two quenchings. This mapping enabled us to show numerically that the system reaches more polarized states than the no-delay case, corresponding to the canonical distribution. The larger the system size, the greater this effect appears to be, but this conclusion remains to be confirmed by further numerical studies.

Although the main results presented, namely the conservation of the stationary dis-

tribution in the Markovian case, may appear disappointing in their apparent simplicity, they nevertheless pave the way for the study of non-Markovian systems, in particular the coupling between delay between interactions and waiting time between two quenches. Our preliminary study seems to indicate that there is an area of domain $(a, \Delta T)$ where this effect is optimal.

In addition, Progressive Quenching applied to the Curie-Weiss model allows the application of martingale theory to processes that differ from the standards of stochastic thermodynamics. Given the generality of systems in which specific parameters become fixed with time, primarily systems cooling non-homogeneously, we are convinced that these processes go beyond pure statistical physics. Also, we have yet to study the consequences when T is a stopping time [47, 49, 27]. Often, the many advantages of the martingale theory come with this concept. With a broader scope, hidden martingales under non-Markovian processes mentioned at the end of should be exploited in concrete evolution models beyond the quasi-static protocol. We believe that beyond analytical tools, martingales represent a class of mathematical and physical objects that has yet to be democratized.

Bibliography

[1] Bruno Ventéjou and Ken Sekimoto. Progressive quenching: Globally coupled model. *Physical Review E*, 97(6):062150, 2018.

[2] Charles Moslonka and Ken Sekimoto. Memory through a hidden martingale process in progressive quenching. *Physical Review E*, 101(6):062139, June 2020.

[3] Charles Moslonka and Ken Sekimoto. Martingale-induced local invariance in progressive quenching. *Phys. Rev. E*, 105:044146, Apr 2022.

[4] Charles Moslonka and Ken Sekimoto. Interplay between markovianity and progressive quenching. *arXiv preprint arXiv:2306.05831*, 2023.

[5] Francesco Avanzini, Massimo Bilancioni, Vasco Cavina, Sara Dal Cengio, Massimiliano Esposito, Gianmaria Falasco, Danilo Forastiere, Nahuel Freitas, Alberto Garilli, Pedro E Harunari, et al. Methods and conversations in (post) modern thermodynamics. *arXiv preprint arXiv:2311.01250*, 2023.

[6] Nicolaas Godfried Van Kampen. *Stochastic processes in physics and chemistry*, volume 1. Elsevier, 1992.

[7] C. Jarzynski. Nonequilibrium Equality for Free Energy Differences. *Physical Review Letters*, 78(14):2690–2693, April 1997.

[8] Udo Seifert. Entropy production along a stochastic trajectory and an integral fluctuation theorem. 95:040602, 2005.

[9] Udo Seifert. Stochastic thermodynamics, fluctuation theorems and molecular machines. *Reports on Progress in Physics*, 75(12):126001, nov 2012.

[10] K. Sekimoto. *Stochastic Energetics (Lecture Notes in Physics, vol. 799)*. Springer, 2010.

[11] Christopher Jarzynski. Equalities and inequalities: Irreversibility and the second law of thermodynamics at the nanoscale. *Annual Review of Condensed Matter Physics*, 2(1):329–351, 2011.

[12] Bruno Bresson, Coralie Brun, Xavier Buet, Yong Chen, Matteo Ciccotti, Jérôme Gâteau, Greg Jasion, Marco N. Petrovich, Francesco Poletti, David J. Richardson, Seyed Reza Sandoghchi, Gilles Tessier, Botond Tyukodi, and Damien Vandembroucq. Anisotropic superattenuation of capillary waves on driven glass interfaces. *Phys. Rev. Lett.*, 119:235501, Dec 2017.

[13] Marc Mézard, Giorgio Parisi, and Miguel Angel Virasoro. *Spin glass theory and beyond: An Introduction to the Replica Method and Its Applications*, volume 9. World Scientific Publishing Company, 1987.

[14] J-P Bouchaud and David S Dean. Aging on parisi's tree. *Journal de Physique I*, 5(3):265–286, 1995.

[15] SN Kaul. Static critical phenomena in ferromagnets with quenched disorder. *Journal of magnetism and magnetic materials*, 53(1-2):5–53, 1985.

[16] Viktor S Dotsenko. Critical phenomena and quenched disorder. *Physics-Uspekhi*, 38(5):457, 1995.

[17] Jannik C Meyer, Andre K Geim, Mikhail I Katsnelson, Konstantin S Novoselov, Tim J Booth, and Siegmar Roth. The structure of suspended graphene sheets. *Nature*, 446(7131):60–63, 2007.

[18] LL Bonilla, A Carpio, A Prados, and RR Rosales. Ripples in a string coupled to glauber spins. *Physical Review E*, 85(3):031125, 2012.

[19] Michael Widom, Katherine J Strandburg, and Robert H Swendsen. Quasicrystal equilibrium state. *Physical review letters*, 58(7):706, 1987.

[20] Katherine J Strandburg, Lei-Han Tang, and Marko V Jarić. Phason elasticity in entropic quasicrystals. *Physical review letters*, 63(3):314, 1989.

[21] Ken Sekimoto. Phason freezing in quasicrystals—a simple model using the freezing boundary condition. *Physica A: Statistical Mechanics and its Applications*, 170(1):150–186, 1990.

[22] M Etienne and K Sekimoto. Progressive quenching-ising chain models. *Acta Physica Polonica B*, 49(5):883, 2018.

[23] Joseph L Doob. The brownian movement and stochastic equations. *Annals of Mathematics*, pages 351–369, 1942.

[24] Raphaël Chetrite and Shamik Gupta. Two refreshing views of fluctuation theorems through kinematics elements and exponential martingale. 143(3):543, Apr 2011.

[25] Simone Pigolotti, Izaak Neri, Édgar Roldán, and Frank Jülicher. Generic properties of stochastic entropy production. *Physical review letters*, 119(14):140604, 2017.

[26] Raphaël Chétrite, Shamik Gupta, Izaak Neri, and Édgar Roldán. Martingale theory for housekeeping heat. *Europhysics Letters*, 124(6):60006, 2019.

[27] Izaak Neri. Second law of thermodynamics at stopping times. *Physical review letters*, 124(4):040601, 2020.

[28] Édgar Roldán, Izaak Neri, Raphael Chetrite, Shamik Gupta, Simone Pigolotti, Frank Jülicher, and Ken Sekimoto. Martingales for physicists, 2023.

[29] Bernard Bercu and Djalil Chafaï. *Modélisation stochastique et simulation-Cours et applications*. Dunod, 2007.

[30] Gonzalo Manzano, Diego Subero, Olivier Maillet, Rosario Fazio, Jukka P Pekola, and Édgar Roldán. Thermodynamics of gambling demons. *Physical Review Letters*, 126(8):080603, 2021.

[31] Ken Sekimoto. Derivation of the first passage time distribution for markovian process on discrete network, 2021.

[32] Hendrik Anthony Kramers. Brownian motion in a field of force and the diffusion model of chemical reactions. *Physica*, 7(4):284–304, 1940.

[33] Roger A Horn and Charles R Johnson. *Matrix analysis*. Cambridge university press, 2012.

[34] Carolyne M Van Vliet. *Equilibrium And Non-equilibrium Statistical Mechanics (New And Revised Printing)*. World Scientific Publishing Company, 2008.

[35] Hidetoshi Nishimori and Gerardo Ortiz. *Elements of phase transitions and critical phenomena*. Oup Oxford, 2010.

[36] RL Stratonovich. On a method of calculating quantum distribution functions. In *Soviet Physics Doklady*, volume 2, page 416, 1957.

[37] John Hubbard. Calculation of partition functions. *Physical Review Letters*, 3(2):77, 1959.

[38] Werner Krauth. *Statistical mechanics: algorithms and computations*. Number 13 in Oxford master series in physics. Oxford University Press, Oxford, 2006.

[39] Robert H. Swendsen and Jian-Sheng Wang. Nonuniversal critical dynamics in monte carlo simulations. *Phys. Rev. Lett.*, 58:86–88, Jan 1987.

[40] Ulli Wolff. Collective monte carlo updating for spin systems. *Physical Review Letters*, 62(4):361, 1989.

[41] Rick Durrett. *Probability: theory and examples*, volume 49. Cambridge university press, 2019.

[42] M. Baxter and A. Rennie. *Financial Calculus: An Introduction to Derivative Pricing*. Cambridge University Press, 1996.

[43] Izaak Neri, Édgar Roldán, and Frank Jülicher. Statistics of infima and stopping times of entropy production and applications to active molecular processes. *Phys. Rev. X*, 7:011019, Feb 2017.

[44] Gavin E. Crooks. Nonequilibrium measurements of free energy differences for microscopically reversible markovian systems. 90:1481–1487, 1998.

[45] S.A. Curtis. The classification of greedy algorithms. *Science of Computer Programming*, 49(1):125 – 157, 2003.

[46] Joseph L. Doob. What is a martingale? *Amer. Math. Monthly*, 78:451–463, 1971.

[47] Izaak Neri, Édgar Roldán, Simone Pigolotti, and Frank Jülicher. Integral fluctuation relations for entropy production at stopping times. *Journal of Statistical Mechanics: Theory and Experiment*, 2019(10):104006, oct 2019.

[48] Shilpi Singh, Paul Menczel, Dmitry S. Golubev, Ivan M. Khaymovich, Joonas T. Peltonen, Christian Flindt, Keiji Saito, Édgar Roldán, and Jukka P. Pekola. Universal first-passage-time distribution of non-gaussian currents. *Phys. Rev. Lett.*, 122:230602, Jun 2019.

[49] Gonzalo Manzano, Rosario Fazio, and Édgar Roldán. Quantum martingale theory and entropy production. *Phys. Rev. Lett.*, 122:220602, Jun 2019.

[50] Ken Sekimoto. Autonomous free-energy transduceer working under thermal fluctuations. *Physica D*, 205:242, 2005.

[51] Édgar Roldán, Izaak Neri, Raphael Chetrite, Shamik Gupta, Simone Pigolotti, Frank Jülicher, and Ken Sekimoto. Martingales for physicists. *arXiv preprint arXiv:2210.09983*, 2022.

[52] Lars Onsager. Reciprocal relations in irreversible processes. i. *Phys. Rev.*, 37:405–426, Feb 1931.

[53] H. B. G. Casimir. On onsager's principle of microscopic reversibility. *Rev. Mod. Phys.*, 17:343–350, Apr 1945.

[54] Ryogo Kubo. The fluctuation-dissipation theorem. *Reports on progress in physics*, 29(1):255, 1966.

[55] Umberto Marini Bettolo Marconi, Andrea Puglisi, Lamberto Rondoni, and Angelo Vulpiani. Fluctuation–dissipation: response theory in statistical physics. *Physics reports*, 461(4-6):111–195, 2008.

[56] Hugo Touchette. The large deviation approach to statistical mechanics. *Physics Reports*, 478(1-3):1–69, 2009.

[57] P. Malliavin. Stochastic calculus of variations and hypoelliptic operators. *Proceedings of the International Conference on Stochastic Differential Equations (Wiley, New York)*, :195–263, 1976.

[58] David Nualart and Eulalia Nualart. *Introduction to Malliavin calculus*, volume 9. Cambridge University Press, 2018.

[59] David Nualart. *The Malliavin calculus and related topics*. Probability and its applications. Springer, Berlin ; New York, 2nd ed edition, 2006.

[60] Ludovic Berthier. Efficient measurement of linear susceptibilities in molecular simulations: Application to aging supercooled liquids. *Phys. Rev. Lett.*, 98:220601, May 2007.

[61] Patrick B. Warren and Rosalind J. Allen. Malliavin weight sampling for computing sensitivity coefficients in brownian dynamics simulations. *Phys. Rev. Lett.*, 109:250601, Dec 2012.

[62] Patrick B Warren and Rosalind J Allen. Malliavin weight sampling: a practical guide. *Entropy*, 16(1):221–232, 2013.

[63] P. C. Martin, O. Parodi, and P. S. Pershan. Unified hydrodynamic theory for crystals, liquid crystals, and normal fluids. *Phys. Rev. A*, 6:2401–2420, Dec 1972.

[64] P. Hall and C.C. Heyde. *Martingale Limit Theory and its Application*. Academic Press, 1980.

[65] R.P. Feynman, R.B. Leighton, and M. Sands. *The Feynman Lectures on Physics, Vol. I: The New Millennium Edition: Mainly Mechanics, Radiation, and Heat*. Basic Books, 2015.

[66] David Williams. *Probability with Martingales*. Cambridge University Press, 1991.

[67] Thomas M. Liggett. The 1996 wald memorial lectures, stochastic models of interacting systems. *The Annals of Probability*, 25(1):1–29, 1997.

[68] Achim Klenke. *Probability theory: a comprehensive course*. Springer Science & Business Media, 2013.

[69] John B. Kogut. An introduction to lattice gauge theory and spin systems. *Rev. Mod. Phys.*, 51:659–713, Oct 1979.

[70] J. L. Doob. Semimartingales and subharmonic functions. *Trans. Amer. Math. Soc.*, 77:86–121, 1954.

[71] Roy J Glauber. Time-dependent statistics of the ising model. *Journal of mathematical physics*, 4(2):294–307, 1963.

[72] Fabio Martinelli. Lectures on glauber dynamics for discrete spin models. In *Lectures on probability theory and statistics*, pages 93–191. Springer, 1999.

[73] R. Landauer. Irreversibility and heat generation in the computing process. *IBM J. Res. Dev.*, 5:183–191, 1961) Reprint: **44**, 261-269 (2000).

[74] Naoto Shiraishi, Takumi Matsumoto, and Takahiro Sagawa. Measurement-feedback formalism meets information reservoirs. *New Journal of Physics*, 18(1):013044, 2016.

[75] Naoto Shiraishi and Keiji Saito. Incompatibility between carnot efficiency and finite power in markovian dynamics. *arXiv preprint arXiv:1602.03645*, 2016.

[76] Naoto Shiraishi, Keiji Saito, and Hal Tasaki. Universal trade-off relation between power and efficiency for heat engines. *Phys. Rev. Lett.*, 117:190601, Oct 2016.

[77] Massimiliano Esposito and Christian Van den Broeck. Three faces of the second law. i. master equation formulation. *Physical Review E*, 82(1):011143, 2010.

[78] Naoto Shiraishi and Takahiro Sagawa. Fluctuation theorem for partially masked nonequilibrium dynamics. *Phys. Rev. E*, 91:012130, 2015.

[79] James R Norris. *Markov chains*. Number 2. Cambridge university press, 1998.

[80] Geoffrey Grimmett and David Stirzaker. *Probability and random processes*. Oxford university press, 2020.

[81] Riccardo Rao and Massimiliano Esposito. Nonequilibrium thermodynamics of chemical reaction networks: wisdom from stochastic thermodynamics. *Physical Review X*, 6(4):041064, 2016.

[82] Linda JS Allen. *An introduction to stochastic processes with applications to biology*. CRC press, 2010.

[83] Kurt Jacobs. *Stochastic processes for physicists: understanding noisy systems*. Cambridge University Press, 2010.

[84] Terrell L. Hill. Studies in irreversible thermodynamics iv. diagrammatic representation of steady state fluxes for unimolecular systems. *Journal of Theoretical Biology*, 10(3):442–459, 1966.

[85] Jürgen Schnakenberg. Network theory of microscopic and macroscopic behavior of master equation systems. *Reviews of Modern physics*, 48(4):571, 1976.

[86] Pedro E. Harunari, Annwesha Dutta, Matteo Polettini, and Édgar Roldán. What to learn from a few visible transitions' statistics? *Phys. Rev. X*, 12:041026, Dec 2022.

[87] Jann van der Meer, Benjamin Ertel, and Udo Seifert. Thermodynamic inference in partially accessible markov networks: A unifying perspective from transition-based waiting time distributions. *Phys. Rev. X*, 12:031025, Aug 2022.

[88] Terrell L. Hill. Studies in irreversible thermodynamics iv. diagrammatic representation of steady state fluxes for unimolecular systems. *Journal of Theoretical Biology*, 10(3):442–459, 1966.

[89] R Bott and JP Mayberry. Matrices and trees, economic activity analysis. *Economic activity analysis, New York*, pages 391–400, 1954.

[90] F Leighton and Ronald Rivest. Estimating a probability using finite memory. *IEEE Transactions on Information Theory*, 32(6):733–742, 1986.

[91] Norman Biggs. *Algebraic graph theory*. Number 67. Cambridge university press, 1993.

[92] Ronald L Graham and Pavol Hell. On the history of the minimum spanning tree problem. *Annals of the History of Computing*, 7(1):43–57, 1985.

[93] Radia Perlman. An algorithm for distributed computation of a spanningtree in an extended lan. *ACM SIGCOMM computer communication review*, 15(4):44–53, 1985.

[94] Joel L Lebowitz and Peter G Bergmann. Irreversible gibbsian ensembles. *Annals of Physics*, 1(1):1–23, 1957.

[95] MY Choi and BA Huberman. Collective excitations and retarded interactions. *Physical Review B*, 31(5):2862, 1985.

[96] Prajwal Padmanabha, Daniel Maria Busiello, Amos Maritan, and Deepak Gupta. Fluctuations of entropy production of a run-and-tumble particle. *Phys. Rev. E*, 107:014129, 2023.

RÉSUMÉ

Dans un système dynamique, les différents degrés de libertés paramétrisant l'état du système peuvent fluctuer au cours du temps. L'objet principal de cette thèse est d'étudier l'effet d'une fixation (un "quench") progressive de tout ou d'une partie de ces degrés de libertés, à un instant donné, sur l'évolution du reste du système via une étude statistique. Le processus stochastique en découlant est appelé "Progressive Quenching". En nous basant sur un modèle simple de spins en interaction (modèle de Curie-Weiss), nous étudions l'évolution des trajectoires individuelles de son état dans l'espace des phases, et leur répartition statistique. Le rôle des martingales, vues comme des quantités stochastiquement conservées pendant ces processus, est crucial. Elles permettent à la fois d'estimer efficacement l'état final à partir de peu d'observations, mais aussi de comprendre leur répartition. L'invariance sous-jacente à cette loi de conservation permet de dresser un lien explicite entre la distribution finale du système et la distribution canonique initiale. Ce lien est explicitement prouvé par une étude combinatoire, et justifié thermodynamiquement. Nous étendons notre étude à l'ensemble des systèmes Markoviens et généralisons les précédents résultats. Pour un système Markovien admettant une distribution stationnaire, cette dernière est invariante par Progressive Quenching si le bilan détaillé est respecté. Nous abordons brièvement ce résultat du point de vue des graphes, et des flux de probabilité qui les parcourent. Enfin, une étude du cas non-Markovien est réalisée en considérant une information incomplète sur le système ainsi qu'en introduisant des délais dans les interactions entre les spins. Dans ce dernier cas, nous étudions numériquement l'influence des paramètres cinétiques du système sur les distributions finales.

MOTS CLÉS

Processus Stochastiques, Martingales, Théorie de l'information, Thermodynamique stochastique

ABSTRACT

In a dynamical system, the various degrees of freedom parameterizing the state of the system can fluctuate over time. The main aim of this thesis is to study the effect of a progressive fixing of all or part of these degrees of freedom, at a given instant, on the evolution of the rest of the system via a statistical study. The resulting stochastic process is called "Progressive Quenching". Based on a simple model of interacting spins (Curie-Weiss model), we study the evolution of individual trajectories of its state in phase space, and their statistical distribution. The role of martingales, seen as stochastically conserved quantities during these processes, is crucial. They enable us to efficiently estimate the final state from a small number of observations, and also to understand their distribution. The invariance underlying this conservation law enables an explicit link to be established between the final distribution of the system and the initial canonical distribution. This link is explicitly proven by a combinatorial study, and thermodynamically justified. We extend our study to all Markovian systems and generalize the previous results. For a Markovian system admitting a stationary distribution, the latter is invariant by Progressive Quenching if the detailed balance is verified. We briefly discuss this result from the point of view of graphs, and the probability flows that run through them. Finally, a study of the non-Markovian case is carried out by considering incomplete information about the system and introducing delays in the interactions between spins. In the latter case, we numerically study the influence of the system's kinetic parameters on the final distributions.

KEYWORDS

Stochastic processes, Martingales, Information theory, Stochastic thermodynamics